

Psychologie

**Attention Induced Distortions of Neural  
Population Responses, Receptive Fields, and  
Tuning Curves**

Inaugural-Dissertation

zur Erlangung des Doktorgrades

der

Philosophischen Fakultät

der

Westfälischen Wilhelms-Universität

zu

Münster (Westf.)

vorgelegt von

Marc Zirnsak

aus

Hamm (Westf.)

2009

Tag der mündlichen Prüfung: 20.08.2009

Dekan: Herr Prof. Dr. Christian Pietsch

Referent: Herr Prof. Dr. Markus Lappe

Korreferent: Herr Prof. Dr. Fred H. Hamker

*Für*  
*Elisabeth Weischer*  
*geb. Schütze*  
*20.05.1926 - 02.03.2008*

---

## Synopsis

Selective visual attention is generally conceptualized to control the flow of information with respect to the task at hand. Various studies in the space-based and feature-based domain of attention have demonstrated that the visual system achieves this via gain-control mechanisms. These mechanisms are supposed to result in an enhanced neural representation of relevant stimuli or features while irrelevant ones are suppressed. Thus, attention is suggested to modulate the strength of neural representations without altering their content. In this thesis, however, it will be argued that attention is able to change the very nature of these neural representations both at the level of population responses and of single neurons. This will be demonstrated for overt shifts of space-based attention as well as for the directing of feature-based attention.

Although we are able to covertly attend to regions which differ from the actual fixation of our eyes, shifts of space-based attention are typically accompanied by eye movements. By means of such overt shifts of space-based attention, that is, rapid eye movements called saccades, we constantly scan our environment. As a consequence the retinal images of our environment change as well as the processing of information in retinocentric areas of the visual system. A multitude of studies have demonstrated that several dynamic phenomena can be observed at the time of an impending saccade. Among them are firstly the observation that visual performance increases at the future fixation, that is, the saccade target, and secondly the fact that briefly presented visual stimuli are mislocalized. Under certain conditions these mislocalizations resemble a compression of visual space, so that stimuli are perceived closer towards the saccade target than expected from their veridical positions. Thirdly, at the same time changes of receptive fields can be observed in several retinocentric areas. Two types of receptive field dynamics can be distinguished. The first type basically consists of a shrinkage and shift of receptive fields towards the saccade target. Their suggested function is an enhanced processing at the future fixation. The second type is characterized by the finding that some cells become responsive to stimuli presented in their future receptive field. This is the region where the receptive field will be located after the saccade. The latter observations suggest that the visual system anticipates the consequences of an eye movement and already remaps the receptive fields before saccade onset in order to provide sufficiently accurate spatial processing across saccades within the involved areas. Thus, it is often assumed that this type of receptive field changes plays an important role for visual stability, which designates our stable perception of the world despite saccade induced changes of the retinal images.

In the first part of the thesis, the attempt is made to provide a unifying explanation of the above described phenomena. Based on a computational model, it will be argued that immediately before a saccade, the activity of neurons which are located in the surrounding of the internal representation of the saccade target, is enhanced by a spatially selective feedback signal. It is assumed that this feedback signal encodes the saccade target and originates in oculomotor areas, that is, areas that participate in the planning and execution of eye movements. At the level of neural populations the induced gain modulations cause distortions of the activity profile, that is, distortions of the neural representation of spatial positions. As a consequence these distortions lead to alterations of receptive fields and to spatial mislocalizations of visual stimuli.

In the course of the description it will be demonstrated that the developed model is able to quantitatively account for three particular aspects of the empirically observed mislocalizations: the time course of the mislocalization, the two-dimensional spatial pattern of the mislocalization, and the spatial range of the mislocalization. Furthermore, detailed analyses of the predicted receptive field changes will reveal that the model is able to unify both types of receptive field dynamics, namely saccade target shifts and predictive remapping. Thereby, the overall effect of the receptive field alterations in the model leads to an increase in the number of neurons which are effectively processing the saccade target region. Thus, it will be suggested that the observed mislocalizations are an inevitable consequence of an enhanced processing capacity of the future fixation.

In the second part of this thesis, it will be argued that related mechanisms are also involved in the domain of feature-based attention. Previous studies have shown that the response of neurons is either enhanced or suppressed, depending on whether their tuning characteristics match with the content of attention. This feature-based attention is supposed to operate globally throughout the whole visual space in order to gate relevant features for further processing, that is, the activity of neurons is enhanced respectively suppressed even if their receptive field location is distinct from the present focus of space-based attention.

Based on experimental results and computational modeling, it will be shown that global feature-based attention does not only render relevant features more salient by a simple scaling of the population response, but that global feature-based attention has a direct impact on the metric of feature space. This means that feature-based attention increases the distance between relevant and irrelevant features in feature space. Again this effect is based on a feedback signal which induces distortions of the population response. In turn these distortions are responsible for changes in

the tuning of neurons. Thus, similar to the postulated spatial feedback signal, the proposed feature-based feedback signal can enhance the processing capacity of the attended feature. In contrast to the spatial mislocalizations which are suggested to be the costs that the visual system has to pay for an increased processing, the mislocalizations in feature space are themselves of functional relevance.

Selektive visuelle Aufmerksamkeit bezeichnet im Allgemeinen die zielgerichtete Steuerung des Informationsflusses. Zahlreiche Studien im Bereich der raum- und merkmalsbasierten Aufmerksamkeit haben gezeigt, dass das visuelle System diese Kontrolle durch aktivitätsmodulierende Mechanismen ausübt. Es wird angenommen, dass diese Mechanismen zu einer verstärkten neuronalen Repräsentation von relevanten Stimuli oder Merkmalen führen, während irrelevante Aspekte unterdrückt werden. Dies bedeutet, dass typischerweise angenommen wird, dass Aufmerksamkeit lediglich die Stärke der neuronalen Repräsentationen, nicht aber die repräsentierten Inhalte selbst ändert. In dieser Arbeit wird jedoch argumentiert, dass Aufmerksamkeit die neuronalen Repräsentationen grundlegend sowohl auf Populationsebene als auch auf der Ebene einzelner Neurone verändern kann. Dies wird anhand offener Aufmerksamkeitsverlagerungen und der Ausrichtung von merkmalsbasierter Aufmerksamkeit gezeigt werden.

Obwohl wir in der Lage sind, räumliche Aufmerksamkeit verdeckt auszurichten, das heißt, örtlich abweichend von der gegenwärtigen Fixation unserer Augen, so gehen doch typischerweise Verlagerungen der räumlichen Aufmerksamkeit einher mit der Repositionierung unserer Augen. Mittels einer beständigen Sequenz dieser offenen Verlagerung der räumlichen Aufmerksamkeit, das heißt, schnellen Augenbewegungen, den sogenannten Sakkaden, analysieren wir unsere Umwelt. Im Verlauf dieser Sequenz ändern sich die retinalen Projektionen unserer Umgebung und demzufolge auch die Informationsverarbeitung innerhalb retinozentrisch organisierter Bereiche des visuellen Systems. Wie eine Vielzahl von Untersuchungen bislang demonstriert hat, lässt sich bereits im unmittelbaren Zeitraum vor einer Sakkade eine Reihe dynamischer Phänomene beobachten. Unter anderem zeigt sich, dass zum einen die visuelle Leistungsfähigkeit am Ort der zukünftigen Fixation, das heißt dem Sakkadenziel, erhöht ist und dass zum anderen visuelle Stimuli mislokalisiert werden. Unter bestimmten Bedingungen ähnelt das beobachtete Mislokalisationsmuster einer Kompression des visuellen Raumes, so dass Stimuli, die nur für den Bruchteil einer Sekunde präsent sind, näher am Sakkadenziel wahrgenommen werden, als es ihre tatsächliche Position vermuten lässt. Die Distanz zwischen dem Sakkadenziel

und der wahrgenommenen Stimulusposition relativ zu der Distanz zwischen dem Sakkadenziel und der tatsächlichen Stimulusposition erscheint demnach verkürzt. Zusätzlich zu der gesteigerten visuellen Leistungsfähigkeit am Sakkadenziel und der beschriebenen Mislokalisierung zeigen elektrophysiologische Studien, dass sich im selben Zeitraum auch die rezeptiven Felder von Neuronen in verschiedenen retinazentrisch organisierten Gehirnarealen ändern. Es lassen sich zwei Klassen rezeptiver Felddynamiken unterscheiden. Dabei besteht die erste Klasse in ihrer Mehrheit aus einer Verkleinerung und einer Verschiebung von rezeptiven Feldern zum Zeitpunkt der Sakkade. Diese beruht auf einer Erhöhung der Neuronenanzahl, die diesen Bereich verarbeiten und auf einer aus der Verkleinerung der rezeptiven Felder resultierenden, verbesserten räumlichen Selektivität. Die zweite Klasse ist folgendermaßen gekennzeichnet: Vor einer Sakkade antworten einige Neurone bereits auf Stimuli, die an der zukünftigen Position des rezeptiven Feldes präsentiert werden. Aus diesen Beobachtungen wird häufig geschlossen, dass sich die rezeptiven Felder besagter Neurone bereits vor der Sakkade an der Position befinden, die sie erst nach der Sakkade einnehmen würden und dass das visuelle System somit die Konsequenzen einer Sakkade gewissermaßen antizipiert, um eine die Sakkade überbrückende, räumlich akkurate Verarbeitung in den betroffenen Arealen zu ermöglichen. Demzufolge wird dieser Klasse von rezeptiven Feldänderungen eine bedeutende Rolle in der Generierung der visuellen Stabilität zugesprochen, das heißt unserer im Allgemeinen kontinuierlichen und stabilen Wahrnehmung der Welt, welche trotz der durch eine Sakkade verursachten retinalen Veränderungen aufrechterhalten wird.

Im ersten Teil dieser Arbeit wird der Versuch unternommen, eine vereinheitlichende Erklärung der oben beschriebenen Phänomene zu geben. Mittels eines quantitativen Modells wird argumentiert, dass unmittelbar vor einer Sakkade die Aktivität von Neuronen, welche in der Umgebung der internen Repräsentation des Sakkadenziels angeordnet sind, durch ein räumlich-selektives Rückkopplungssignal verstärkt wird. Dabei wird angenommen, dass das Rückkopplungssignal in okulomotorischen Gehirnarealen, das heißt in Arealen, die an der Planung und Ausführung von Augenbewegungen beteiligt sind, entsteht und das Sakkadenziel kodiert. Auf neuronaler Populationsebene verursacht dieses Signal Verzerrungen des Aktivitätsprofils. Diese Verzerrungen der Population führen wiederum zu Veränderungen von rezeptiven Feldern und zur räumlichen Mislokalisierung von visuellen Reizen.

Im Verlauf der Darstellung wird insbesondere Folgendes gezeigt: Das entwickelte Modell ist in der Lage, essentielle Aspekte der empirisch beobachteten

Mislokalisierung quantitativ zu erfassen. Darunter fallen der zeitliche Verlauf der Mislokalisierung, das räumliche, zweidimensionale Muster der Mislokalisierung und die räumliche Ausdehnung der Mislokalisierung. Detaillierte Analysen der vorhergesagten rezeptiven Feldänderungen zeigen, dass das Modell ebenfalls in der Lage ist, beide Klassen der elektrophysiologisch gemessenen rezeptiven Felddynamiken zu vereinheitlichen. Die Gesamtheit der vom Modell vorhergesagten rezeptiven Feldänderungen führt dabei zu einem Anstieg in der Anzahl von Neuronen, welche effektiv den Bereich der zukünftigen Fixation verarbeiten. Demzufolge wird argumentiert, dass die beobachteten Mislokalisierungen als unvermeidbare Folge einer erhöhten visuellen Verarbeitungskapazität der Region am Sakkadenziel entstehen.

Im zweiten Teil dieser Arbeit wird demonstriert, dass verwandte Mechanismen auch im Bereich der visuellen merkmalsbasierten Aufmerksamkeit wirksam sind. Vorangegangene Studien haben gezeigt, dass die Aktivität von Neuronen verstärkt wird, wenn die von ihnen präferierten Merkmale konsistent mit dem Inhalt der Aufmerksamkeit sind. Sind die präferierten Merkmale inkonsistent mit dem Inhalt der Aufmerksamkeit, wird die Aktivität der entsprechenden Neurone unterdrückt. Diese Effekte treten unabhängig davon auf, ob sich die Neurone im Fokus der räumlichen Aufmerksamkeit befinden. Ihre Funktion kann daher als eine globale, das heißt eine das ganze visuelle Feld betreffende Erhöhung der Salienz von relevanten Merkmalen charakterisiert werden.

Es wird gezeigt, dass der Mechanismus der globalen merkmalsbasierten Aufmerksamkeit dabei nicht nur auf einer Skalierung der Populationsantwort beruht, sondern dass die merkmalsbasierte Aufmerksamkeit einen direkten Einfluss auf die Metrik des Merkmalsraumes hat. Anhand experimenteller Befunde und eines quantitativen Modells wird argumentiert, dass die merkmalsbasierte Aufmerksamkeit mittels eines merkmalsselektiven Rückkopplungssignals die Distanz zwischen relevanten, das heißt mit dem Inhalt der Aufmerksamkeit konsistenten Merkmalen und irrelevanten, das heißt mit dem Inhalt der Aufmerksamkeit inkonsistenten Merkmalen, im Merkmalsraum erhöht. Die Grundlage dafür sind wiederum durch das Rückkopplungssignal induzierte Verzerrungen der Populationsantwort, welche darüber hinaus zu Änderungen der Antwortcharakteristik von Neuronen im Merkmalsraum führen. Das heißt, analog zum postulierten räumlichen Rückkopplungssignal führt das merkmalsbasierte Rückkopplungssignal durch Populationsverzerrungen zu einer Erhöhung der Verarbeitungskapazität des attendierten Merkmals. Im Gegensatz zu den durch das räumliche Rückkopplungssignal induzierten Mislokalisierungen stellen die

Mislokalisationen im Merkmalsraum jedoch keine reinen Kosten einer erhöhten Verarbeitungskapazität dar, sondern sind selbst von funktionaler Bedeutung.

# Contents

<b>1</b>	<b>General introduction</b>	<b>1</b>
<b>2</b>	<b>Overt shifts of space-based attention</b>	<b>3</b>
2.1	Introduction . . . . .	3
2.1.1	The need for saccades . . . . .	3
2.1.2	The enhanced processing of the future fixation . . . . .	5
2.2	Peri-saccadic compression of visual space . . . . .	6
2.2.1	Introduction . . . . .	6
2.2.2	Model of peri-saccadic processing . . . . .	7
2.2.3	Peri-saccadic compression in the model . . . . .	9
2.2.4	The origin of the feedback signal . . . . .	11
2.2.5	Cortical magnification and the shape of the feedback signal in visual space . . . . .	14
2.2.6	Where does visual compression occur in the brain? . . . . .	14
2.2.7	Discussion . . . . .	15
2.3	Peri-saccadic receptive field shifts . . . . .	18
2.3.1	Introduction . . . . .	18
2.3.2	Mapping of model receptive fields . . . . .	19
2.3.3	Changes in receptive field size . . . . .	21
2.3.4	Changes in the number of responsive cells . . . . .	24
2.3.5	One-probe remapping test . . . . .	27
2.3.6	Two-probe remapping test . . . . .	29
2.3.7	Continuous remapping test . . . . .	32
2.3.8	Discussion . . . . .	35
2.4	Discussion . . . . .	38
<b>3</b>	<b>Directing global feature-based attention</b>	<b>42</b>
3.1	Introduction . . . . .	42
3.2	Experimental procedure . . . . .	44
3.3	The altered metric of feature space . . . . .	46
3.4	Discussion . . . . .	50
<b>4</b>	<b>General discussion</b>	<b>53</b>
	<b>References</b>	<b>55</b>

<b>5</b>	<b>Appendix A: Space-based attention</b>	<b>73</b>
5.1	Mathematical description of the model . . . . .	73
5.1.1	Hierarchical visual processing . . . . .	73
5.1.2	Gain modulation . . . . .	76
5.1.3	Visuo-cortical mapping . . . . .	78
5.1.4	Computation of distances in visual space . . . . .	82
5.1.5	Computation of distances in cortical space . . . . .	82
5.1.6	Simulation of eye movements . . . . .	84
5.2	Fitting procedure and parameters of the model . . . . .	87
5.3	Predicting source and targets of the feedback signal . . . . .	88
5.4	Decoding of the population response . . . . .	94
5.5	Computation of mean errors . . . . .	95
5.6	Proportional reduction in error measure . . . . .	96
<b>6</b>	<b>Appendix B: Feature-based attention</b>	<b>98</b>
6.1	Control experiment 1: Contrast dependency . . . . .	98
6.2	Control experiment 2: Unattended motion . . . . .	98
6.3	Statistical analysis . . . . .	99
6.4	Model of feature-based attention . . . . .	99
6.5	Eye movements . . . . .	101

---

# 1 General introduction

Selective visual attention refers to our ability to focus on only a small part of the vast amount of information obtained from our environment. Thereby, the current contents of attention are preferentially processed. Helmholtz (1867/1925) was probably the first to demonstrate in a systematic manner that the latter is true. He observed that attending to a location which differs from the present fixation of his eyes while briefly presenting an array of letters led to a superior recognition of those letters spatially coinciding with his focus of attention. Subsequent studies further investigating these covert shifts of space-based attention, that is, shifts of the focus of attention without corresponding eye movements, have confirmed Helmholtz's observation of an enhanced processing at the attended site in various ways. For example, covert attention has been reported to speed up reactions to stimuli presented at the attended location (Posner, Nissen, & Ogden, 1978; Posner, Snyder, & Davidson, 1980), to improve discrimination performance (Lu & Doshier, 1998; Carrasco, Penpeci-Talgar, & Eckstein, 2000), and even to increase perceived stimulus contrast (Carrasco, Ling, & Read, 2004).

The neural basis of attention is supposed to consist of gain control, that is, mechanisms that alter the input-output ratio of individual neurons in visual brain areas. In the presence of single stimuli, the response of neurons whose receptive field is aligned with the attended region in space is enhanced as compared to when attention is directed elsewhere (Treue & Maunsell, 1996; McAdams & Maunsell, 1999; Reynolds, Pasternak, & Desimone, 2000). Moreover, in the case of multiple stimuli, attention has been reported to bias the processing in favor of the attended one (Moran & Desimone, 1985; Luck, Chelazzi, Hillyard, & Desimone, 1997; Reynolds, Chelazzi, & Desimone, 1999). In their pioneering study Moran and Desimone (1985) reported that when two stimuli, one effectively driving the cell if presented in isolation (preferred stimulus) and the other not (non-preferred stimulus), were presented simultaneously in the same receptive field at non-overlapping locations, the activity of the cell was high if attention was directed to the preferred stimulus. However, if attention was directed towards the non-preferred stimulus, the activity of the cell was much lower. That is, the influence of the preferred stimulus was suppressed. Similar effects have also been reported if attention is directed towards specific non-spatial attributes (Chelazzi, Miller, Duncan, & Desimone, 1993; Motter, 1994a, 1994b; Chelazzi, Duncan, Miller, & Desimone, 1998; Treue & Martinez-Trujillo, 1999; Martinez-Trujillo & Treue, 2004; Bichot, Rossi, & Desimone, 2005). This feature-based attention, in contrast to space-based attention, is supposed to operate globally throughout

the whole visual field. This means that the activity of neurons is enhanced if their tuning characteristics match with the attended feature even if their receptive field location is distinct from the present focus of space-based attention. For example, Treue and Martinez-Trujillo (1999) demonstrated that the response of direction-selective neurons in area MT to their preferred direction was enhanced, relative to a neutral condition, if the monkey attended to the same direction of motion which was presented in a non-overlapping location with respect to the receptive field of the recorded neuron. Furthermore, the response to the preferred direction was suppressed if the monkey attended to the anti-preferred direction of the recorded neuron. This principle has also been confirmed in humans in terms of the strength of the haemodynamic response (Sàenz, Buraças, & Boynton, 2002) and the strength of the motion aftereffect (Boynton, Ciaramitaro, & Arman, 2006). Moreover, feature-based attention has been reported to facilitate the detection of stimuli (Sàenz, Buraças, & Boynton, 2003) and contour integration (Stojanoski & Niemeier, 2007). In Sàenz et al. (2003) subjects had to detect a change in speed of two spatially separated motion stimuli. Detection performance was significantly better when both stimuli moved in the same than in opposite directions.

The above described phenomena suggest that visual attention, both space-based and feature-based, operates by the selective enhancement of relevant sensory signals while irrelevant ones are suppressed. As a consequence, attended stimuli or features are gated through the hierarchy of visual processing and ultimately into consciousness. Although this view seems to be convenient with respect to the processing of single cells, it will be argued in this thesis that attention does not merely modulate the strength of neural representations, but that attention is able to fundamentally alter these representations both at the level of population responses and of single cells. That is, the modulation of single neurons leads to distortions on the level of neural populations which are assumed to encode specific dimensions of visual stimuli. In the space-based domain, as demonstrated via overt shifts of attention, that is, shifts of space-based attention that are accompanied by eye movements, the distorted populations will lead to mislocalizations of stimuli in visual space. Similar, in the feature-based domain, the distorted populations will cause mislocalizations in feature space. Furthermore, in both domains the distorted populations cause shifts in receptive fields and tuning curves resulting in an increase of the number of cells which are effectively processing the content of attention. Thus, attention alters both the contents that are processed respectively represented by single neurons and the populations they constitute.

---

## 2 Overt shifts of space-based attention

### 2.1 Introduction

#### 2.1.1 The need for saccades

Only a small region of the visual field, approximately two degrees of visual angle in size, is processed by the fovea centralis of our retinas, where visual accuracy is highest. With increasing eccentricity visual accuracy drops off. Thus, at any one time only a minimal part of our environment that we are looking at is perceived with maximum detail. Two neuroanatomical properties of the visual system seem to be responsible for this restriction.

Firstly, findings in monkeys and humans indicate that central regions of the visual field are processed by a much greater amount of cortical cells as compared to more peripheral regions. This overrepresentation is referred to as cortical magnification, is usually measured in millimeters of cortex per degree of visual angle (Daniel & Whitteridge, 1961), and has been demonstrated to correlate with visual accuracy (Duncan & Boynton, 2003). Cortical magnification is highest in the primary visual cortex V1 (Dow, Snyder, Vautin, & Bauer, 1981; Gattass, Sousa, & Rosa, 1987), which is the earliest cortical processing stage of visual signals. It is less pronounced in later visual areas like V4 (Gattass, Sousa, & Gross, 1988) and the middle temporal area (MT) (Albright & Desimone, 1987). Figure 1 illustrates the representation of the visual field in early visual cortex.

Secondly, while the number of cells which are processing a certain part of the visual field decreases with increasing eccentricity, the opposite is true for receptive field size. The classical receptive field is defined as the region in visual space where a stimulus has to be presented to drive a given neuron. In many visual areas like V1 (Dow et al., 1981; Gattass et al., 1987), V2 (Gattass, Gross, & Sandell, 1981; Nakamura & Colby, 2000), V4 (Desimone & Schein, 1987; Gattass et al., 1988; Boussaoud, Desimone, & Ungerleider, 1991), TEO (Boussaoud et al., 1991), V3a (Galletti & Battaglini, 1989; Nakamura & Colby, 2000), and MT (Felleman & Kaas, 1984; Albright & Desimone, 1987; Komatsu & Wurtz, 1988; Tanaka, Sugita, Moriya, & Saito, 1993) the size of these receptive fields increases with increasing eccentricity as illustrated in Figure 1c. Thus, central parts of the visual field are not only processed by a larger amount of cells, but also by cells that are characterized by a higher spatial selectivity and are therefore in principle able to extract finer details than cells which are processing the periphery.

In retinocentric brain regions, which constitute early to mid-level visual processing and encompass all the above mentioned areas, the receptive field depends

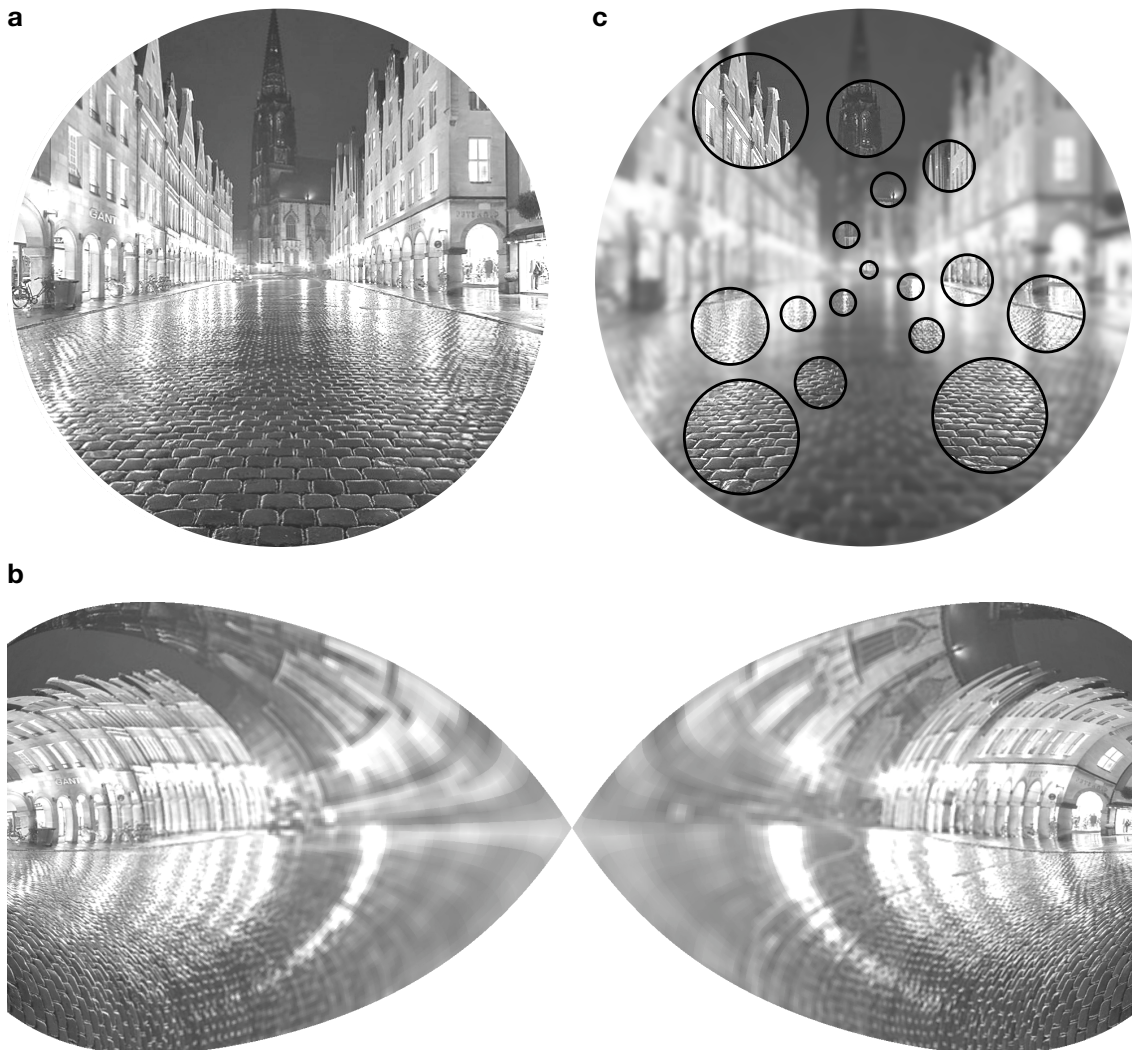


**Figure 1.** The way early visual cortex “sees” the world. (a) Illustration of the visual field. (b) Cortical representation of the visual field in the primary visual cortex. Central parts of the visual field are largely magnified. (c) Hypothetical population of receptive fields (black circles). For the sake of simplicity only the increase of receptive field size with increasing eccentricity is illustrated.

on the eyes’ position. This means that the receptive field is fixed in retinal coordinates but covers different parts of visual space during different fixations of the eyes. Although it was already stated in the General Introduction that we are able to overcome the above described limitations of peripheral vision to some degree by covertly shifting our spatial focus of attention, typically these attentional shifts are accompanied by corresponding shifts of our eyes. Thus, in order to reallocate our central high performance processing resources consisting of a large amount of cells with small receptive fields, we constantly scan our environment by rapid eye movements<sup>1</sup> called saccades. With each of these saccades the retinal images of our environment change as well as the processing in retinocentric areas. However,

various studies have demonstrated that visual processing changes even before the eyes start to move. Among them are the observations that, at the time of an impending saccade, visual performance is enhanced at the future fixation, visual stimuli are mislocalized and receptive fields are subject to change. In the first part of this thesis, the attempt is made to provide a unifying explanation of these three phenomena.

### **2.1.2 The enhanced processing of the future fixation**

Immediately before a saccade visual performance increases at the future fixation. For example, Hoffman and Subramaniam (1995) reported that the detection of a target stimulus was facilitated as compared to a fixation condition, if the stimulus was briefly presented at the saccade target just prior to an eye movement. Furthermore, they demonstrated that when attention was deployed covertly to one location and a saccade was made to a different location, performance remained superior at the saccade target. These and related psychophysical findings (Shepherd, Findlay, & Hockey, 1986; Kowler, Anderson, Doshier, & Blaser, 1995; Deubel & Schneider, 1996; Godijn & Pratt, 2002; Peterson, Kramer, & Irwin 2004) support the view that spatial visual attention does precede a saccade and is automatically locked at the saccade target approximately before the eyes start to move. Consistent with this view the responses of neurons in monkey area V4, an area of the ventral pathway which is supposed to play a key role for object recognition, are pre-saccadically enhanced if a saccade is directed towards a stimulus within their receptive field (Fischer & Boch, 1981a, 1981b; Moore, Tolia, & Schiller, 1998; Mazer & Gallant, 2003). Moreover, the capability of these cells to discriminate between stimuli is increased before an eye movement (Moore & Chang, 2009). Hamker (2003, 2005a) has earlier argued that the enhanced activity is caused by a spatially selective feedback signal. This signal encodes the internal representation of the saccade target, is suggested to arise in oculomotor areas like the frontal eye field (FEF) (Armstrong, Fitzgerald, & Moore, 2006; Armstrong & Moore, 2007) or the superior colliculus (SC) (Cavanaugh & Wurtz, 2004; Müller, Philiastides, & Newsome, 2005), and targets multiple areas of the visual hierarchy. Thereby, the signal induces local gain changes, that is, alterations of the input-output ratio of individual neurons, which are multiplicative in nature. Thus, the signal does not cause activity by itself. In the following it will be demonstrated that due to these local gain modulations, the proposed signal leads to distortions of the population response in the involved areas, which in turn cause

---

<sup>1</sup>Note that throughout the course of the description the use of the term eye movement refers to saccade.

the mislocalization of visual stimuli and changes of receptive fields.

## 2.2 Peri-saccadic compression of visual space

### 2.2.1 Introduction

Around the time of a saccade briefly presented stimuli are mislocalized (e.g., Matin & Pearce, 1965; Bischof & Kramer, 1968; Matin, Pearce, & Pearce, 1969; O'Regan, 1984; Honda, 1989, 1991; Dassonville, Schlag, & Schlag-Rey, 1992, 1995; Schlag & Schlag-Rey, 1995; Cai, Pouget, Schlag-Rey, & Schlag, 1997; for a review see Ross, Morrone, Goldberg, & Burr, 2001). Under certain conditions the observed mislocalization pattern resembles a compression of visual space (e.g., Honda, 1993; Ross, Morrone, & Burr, 1997; Morrone et al., 1997; Lappe, Awater, & Krekelberg, 2000), so that stimuli are perceived as being presented closer towards the saccade target than they really are. Figure 2 displays a schematic illustration of this effect. Stimuli that are presented between the fixation point and the saccade target, and stimuli that are presented left to the fixation point are mislocalized in the direction of the saccade. Stimuli that are presented right to the saccade target are mislocalized against the direction of the saccade. The spatial range of this effect can extend to stimuli presented up to  $10^\circ$  left and  $30^\circ$  right of the fixation point (Ross et al., 1997; Morrone et al., 1997). As it was demonstrated by Kaiser and Lappe (2004), compression also occurs orthogonal to saccade direction, revealing a two-dimensional spatial pattern of mislocalization. According to the temporal pattern, the mislocalization begins about 50 ms before the eyes start to move, reaches its maximum around saccade onset, and usually vanishes at the end of the saccade.

Which factors do influence or even cause compression? It has been demonstrated that the strength of the effect depends on stimulus contrast (Michels & Lappe, 2004), saccadic peak velocity (Ostendorf, Fischer, Finke, & Ploner, 2007), and the presence of post-saccadic visual references (Lappe et al., 2000). Although the latter has originally been interpreted as the causal factor to give rise for compression, Morrone, Ma-Wyatt, and Ross (2005) have demonstrated that post-saccadic visual references are not necessary for compression to occur. Compression has also been attributed to a translation of spatial locations in cortical coordinates (Van Rullen, 2004). While this account is able to explain in principle the observed spatial pattern of compression (Kaiser & Lappe, 2004), it remains unclear how the characteristic time course of compression arises. Furthermore, compression has been linked to peri-saccadic receptive field dynamics (Ross et al., 1997; Morrone et al., 1997; Ross et al., 2001). However, this proposal has never been formalized. Thus, the

cause of peri-saccadic compression of visual space is virtually not understood. In particular, a quantitative, comprehensive, and physiologically plausible explanation of the observed effect is missing.

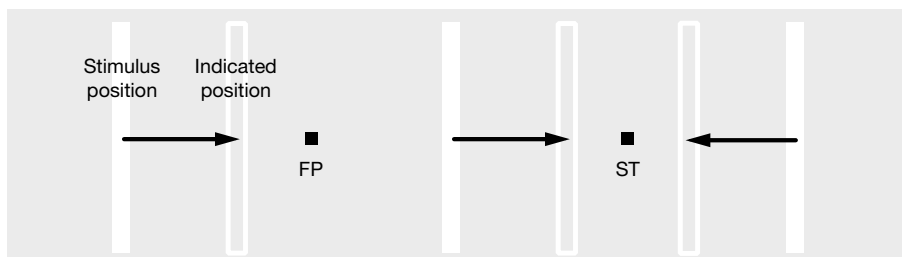


**Figure 2.** Schematic illustration of the mislocalization pattern and the experimental setup used by Ross et al. (1997). The solid white bars denote the veridical positions of three stimuli. In a given trial only one of these stimuli was briefly presented (8 ms) around the time of a saccade, which was made from the fixation point (FP) to the saccade target (ST). As illustrated by the arrows, subjects indicated that they perceived these stimuli as being presented closer towards the saccade target.

### 2.2.2 Model of peri-saccadic processing

Early to mid-level visual processing is organized in retinotopic maps in many brain areas. Likewise, information about the saccade target is organized in visuo-motor maps in cortical and subcortical structures, that is, the FEF and the SC, respectively. In the model, it is assumed that around the time of an eye movement, saccade target information is sent back as a spatially selective feedback signal from these oculomotor areas to multiple visual areas in which the feedback signal leads to modulations of the neural activity. A single visual area, which will be referred to as *layer*, consists of an *input stage* with “simple” cells for feature detection, a *spatial pooling stage* with “complex” cells, that is, cells which share the same non-spatial feature space with the simple cells, but have larger receptive fields leading to an increased spatial invariance (Fukushima, 1980; Riesenhuber & Poggio, 1999), and an *intermediate gain stage* at which the oculomotor feedback signal acts.

A hierarchy of visual processing (Figure 3a) can be obtained by simulating multiple layers. A given layer receives its input exclusively from the preceding layer and the first layer in the hierarchy is driven directly by a visual stimulus. In each layer, cells are organized according to cortical magnification functions which constitute cortical space (Figure 3b) and the size of their receptive fields increases as a function of eccentricity.

Figure 3c illustrates the processing in a given layer. In this case, it is the first layer of the hierarchy. A stimulus presented in visual space (yellow dot) initially exerts a

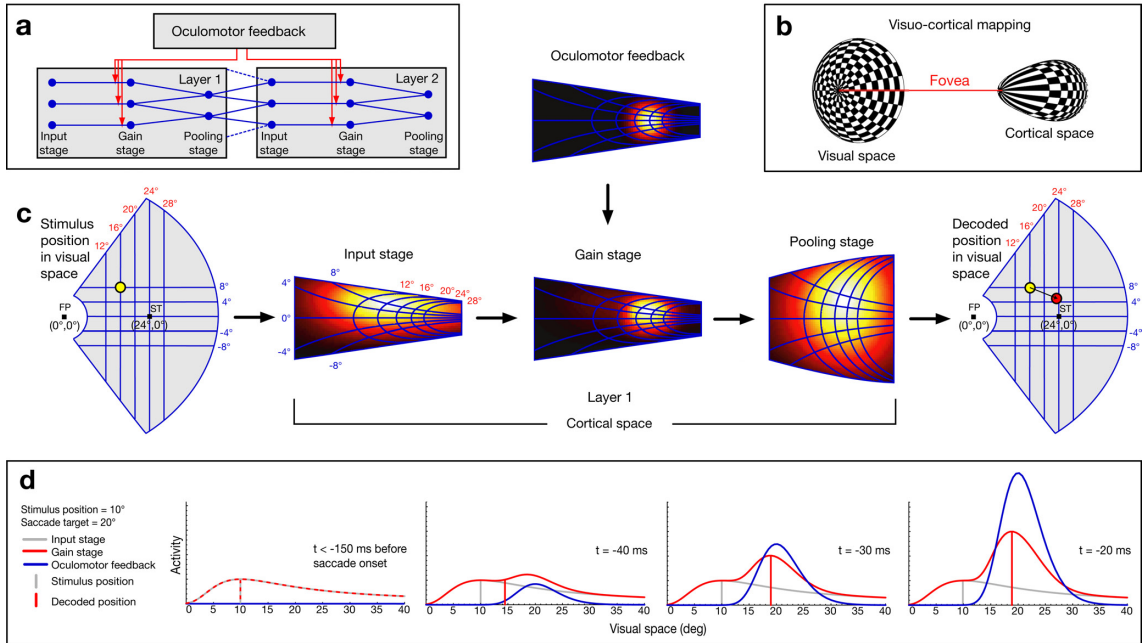


**Figure 3.** Model of peri-saccadic processing. (a) Simplified hierarchy of visual processing. Each layer consists of three stages (input, gain, and pooling). Each dot represents a cell in the respective stage. The stream of the bottom-up activity is from left to right. The encoded saccade target position is fed back (red arrows) by the oculomotor system into multiple layers and modulates the gain of the cells prior to spatial pooling. (b) Illustration of the visuo-cortical mapping. (c) Detailed view of the computations within a single layer (layer 1). The effect of the feedback signal on the population response is illustrated for a stimulus at position  $(16^\circ, 8^\circ)$  immediately before the onset of a  $24^\circ$  saccade where the signal is strong. The population activities of the model are shown in cortical space. Thereby, the shown area of cortical space corresponds to the (gray) area of visual space which is presented to the left and right of the cortical space. The population response in the input stage is a function of stimulus and eye position, receptive field size, and cortical magnification. The gain factor is determined by the strength of the feedback signal. If the signal is sufficiently strong, the modulated population response will be distorted towards the saccade target and is then spatially pooled. The perceived position of the stimulus is decoded from the activity in the neural ensemble. (d) Population responses along the horizontal meridian of the input and the gain stage are shown together with the feedback signal in visual space. A stimulus is presented at  $10^\circ$  and the saccade target is located at  $20^\circ$ . Long before saccade onset ( $t < -150$ ms) the oculomotor feedback is inactive and thus, the population responses in the input and the gain stage are identical. As a result, the decoding of the stimulus position from the population response leads to the true position. At  $t = -40$ ms the oculomotor feedback is sufficiently strong to distort the population response with the consequence that the decoded position is already shifted towards the saccade target. As the presentation time of the stimulus gets closer to saccade onset, the feedback signal, and thus the gain factor, increases further and the decoded position gets closer to the saccade target. However, a further increase of the signal at  $t = -20$ ms does not lead to a stronger mislocalization for a stimulus presented at this time, that is, the magnitude of the mislocalization saturates.

corresponding activity hill in the cortical space of the input stage (Figure 3c, left). Prior to an eye movement, activity increases at the location of the saccade target in the oculomotor map (Figure 3c, top). Prior to the pooling the feedback of this activity distorts the population response of the stimulus towards the saccade target

(Figure 3c, center). By assuming that the visual system relies on this population response for stimulus localization, we can decode the “perceived” position (Figure 3c, right, red dot). Consistent with the distortion of the population activity the stimulus is mislocalized towards the saccade target. Further, as it will be demonstrated later, the distorted population response of the gain stage leads to receptive field changes of pooling stage cells.

In analogy to cells in oculomotor areas the feedback signal in the model builds up before the saccade and reaches its maximum at saccade onset. Figure 3d illustrates the time course of the oculomotor feedback build up and the corresponding distortion of the population activity. Each panel shows the activity profiles in the input (gray) and gain (red) stage, and the activity profile of the feedback signal (blue), along the horizontal meridian of visual space. The leftmost panel illustrates the case when the visual stimulus is presented 150 ms before the saccade and the feedback is inactive. In this case, the activity profiles of the input and gain stage are identical and peak at the position where the stimulus was presented ( $10^\circ$ ). Thus, the model perceives the stimulus at its veridical position, that is, the true stimulus position in visual space. The three panels on the right illustrate the interaction between the feedback signal and the gain stage for the case that the stimulus is presented closer in time towards saccade onset (-40 ms, -30 ms, and -20 ms). The feedback signal (blue) rises in strength but is always centered at the saccade target position at  $20^\circ$ . In the gain stage the activity of neurons near the saccade target is enhanced and the shape of the population profile is distorted. The decoded stimulus position (red vertical line) shifts away from the true position (gray vertical line) towards the saccade target as a function of feedback strength. Mathematical details of the model are described in Section 5.

### 2.2.3 Peri-saccadic compression in the model

Extensive simulations revealed that a model with a hierarchy of only two gain modulated layers with increasing receptive field sizes is consistent with three particularly relevant experimental data sets of peri-saccadic compression, namely the spatial range of compression (Morrone et al., 1997), the time course of compression (Morrone et al., 1997), and the two-dimensional spatial pattern of compression (Kaiser & Lappe, 2004). For details of the fitting process and the involved parameters please refer to Section 5.2. Figure 4 summarizes the main results. The goodness of fit of the model is given by the proportional reduction in error measure (*pre*), which is the reduction in the sum of squared error (*SSE*) of the data by the model (see Section 5.6). Figure 4a shows the spatial range of compression for a

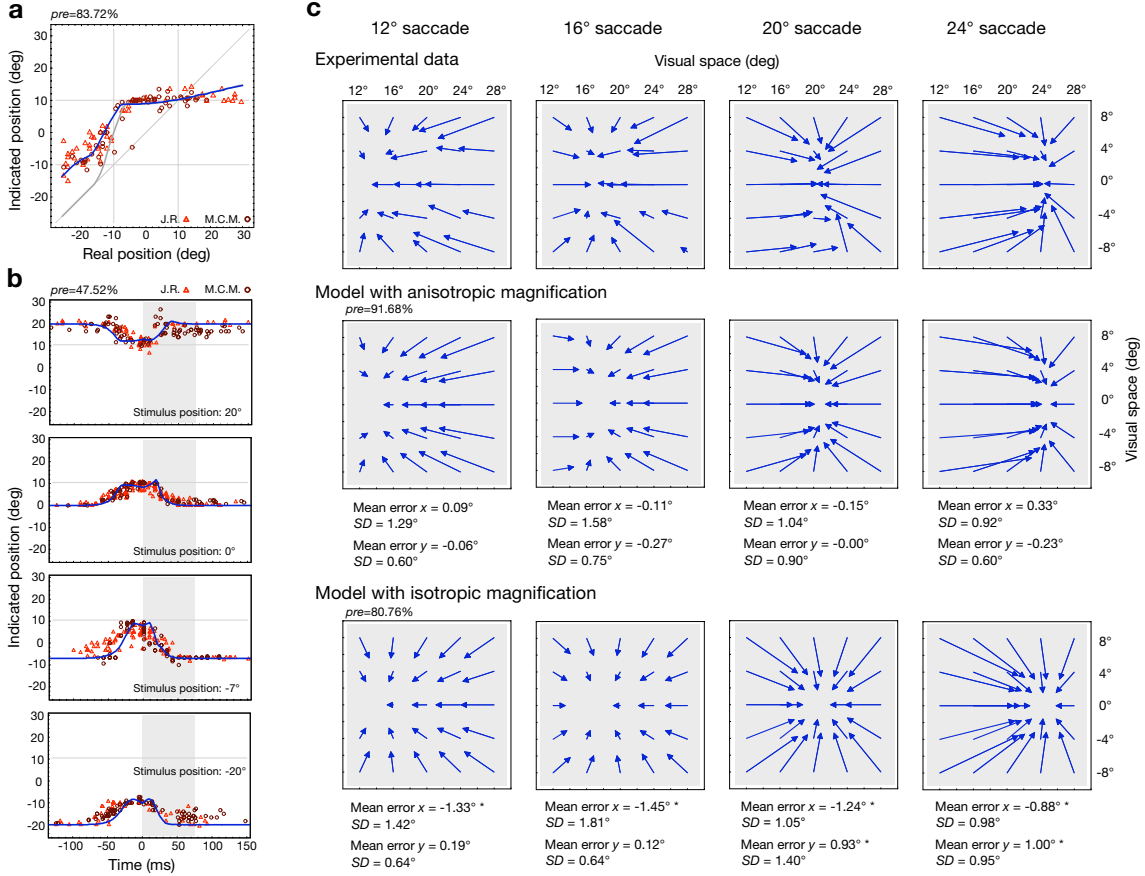


**Figure 4.** Peri-saccadic compression in the model. **(a)** Spatial range of compression. The data show the indicated versus real stimulus position of briefly presented bars in the critical phase from  $-25$  to  $0$  ms before a  $20^\circ$  saccade for two subjects (data from Morrone et al. 1997) together with the predicted stimulus location by the model simulating both layer 1 and layer 2 (blue curve) and layer 1 only (gray curve). The fixation point is at  $-10^\circ$  and the saccade target at  $10^\circ$ . **(b)** The time course of compression. The data show the indicated position of bars presented at four different locations as a function of time relative to saccade onset for two subjects (data from Morrone et al. 1997). The blue lines represent the predicted mislocalization of the model. The gray area denotes the time period of the simulated saccade (see Section 5.1.6). **(c)** The spatial pattern of compression. The data show the absolute mislocalization with reference to the true position of a briefly presented dot randomly chosen from an array of 24 possible positions for four different saccade amplitudes (data replotted from Kaiser and Lappe 2004). The fixation point lies outside the shown area. The  $y$ -coordinate of the saccade target is always zero and the  $x$ -coordinate is equal to the respective saccade amplitude. Vector origins indicate the veridical stimulus position and vector endpoints denote the indicated position shortly after saccade onset. The simulation results show the best fits of two models with either anisotropic or isotropic magnification (see Section 5.1.3). In contrast to the isotropic model, the anisotropic model on average does not significantly deviate from the data (see Section 5.5 for the computation of mean errors). Significant deviations ( $p < 0.05$ ) are indicated by asterisks (two-sided, one-sample  $t$ -test,  $\alpha = 0.05$ ,  $df = 23$ ).

planned  $20^\circ$  saccade close to saccade onset, where the effect is strong. Consistent with the experimental data the model shows strong compression in the range of roughly  $\pm 20^\circ$  around the saccade target ( $10^\circ$ ), which gradually decreases for stimuli presented farther to the left of the fixation point ( $-10^\circ$ ). For stimuli presented

close to the saccade target the mislocalization originates in layer 1, that is, the gain modulation in this layer is strong enough to affect the localization of stimuli in the range of  $-10^\circ$  to  $30^\circ$  with reasonable strength. However, due to the relatively small receptive fields and a relatively small spatial extent of the feedback signal in this layer, the gain modulation is too weak to result in a sufficiently mislocalization of stimuli presented farther to the left of the fixation point ( $-10^\circ$ ). Thus, the model predictions fall below the empirical observations, which is indicated by the gray curve. Note that in the range of  $-8^\circ$  to  $30^\circ$  the gray curve is identical to the blue curve. In order to account for the full range of compression, an additional gain modulation in a second subsequent layer has to be assumed. In this layer 2 the central receptive fields are larger than in layer 1 and the same is true for the estimated spatial extent of the feedback signal. Thus, the gain modulation in layer 2 leads to sufficiently large mislocalizations for stimuli presented farther to the left of the fixation point without further affecting the mislocalization of stimuli presented in the close range of the saccade target (blue curve). Figure 4b shows the corresponding time course of compression for a  $20^\circ$  saccade in the range of -150 ms to 150 ms around saccade onset for four stimulus positions ( $-20^\circ$ ,  $-7^\circ$ ,  $0^\circ$ ,  $20^\circ$ ). The mislocalization begins about 50 ms before the saccade, reaches its maximum at saccade onset and ceases during the eye movement. Finally, Figure 4c shows the spatial pattern of compression for four saccade amplitudes ( $12^\circ$ ,  $16^\circ$ ,  $20^\circ$ ,  $24^\circ$ ) about saccade onset. The predictions of two models with either isotropic or anisotropic magnification in layer 1 (see Section 5.1.3) are reported. It becomes obvious that the latter accounts best for the experimentally observed data.

#### **2.2.4 The origin of the feedback signal**

In the model it is assumed that the feedback signal arises in oculomotor areas. However, cells in these areas show a variety of response characteristics. The FEF shows a continuum of saccade-related cells ranging from a strong visual to no visual response (Bruce & Goldberg, 1985). Similarly, some cells in the SC initially build up their activity slowly and others show a burst of activity only around saccade onset (Munoz & Wurtz, 1995). The movement fields of saccade-related cells in the FEF and SC can be closed and open-ended (Bruce & Goldberg, 1985; Munoz & Wurtz, 1995; Sommer & Wurtz, 2004). Cells with closed movement fields only fire when the actual saccade amplitude is close to the preferred amplitude of the cell, whereas cells with open movement fields continue to discharge also for larger saccade amplitudes. Furthermore, saccade-related cells can be classified as clipped, partially clipped or unclipped (Munoz & Wurtz, 1995). A cell is classified as clipped if the

activity drops close to baseline by the end of the saccade, is classified as partially clipped if the activity drops close to baseline shortly after the end of the saccade, and is classified as unclipped if the cell continues to discharge above baseline well beyond the end of a saccade. Although several neurons with open movement fields, primarily of a build-up type, can be found in the SC, the majority of burst cells has closed movement fields and a clipped activity profile (Munoz & Wurtz, 1995).

Since the properties of the feedback signal in the model are constrained by the temporal and spatial dynamics of the mislocalization, these properties can be used to predict the type of cell which should predominately drive the feedback. Therefore, the time course and shape of the feedback signal was systematically varied and the model was fitted to the data, that is, the spatial range and time course of compression, with the constraint that the resulting model specification remained consistent with the two-dimensional pattern of compression (see Section 5.3).

By assuming that the feedback to both model layers originates from cells which share the same oculomotor related characteristics, but differ in their effective back-projections resulting in a smaller feedback signal in earlier visual areas (feedback width in layer 1) than in later visual areas (feedback width in layer 2), the model predicts that the main contribution should originate from cells with closed movement fields (Figure 5a). Open movement fields systematically reduce the magnitude of the predicted mislocalization as it is shown in Figure 5b for stimuli presented beyond the saccade target, which is due to a weaker gradient of the feedback signal for larger eccentricities. Furthermore, the main contribution to the feedback signal should originate from clipped cells, since the discharge of unclipped cells results in too large mislocalizations during the eye movement. Finally, the activity in the oculomotor map should exceed its half-maximum value not earlier than 30 ms prior to saccade onset, which is consistent with the firing pattern of burst cells. However, this value depends on the assumption that the gain is instantaneous, that is even a low activity of the cells in the oculomotor map leads to a significant gain increase (Figure 28a in Section 5.1.2). The model was also tested using a damped gain function with little increase at the target site for low oculomotor activity (Figure 28b), with the result that the half-maximum activity can occur much earlier. Thus, while an instantaneous gain function requires that the feedback signal primarily originates in oculomotor burst cells, a damped gain function allows that build-up, and/or visual activity contributes to the feedback signal (Thompson, Biscoe, & Sato, 2005). In both cases, however, the effective feedback signal would be primarily driven by late saccade-related activity, since the early prelude activity would have little impact on the gain.

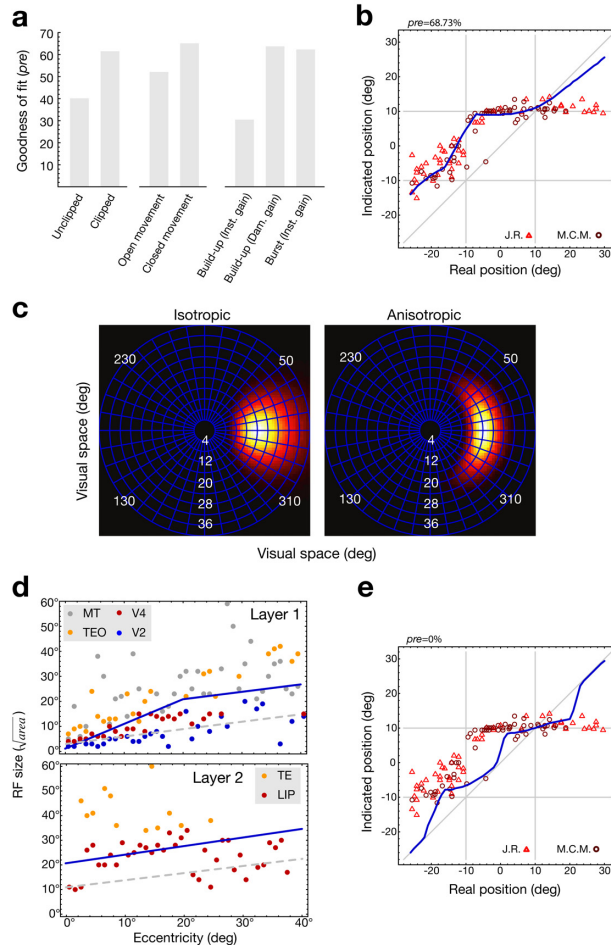


**Figure 5.** Predicted source and shape of oculomotor feedback, and predicted target area of compression. (a) Goodness of fit (*pre*) for the time course and spatial range of compression with respect to typical properties of cells in oculomotor areas. Unclipped activity and open movement fields lead to a decrease in the goodness of fit. A time course which resembles the firing pattern of burst cells is consistent with the data, whereas build-up like activity with a half-maximum value around 46 ms prior to saccade requires a damped gain function in the target area to compensate the early distortion which would arise otherwise. (b) Effect of open movement fields on the localization of flashed bars in the critical phase from  $-25$  to the onset of a  $20^\circ$  saccade. (c) Predicted shape of the feedback signal in visual space for a  $20^\circ$  saccade. The left panel shows the prediction of a model with isotropic magnification and the right panel the prediction of a model with anisotropic magnification. (d) Comparison of monkey receptive field sizes with the model prediction (see Section 5.3). The solid line shows the required minimal receptive field size for each layer. Please note, due to the non-linear spatial pooling in the model, the receptive field values are upper bounds and not mean values. The dots indicate the maximal receptive field size for a particular eccentricity in the respective cortical area as reported in the literature. For the area to be consistent with the model the dots should be close to or exceed the constraint given by the model. Layer 1: The receptive field sizes in V4 are close to the minimal receptive field sizes required by the model. Receptive field sizes in MT and TEO are sufficiently large. Layer 2: Both TE and LIP are consistent with the prediction of the model for layer 2. For larger eccentricities, receptive field sizes in LIP are below the lower limit obtained from the model. However, since the critical stimuli in the data (Figure 4a) which constrain the receptive field size in layer 2 were all presented at an eccentricity of less than  $20^\circ$  (in the opposite hemifield than the one where the saccade target appeared) LIP should not be excluded. (e) Effect of (too) small receptive field sizes in layer 1 and layer 2 (dashed lines in d) on the localization of flashed bars in the critical phase from  $-25$  to the onset of a  $20^\circ$  saccade.

### 2.2.5 Cortical magnification and the shape of the feedback signal in visual space

Another prediction is concerned with the shape of the feedback signal in visual space. The feedback signal was modeled as a Gaussian in cortical space similar to collicular neurons with closed movement fields (Munoz & Wurtz, 1995; Sommer & Wurtz, 2004). Under this assumption the model predicts an anisotropic magnification in early visual areas. This qualitatively resembles findings in striate cortex of monkey (Van Essen, Newsome, & Maunsell, 1984; Adams & Horton, 2003) and human V1 and V2 (Schira, Wade, & Tyler, 2007). As a consequence of this anisotropic magnification the feedback signal appears elongated in visual space (Figure 5c). This prediction seems to be supported by at least some evidence from a recent fMRI study (Datta & DeYoe, 2009), in which a similar circumferential spread of the attentional “spotlight” was reported in early visual cortex during the allocation of covert attention.

### 2.2.6 Where does visual compression occur in the brain?

Anatomical investigations in monkeys revealed that the oculomotor system is widely connected to visual areas via indirect (SC) (Wurtz, Sommer, & Cavanaugh, 2005) and direct (FEF) projections. The FEF is linked with areas of both the ventral and dorsal stream. Among them are V2, V4, TEO, TE, V3a, MT, the medial superior temporal area (MST), and the lateral intraparietal area (LIP) (Webster, Bachevalier, & Ungerleider, 1994; Stanton, Bruce, & Goldberg, 1995; Schall, Morel, King, & Bullier, 1995; Bullier, Schall, Morel, 1996). The FEF projections to these areas appear to be topologically organized in terms of saccadic amplitude (Stanton et al., 1995), as required by the model. In addition to these anatomical considerations stronger constraints for the involved areas can be formulated by tuning the parameters of the model to the minimal possible receptive field sizes and compare them to the receptive field sizes of several areas in question (Figure 5d). For the strong compression in the spatial range of  $\pm 20^\circ$  around the saccade target (Figure 4a), the model (layer 1) requires at least a receptive field size as observed in areas V4, MT, or TEO, alternatively in V3a (not shown) as well. The receptive field constraint of layer 2 is consistent with the receptive field sizes found in TE, LIP, and MST (not shown). Too small receptive field sizes, for example at the level of V2 for layer 1 and between  $10^\circ$  and  $20^\circ$  for layer 2, still allow to fit the data for stimuli presented close to the saccade target, but effects from stimuli presented at a larger distance cannot be accounted for (Figure 5e). The reason is that with a small receptive field size the population response becomes too narrow

to be affected by the feedback signal so that the spatial range of strong compression is reduced to less than  $\pm 10^\circ$  around the saccade target. Increasing the width of the feedback signal is not a solution since a broader feedback signal would increase the gain of large parts of the population to a similar degree. However, a mislocalization only occurs when the population response is sufficiently distorted, which requires a difference in the gain across the population. Thus, a broader feedback signal would increase the range of compression, but the amount of compression would be reduced (slope of the line through  $(10^\circ, 10^\circ)$  in Figure 5e would approach 1).

Thus, the model predicts that the encoded position of a peri-saccadic stimulus is already sufficiently distorted, with respect to the magnitude of the observed mislocalizations, in retinocentric areas at intermediate levels of the visual hierarchy, that is, at the levels of V4, TEO, V3a, MT, and MST. Consistent with this prediction, observations in MT/MST (Krekelberg, Kubischik, Hoffmann, Bremmer, 2003) revealed that the decoding of the population response to peri-saccadic stimuli leads to a pattern resembling compression. Furthermore, since no significant compression has been observed in the case of “open-loop” pointing (Burr, Morrone, & Ross, 2001; Morrone, Ma-Wyatt, & Ross, 2005), the model predicts that areas that are rather participating in action than perception (e.g., Rizzolatti & Matelli, 2003) should receive at best weak oculomotor feedback and thus no or at least much less distortions of the population response should be observable.

### 2.2.7 Discussion

It was demonstrated that the model is able to sufficiently account for three essential aspects of compression, namely the spatial range, the time course, and the two-dimensional spatial pattern of compression. Thereby, compression in the model arises exclusively due to distortions of the population response in retinocentric visual maps.

However, besides these distortions caused by the oculomotor feedback, other factors might also influence the pattern of mislocalization. In the considered experiments (Morrone et al., 1997; Kaiser & Lappe, 2004) and in related work, subjects have to report the perceived position after the eye movement. Thus, they must take the saccade into account to avoid any systematic offset in their location estimate. This means that subjects have to rely on additional retinal or extraretinal information, such as the relative distance to other stimuli that can be used as visual references (McConkie & Currie, 1996; Currie, McConkie, Carlson-Radvansky, & Irwin, 2000; Deubel, Schneider, & Bridgeman, 2002) or an eye-position signal (Honda, 1990, 1991; Dassonville et al., 1992, 1995; Schlag & Schlag-Rey, 2002;

Pola, 2004; Binda, Bruno, Burr, & Morrone, 2007). Regarding the limits of this information, its usage allows to establish a stimulus location which is invariant of eye position. For the reported data, any additional systematic localization error that might arise due to such a transformation, however, seems to be small with respect to the localization error which, as predicted by the model, already arises in retinal coordinates prior to any transformation.

If compression is caused by distortions in retinocentric maps due to an oculomotor feedback signal, why is mislocalization in “total” darkness predominantly characterized by a uniform shift with only little evidence of compression (e.g., Matin & Pearce, 1965; Matin et al., 1969; Honda, 1989, 1991; Dassonville et al., 1992, 1995; Schlag & Schlag-Rey, 1995; Lappe, Awater, & Krekelberg; 2000)? While in principle under normal illuminated conditions the relative distance to additional visual information serving as references can be used for eye position-invariant localization, experiments in total darkness, that is, in the absence of such additional visual information, presumably require the use of an extraretinal eye-position signal. Although it appears well established that such a signal does not allow for a perfect compensation of the saccade induced retinal changes leading to the observed uniform mislocalization (Honda, 1990, 1991; Dassonville et al., 1992, 1995; Schlag & Schlag-Rey, 2002; Pola, 2004), the missing compression appears puzzling. Since there is no obvious reason to postulate the absence of the oculomotor feedback signal in total darkness, one would expect compression also to occur under these conditions. However, at least two factors are supposed to reduce or even diminish compression. Firstly, experiments in total darkness often require memory guided saccades or at least saccades with less visual guidance. In memory guided saccades and saccades that are made to the center of a homogeneous target, movement related neurons typically fire less vigorously (Edelman & Goldberg, 2001, 2003) and thus, the gain increase should be reduced. An indirect link between the activity of movement cells and the amount of peri-saccadic compression is also suggested by the correlation of compression with saccadic peak velocity (Ostendorf, Fischer, Finke, & Ploner, 2007), since the peak velocity depends on the activity of movement related cells (Waitzman, Ma, Optican, & Wurtz, 1991). Secondly, in the model the gain increase depends on the stimulus strength, consistent with the observation that the magnitude of compression decreases with increasing contrast (Michels & Lappe, 2004). Thus, the model predicts weak or diminished compression in total darkness if stimulus contrast is high. Although the exact type of gain function is still under debate (Williford & Maunsell, 2006), cell recordings in V4 and MT have indeed revealed that the gain enhancement due to covert shifts of space-based attention, that is, shifts of

space-based attention which are not immediately succeeded by a saccade, is limited for high contrast stimuli (Reynolds, Pasternak, & Desimone, 2000; Martinez-Trujillo & Treue, 2002). Furthermore, it is not clear whether the predicted oculomotor feedback signal is identical to the mechanism causing shifts of space-based attention in those experiments, but the mechanism of gain enhancement might be independent of the source of the modulatory signal. Thus, for low contrast stimuli the model predicts compression even in total darkness. This prediction is supported by a recent psychophysical study conducted in total darkness (Georg, Hamker, & Lappe, 2008) in which it has been demonstrated that peri-saccadic stimuli are compressed if their intensity, that is, their luminance is near-threshold. However, in contrast to experiments performed under illuminated conditions, the center of compression was not at the saccade target position, but was located farther in the direction of the saccade, resembling a superposition of compression and shift. This result seems to be consistent with a two step theory of peri-saccadic (mis)localization proposed by Awater and Lappe (2006), according to which the positions of peri-saccadic stimuli, in a first step, are encoded relatively to the saccade target in retinal coordinates and, in a second step, are transformed into exocentric coordinates. As in the present model, compression is already manifested in retinal coordinates, but its final form, that is, the subject's response depends on the transformation in the second step, which in the case of total darkness must rely on less accurate information, as compared to an illuminated condition where visual references are available. This results in an additional error.

Furthermore, the process of determining the position of a stimulus in eye-position invariant coordinates may also influence the mislocalization effects observed after saccadic adaptation, where it has been shown that peri-saccadic compression is directed to the adapted end-point of the saccade (Awater, Burr, Lappe, Morrone, Goldberg, 2005; Georg & Lappe, 2009), whereas the activity in the SC appears to encode the initial, unadapted saccade target (Frens & Van Opstal, 1997) (see however Hopp & Fuchs 2004; Takeichi, Kaneko, & Fuchs, 2007). There are two possibilities to explain the observed compression towards the adapted saccade end-point with the present model. Firstly, it may be possible that the pre-saccadic compression is directed to the unadapted target location in retinocentric maps and that it is subsequently shifted towards the post-saccadic gaze direction by adaptation specific spatial transformations. The latter is supported by observations of general shifts of perceived visual location induced by saccadic adaptation outside the time period of compression (Collins, Doré-Mazars, & Lappe, 2007). Secondly, in humans the feedback signal might indeed be pre-saccadically directed towards the adapted

saccade target. Evidence for this view is provided by observations of mandatory pre-saccadic allocation of attention towards the adapted saccade target after saccadic adaptation (Doré-Mazars, & Collins, 2005).

To summarize, while the observed compression presumably arises in retinal coordinates, the observed uniform shift in total darkness or in general, any additional error, might be the result of eye-position invariant transformations.

## 2.3 Peri-saccadic receptive field shifts

### 2.3.1 Introduction

Remember, the classical receptive field of a visual cell is defined as the region in visual space where a stimulus has to be presented to drive the cell. In retinocentric areas this region depends on the eyes' position. This means that the receptive field is fixed in retinal coordinates, but covers different parts of the visual space during different fixations of the eyes. At the time of the observed processing enhancement at the future fixation and the mislocalization of briefly presented visual stimuli, cells in several monkey visual areas transiently change the location and the extension of their receptive field, that is to say their receptive field profile is altered. According to the conception of predictive remapping (Duhamel, Colby, & Goldberg, 1992), a motor-related signal from the plan to move the eyes - known as corollary discharge - provides the visual system the necessary information to shift the receptive fields in retinocentric maps to the post-saccadic receptive field location (Sommer & Wurtz, 2006). This is extrapolated from the observation that even prior to saccade onset cells become responsive to stimuli presented in their so-called future receptive field (Figure 6b). This phenomenon has been observed in LIP (Duhamel, et al., 1992), the SC (Walker, Fitzgibbon, & Goldberg, 1995), the FEF (Umeno & Goldberg, 1997; Sommer & Wurtz, 2006), and even in earlier visual areas like V3 and V3a (Nakamura & Colby, 2002). Assuming that predictive remapping is uniform across the visual field and is a function of the saccade vector, this mechanism is suggested to provide sufficiently accurate spatial processing across saccades within the involved areas. Furthermore, it has explicitly been proposed to play a key role in the generation of visual stability (Sommer & Wurtz, 2006; Melcher & Colby, 2008; Wurtz, 2008), that is, our apparently stable percept of the world across saccades.

Measurements in monkey V4 have also revealed the change of receptive fields around the time of a saccade (Tolias, Moore, Smirnakis, Tehovnik, Siapas, & Schiller, 2001). Like the receptive field dynamics described above, these receptive field changes begin prior to saccade onset, but the spatial pattern is different. Instead of a

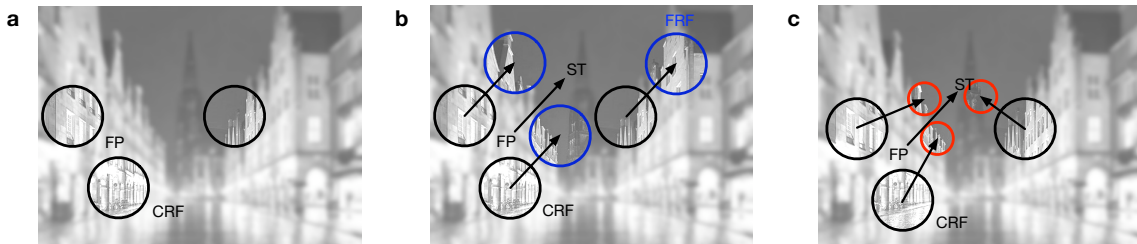


**Figure 6.** Illustration of the two observed receptive field dynamics. Three hypothetical example cells are shown in each panel. **(a)** The current receptive field (CRF), as measured during fixation long before a saccade, is plotted in black. FP denotes the current fixation point. **(b)** Predictive remapping. Before saccade onset cells become responsive to stimuli presented in their future receptive field (FRF) (blue). ST denotes the saccade target. **(c)** V4 receptive field dynamics. Before saccade onset receptive fields shrink and shift (red) towards the saccade target.

translation of the receptive fields parallel to the saccade, the overall effect consists of a shrinkage and shift of receptive fields towards the saccade target (Figure 6c). This suggests that just before the eye movement the region around the saccade target is already processed by a greater amount of finer tuned receptive fields in order to facilitate the processing of this region.

A simple conclusion drawn from these two apparently different observations could be that peri-saccadic receptive field dynamics in V4 are fundamentally different from those in the other areas as mentioned above. However, it will be demonstrated that both receptive field dynamics, namely predictive remapping and the observed V4 receptive field shifts, can be explained by the developed model of peri-saccadic processing. It will be shown that the feedback induced distortions of neural populations leading to the mislocalization of peri-saccadic stimuli cause peri-saccadic changes of receptive fields as well, which are consistent with both observed dynamics.

### 2.3.2 Mapping of model receptive fields

In order to analyze the receptive field dynamics predicted by the model, a systematic mapping of the receptive fields was performed in two conditions (Figure 7). In the first condition, which will be called the *fixation condition*, the current receptive fields were mapped. This mapping was done pre-saccadically long before saccade onset without any feedback. In the second condition, the mapping was done immediately before saccade onset when the feedback signal was strong. This condition will be called the *peri-saccadic condition*. For the mappings in both conditions the same model as outlined in Section 2.2.2 was used with the parameters obtained from the model’s fit to the experimental mislocalization data (see Section 5.2). Stimuli, in the following referred to as *probes*, were systematically presented in steps of  $4^\circ$  in visual space. For a given cell the obtained activity profile for each condition was then

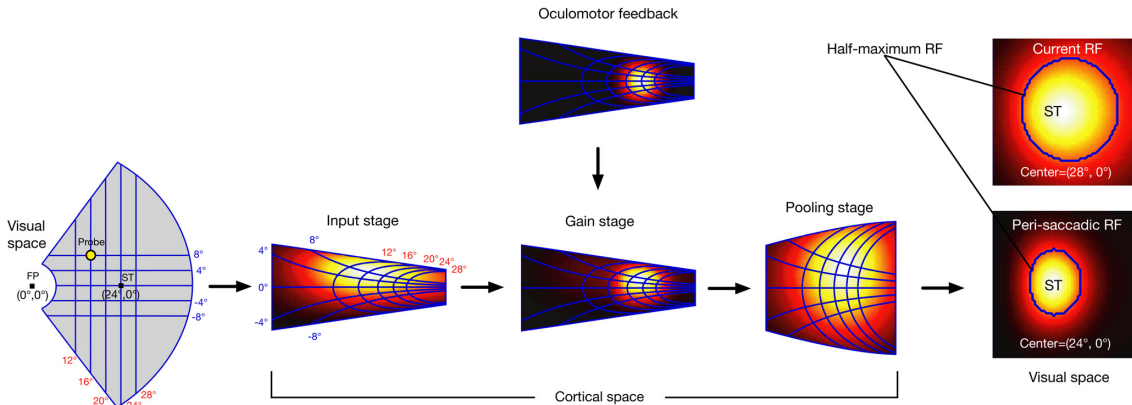


**Figure 7.** Model receptive fields were systematically mapped by presenting visual stimuli, in the following referred to as *probes*, at various positions in visual space in two conditions. In the first condition the mapping was done long before a saccade without any oculomotor feedback. This condition will be referred to as the *fixation condition* and the resulting receptive fields (RFs) will be referred to as *current receptive fields*. In the second condition the mapping was done immediately before saccade onset where the feedback is strong. This condition will be referred to as the *peri-saccadic condition* and the resulting receptive fields will be called *peri-saccadic receptive fields*. On the right, an example of the current (top) and the peri-saccadic receptive field (bottom) of a model cell is shown. The blue lines in each panel denote the half-maximum profile (see Text for detail) of the respective receptive field.

normalized and interpolated to a resolution of  $1^\circ \times 1^\circ$ . As in Tolia et al. (2001), the current and peri-saccadic receptive field of a given cell were then defined as the area in visual space where the activity exceeds half of the maximal activity of the cell in the fixation condition and in the peri-saccadic condition, respectively. As a result current and peri-saccadic receptive fields were obtained for all cells in the pooling stage of layer 1 and the input stage of layer 2 for all saccade amplitudes ( $12^\circ$ ,  $16^\circ$ ,  $20^\circ$ ,  $24^\circ$ ). Note receptive field dynamics in the model can only be observed after the first gain stage. Thus, the input stage of layer 1 does not possess any receptive field dynamics. Further note that an estimate of the feedback signal in the gain stage of layer 2 could be obtained from the available data only for the  $20^\circ$  saccade. Thus, for the pooling stage of layer 2 receptive fields were only mapped for the  $20^\circ$  saccade. Figure 8 shows six examples of current and peri-saccadic receptive fields in the two layers which consist of combinations of shift, shrinkage, and expansion. While cell 4 and cell 6 show a strong peri-saccadic shrinkage and shift towards the saccade target, cell 1 and cell 3 mainly show a shift and cell 2 and cell 5 an expansion of the peri-saccadic receptive field in the direction of the saccade. Thus, while cell 1, cell 3, cell 4, and cell 6 resemble the observed V4 receptive field dynamics, cell 2 and cell 5 seem to be consistent with predictive remapping. In the following the receptive field dynamics of the model will be described in detail with respect to both predictive remapping and saccade target shifts.

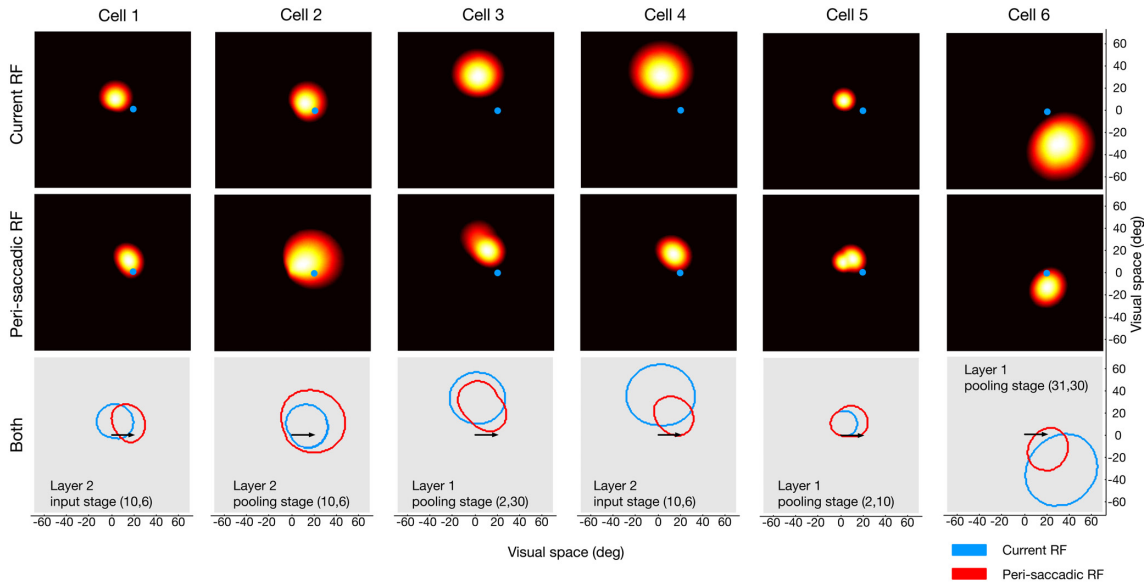


**Figure 8.** Current and peri-saccadic receptive fields (RFs) of six exemplary model cells for a rightward saccade of  $20^\circ$  as determined by a half-maximum threshold (Tolias et al., 2001). The continuous activity profiles, that is, the activity for probes which exceeds half of the maximal activity of each cell in the respective condition are shown in the upper panels (the blue dot denotes the saccade target). The corresponding half-maximum profiles, the layer of origin, and the location of the current receptive field centers in Cartesian  $(x, y)$  coordinates are shown in the lowermost panels. Arrows denote the saccade vector.

### 2.3.3 Changes in receptive field size

To assess the change in receptive field size for each cell, the half-maximum profile of the current receptive field was compared to the half-maximum profile of the peri-saccadic receptive field. The change of receptive field size  $s$  for each cell was obtained by

$$\Delta s_{\text{RF}} = 100 \frac{s_{\text{RF}}^{\text{peri}} - s_{\text{RF}}^{\text{fix}}}{s_{\text{RF}}^{\text{fix}}},$$

where  $s_{\text{RF}}^{\text{peri}}$  and  $s_{\text{RF}}^{\text{fix}}$  denote the half-maximum receptive field size of a given cell in the peri-saccadic condition and the fixation condition, respectively.

Figure 9 shows the amount of size change (shrinkage or expansion) of receptive fields in the peri-saccadic condition relative to the fixation condition for the four saccade amplitudes ( $12^\circ, 16^\circ, 20^\circ, 24^\circ$ ) together with examples of half-maximum profiles of typical cells for the pooling stage of layer 1. The general pattern is similar for the different saccade amplitudes. In the region right to and above the saccade target, cells with current receptive field centers relative close to the saccade target have smaller receptive fields (blue regions) in the peri-saccadic case while cells farther away show an expansion of their receptive fields (red regions). Thereby,

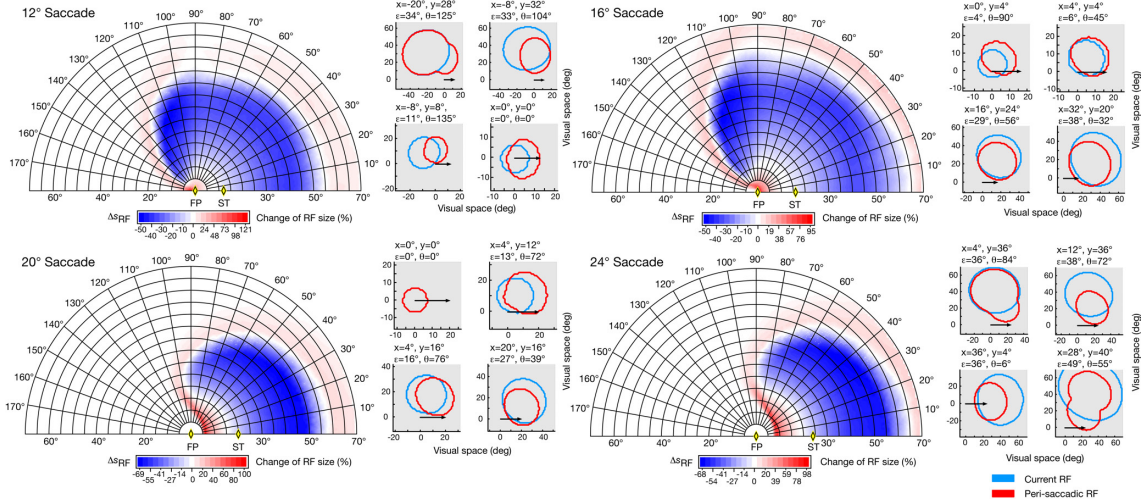


**Figure 9.** Changes in the size of peri-saccadic receptive fields ( $\Delta s_{RF}$ ) in the pooling stage of layer 1 shown as a function of the current receptive fields center in visual space displayed together with representative half-maximum receptive field profiles. Note only the results of the upper part of the visual space are shown. However, the results of the lower part of visual space are identical for all reported simulations (see Figure 12 and 13). An expansion of receptive fields is indicated in red and a shrinkage of receptive fields is indicated in blue. Fixation and peri-saccadic half-maximum profiles are shown in light blue and red, respectively. The center of the current receptive field is given in Cartesian  $(x, y)$  and Polar  $(\epsilon, \theta)$  coordinates. Yellow diamonds indicate the fixation point (FP) and the saccade target (ST).

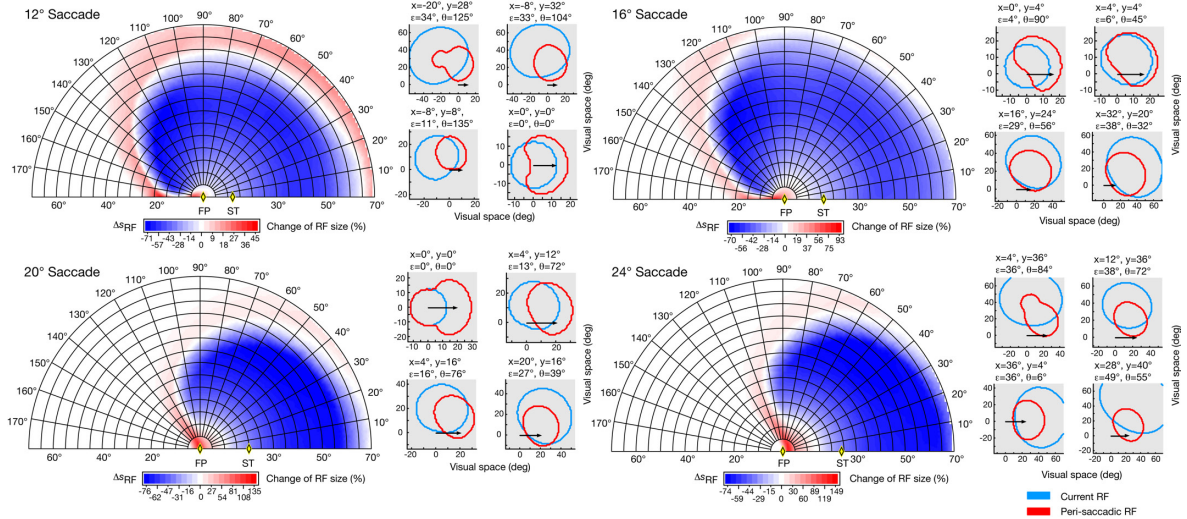


**Figure 10.** Changes in the size of peri-saccadic receptive fields ( $\Delta s_{RF}$ ) in the input stage of layer 2 shown as a function of the current receptive field center in visual space displayed together with representative half-maximum receptive field profiles. Same notation as in Figure 9.

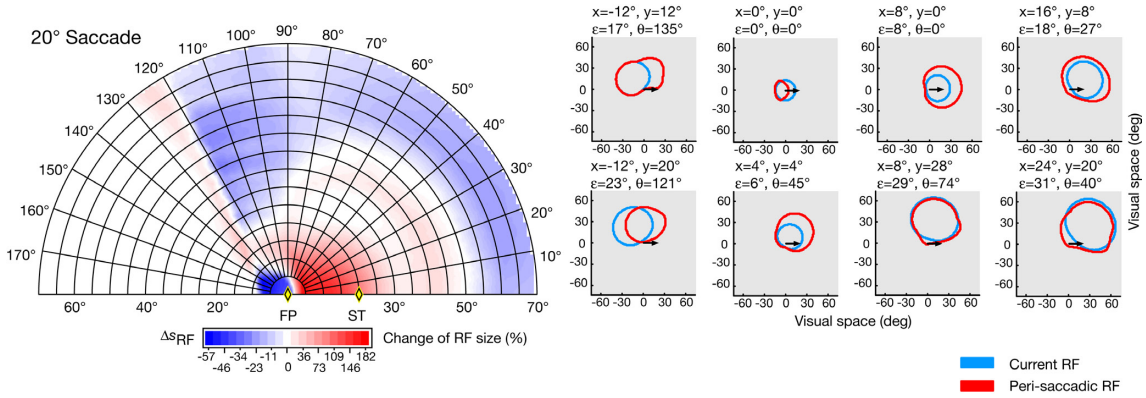


**Figure 11.** Changes in the size of peri-saccadic receptive fields ( $\Delta s_{RF}$ ) in the pooling stage of layer 2 shown as a function of the current receptive field center in visual space displayed together with representative half-maximum receptive field profiles. An expansion of receptive fields is indicated in red and a shrinkage of receptive fields is indicated in blue. Fixation and peri-saccadic half-maximum profiles are shown in light blue and red, respectively. The center of the current receptive fields is given in Cartesian  $(x, y)$  and Polar  $(\epsilon, \theta)$  coordinates. Yellow diamonds indicate the fixation point (FP) and the saccade target (ST).

for all saccade amplitudes the expansion is largest for cells with current receptive field centers located around the region of the fixation point. Between these cells showing expansion and shrinkage, there are cells which do not alter in receptive field size (enclosed white regions) but nevertheless show a translation (e.g., see the cell with its current receptive field center at  $x = 4^\circ$  and  $y = 16^\circ$  during a  $20^\circ$  saccade). The majority of cells with current receptive field centers located in the opposite hemisphere relative to the saccade target location do not show any change in their receptive field profile. This is more prominent for the  $20^\circ$  and  $24^\circ$  saccade than for the  $12^\circ$  and the  $16^\circ$  saccade and is a function of the current receptive field center relative to the saccade target, the current receptive field size and the saccade amplitude. For example, the receptive field size of cells with their current receptive field centers located close to the fixation point is too small to be affected by the feedback signal of the  $20^\circ$  and  $24^\circ$  saccade. However, for the  $12^\circ$  and  $16^\circ$  saccade the same cells are sufficiently close to the feedback signal. As a consequence their receptive field properties are altered. In general, irrespective of shrinkage or expansion, the resulting receptive field dynamics lead to peri-saccadic half-maximum profiles which are located closer to the saccade target in comparison to their current receptive field profiles of the fixation condition (please also refer to the shift direction and amplitude of the continuous remapping test in Section 2.3.7). As it can be seen in Figure 10 the overall results of the input stage of layer 2 are essentially the same as for the pooling stage of layer 1, with the main difference that the area in visual space where the peri-saccadic half-maximum profile is affected by the feedback signal

is larger for the input stage in layer 2 than for the pooling stage of layer 1 (e.g., compare the cell with its current receptive field at  $x = 0^\circ$  and  $y = 0^\circ$  during a  $20^\circ$  saccade for both stages). The similarity between both stages is not surprising since the input stage of layer 2 has larger (current) receptive fields than the pooling stage of layer 1 and is driven by the population activity of the former without the impact of an additional gain stage, which is, however, the case for the pooling stage of layer 2 (Figure 11). Here, the area of visual space between the fixation point and the saccade target is characterized by large expansions of peri-saccadic receptive field profiles (up to 182 %), which is due to the broad feedback signal in layer 2 (see Figure 32 in Section 5.1.5). The expansion is strongly reduced for regions farther to the right of the saccade target. In the right hemifield for eccentricities larger than  $55^\circ$ , the change in the peri-saccadic receptive fields consists of shrinkage, which is largest for peri-saccadic receptive fields with their current receptive field center located left to the fixation point.

#### 2.3.4 Changes in the number of responsive cells

To assess the overall effect of the changes of the peri-saccadic receptive field size together with the shift of the peri-saccadic receptive fields, that is, the region of visual space that is covered by the peri-saccadic half-maximum profile as compared to the current half-maximum profile, the number of cells which respond effectively to a probe of a certain location was compared between the fixation and the peri-saccadic condition as follows. For a given probe location in visual space the number of cells whose responses exceeded the half of the maximum activity of the respective cell, in the following referred to as *responsive cell*, was computed for the fixation condition and the peri-saccadic condition. Figure 12 summarizes the results normalized for each panel. Figure 12a shows the number of responsive cells in the fixation condition for the pooling stage of layer 1, the input stage of layer 2, and the pooling stage of layer 2 from top to bottom. Due to smaller receptive fields the central region consisting of a high number of responsive cells (white and yellow) is smaller for layer 1 than for layer 2. Figure 12b shows the number of responsive cells in the peri-saccadic condition. For all saccade amplitudes ( $12^\circ$ ,  $16^\circ$ ,  $20^\circ$ , and  $24^\circ$  rightwards) the number of responsive cells increases at the saccade target and nearby regions for the pooling stage of layer 1 and the input stage of layer 2, reflecting the shape of the feedback signal in layer 1 (see Figure 34 in Section 5.2).

Because of the larger receptive fields of the input stage of layer 2 the effect is more pronounced in this stage as compared to the pooling stage of layer 1. Due to the broader feedback signal in layer 2, the increase of responsive cells in the

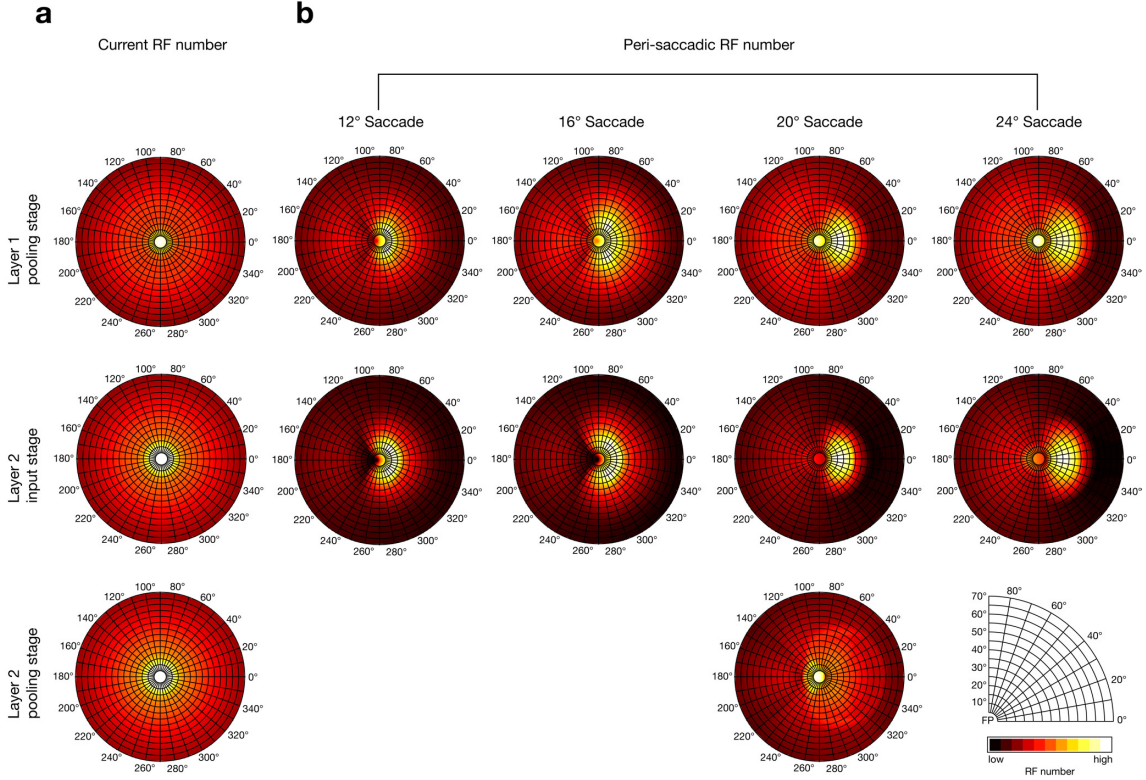


**Figure 12.** Distributions of the number of responsive cells as a function of probe position in visual space. (a) From top to bottom, distributions for the pooling stage of layer 1, the input stage of layer 2, and the pooling stage of layer 2 as obtained from the fixation condition. (b) From top to bottom, distributions for the pooling stage of layer 1, the input stage of layer 2, and the pooling stage of layer 2 as obtained from the peri-saccadic condition for four saccade amplitudes (12°, 16°, 20°, and 24°) are shown. The saccade was always directed to the right with the fixation point (FP) located in the center of each panel. White and yellow colors indicate high numbers of responsive cells.

pooling stage of layer 2 is more modest and spatially uniform. These distributions of the fixation condition and the peri-saccadic condition were then used to compute the peri-saccadic change in the number of responsive cells as a function of spatial location.

$$\Delta n_{\text{RF}} = 100 \frac{n_{\text{RF}}^{\text{peri}} - n_{\text{RF}}^{\text{fix}}}{n_{\text{RF}}^{\text{fix}}},$$

where  $n_{\text{RF}}^{\text{peri}}$  and  $n_{\text{RF}}^{\text{fix}}$  denote the number of responsive cells for a given location in visual space in the peri-saccadic condition and the fixation condition, respectively. The resulting changes are summarized in Figure 13. For the pooling stage of layer 1 and the input stage of layer 2 the number of responsive cells increases (red) at the saccade target and at nearby regions (up to 127 % for the pooling stage of layer 1 and up to 221 % in the input stage of layer 2) and decreases (blue) at surrounding

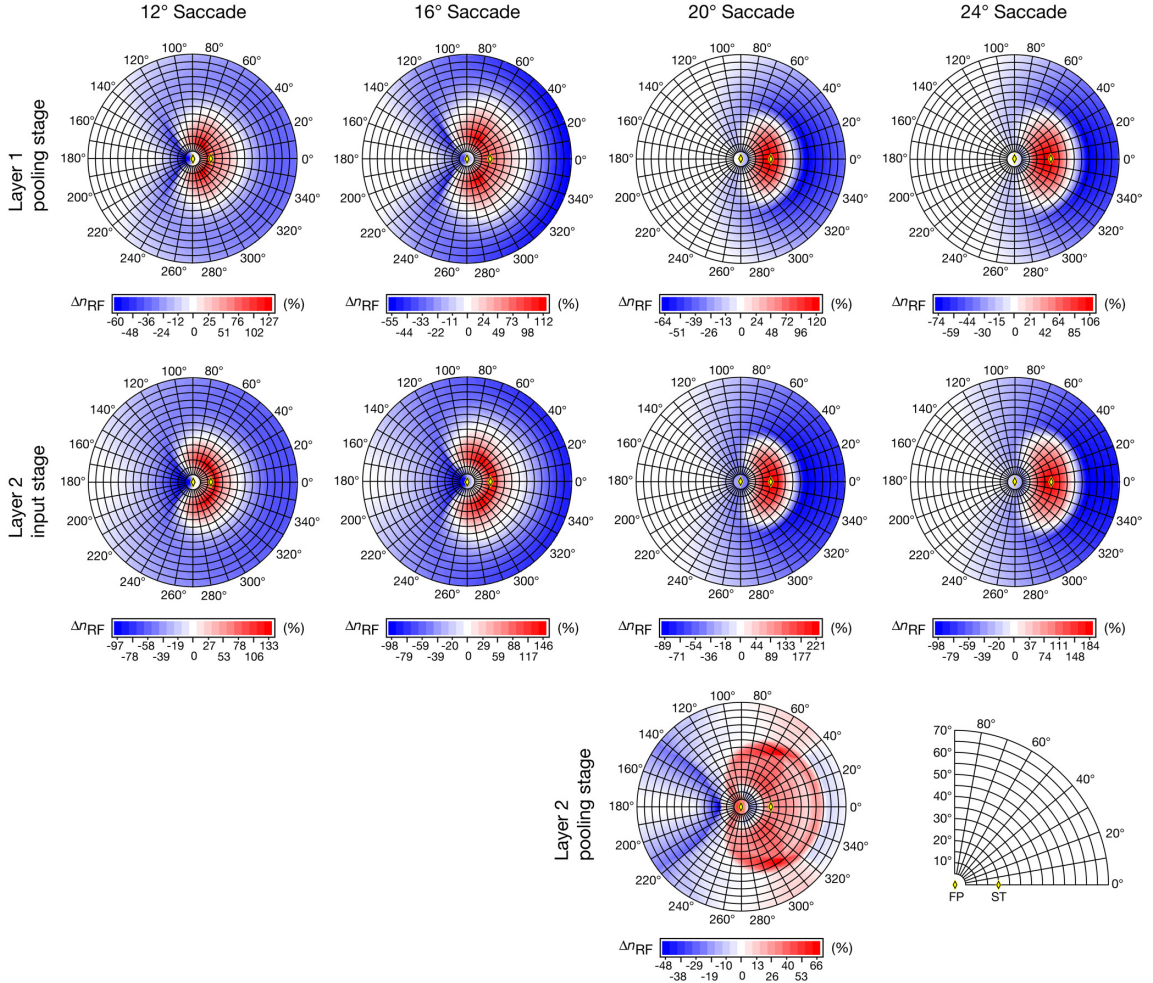


**Figure 13.** Distributions of the peri-saccadic change in number of responsive cells ( $\Delta n_{RF}$ ) as a function of probe position in visual space. From top to bottom, distributions for the pooling stage of layer 1, the input stage of layer 2, and the pooling stage of layer 2 for four saccade amplitudes  $12^\circ$ ,  $16^\circ$ ,  $20^\circ$ , and  $24^\circ$  are shown. The saccade was always directed to the right. Yellow diamonds indicate the fixation point (FP) and the saccade target (ST). An increase in the number of responsive cells is indicated in red and a decrease in blue.

positions (down to  $-74\%$  for the pooling stage of layer 1 and down to  $-98\%$  in the input stage of layer 2) for all saccade amplitudes. The pooling stage of layer 2 shows a more slightly increase (up to  $66\%$ ) for a large part of the right hemisphere around the saccade target and a decrease (down to  $-48\%$  in the left hemisphere). Thus, in terms of the number of responsive cells the processing capacity is enhanced in the peri-saccadic condition (more focused in the pooling stage of layer 1 and the input stage of layer 2 and less focused in the pooling stage of layer 2) at the saccade target region with the cost of a decreased processing capacity at surrounding regions.

### 2.3.5 One-probe remapping test

Although it was already demonstrated that the overall effect of receptive field changes in the model lead to an enhanced processing capacity in terms of the number of responsive cells at the saccade target region, it was also shown that some cells rather shift or expand their receptive field parallel to the saccade vector than directly towards the saccade target. Thus, in order to systematically differentiate between cells which seem to be consistent with predictive remapping and cells which seem to be consistent with the observed V4 dynamics, three tests were applied.

The first test is the most common method in the literature (Duhamel et al., 1992; Walker et al., 1995; Umeno & Goldberg, 1997; Nakamura & Colby, 2002). It consists of placing one probe in the center of the future receptive field of a given cell (Figure 14a), whereupon the future receptive field is the region in visual space where the current receptive field will be located after the eye movement. If the cell gets activated by the probe either before the eye movement or with a latency which is shorter than the latency that would be expected for the current receptive field, it will be classified as a predictive remapping cell. Note that the exact latency criterion used in the remapping studies requires that the latency of a neurons response relative to saccade onset to a probe in the future receptive field must be shorter than the latency relative to the onset of a probe in the current receptive field in a fixation task. In the model, all reported receptive fields were measured before saccade onset. In the following this test will be referred to as the *one-probe test*. Note that in the electrophysiological studies, usually cells are selected which do not respond above baseline to a probe presented in the future receptive field during the fixation task. The response of such a cell to a probe in the future receptive field during the saccade task has to be significantly different from baseline activity to be considered as a remapping cell. Since the model is noiseless, this statistical procedure cannot directly be applied. A cell was labeled as a remapping cell in the one-probe test if the activity to a probe in the future receptive field during the saccade task, that is the peri-saccadic condition, increased at least by five percent relative to the maximum activity in the fixation condition.

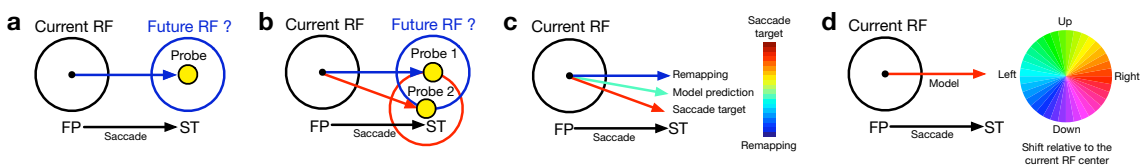


**Figure 14.** Illustration of the applied tests and measures. (a) One-probe test. (b) Two-probe test. (c) Continuous remapping test. (d) Shift direction of the maximum activity increase of the peri-saccadic RF at  $p_{max}$  relative to the CRF center.

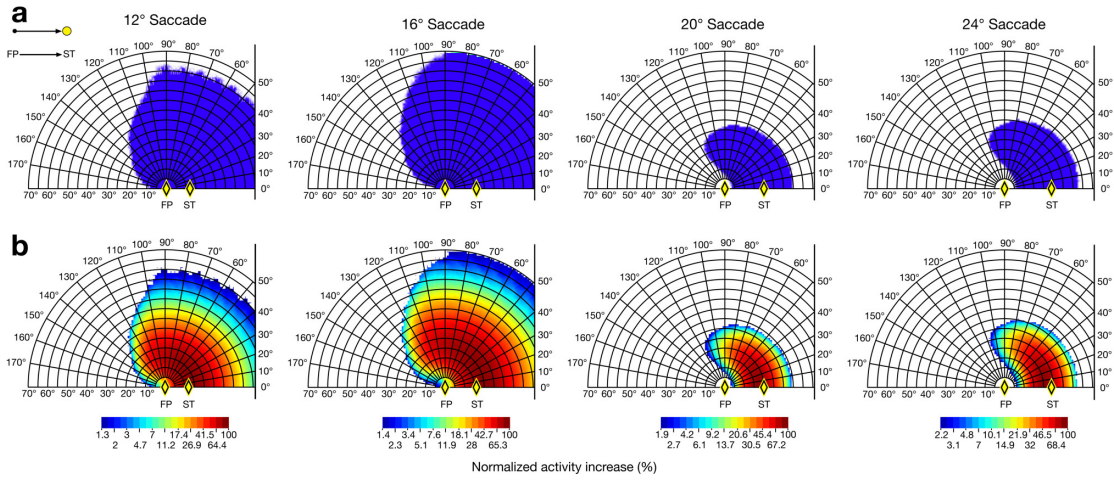


**Figure 15.** Results of the one-probe test for the pooling stage of layer 1. (a) The blue area consists of the positions of current receptive field centers in visual space where cells are classified as predictive remapping cells. (b) Peri-saccadic activity increase shown as a function of the current receptive field center in visual space. Yellow diamonds indicate the fixation point (FP) and the saccade target (ST).

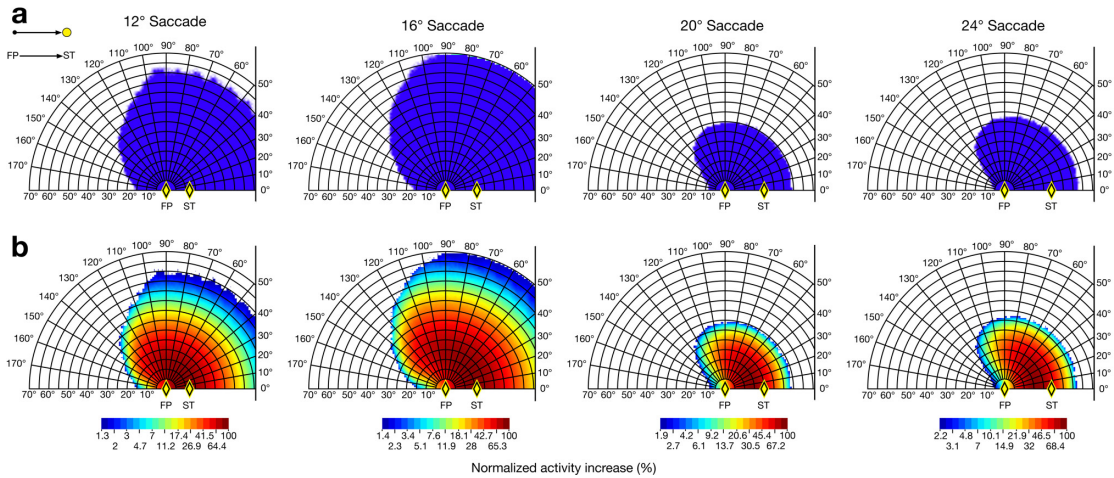


**Figure 16.** Results of the one-probe test for the input stage of layer 2. Same notation as in Figure 15.

The results of the one-probe test for the pooling stage of layer 1 are shown in Figure 15. The blue area in Figure 15a denotes the region where cells are classified as remapping cells. Again, the results for the 12° and the 16° saccade and the results for the 20° and the 24° saccade are very similar. Further, as outlined above, the area where cells are affected by the feedback signal is larger for the 12° and the 16° saccade. The increase of the activity of a given cell is shown in Figure 15b. Note that the activity increase was normalized for each condition, that is each saccade amplitude. In general, cells which are close to the center of the feedback signal, that is the saccade target, show the largest increase in activity. Thereby the observed

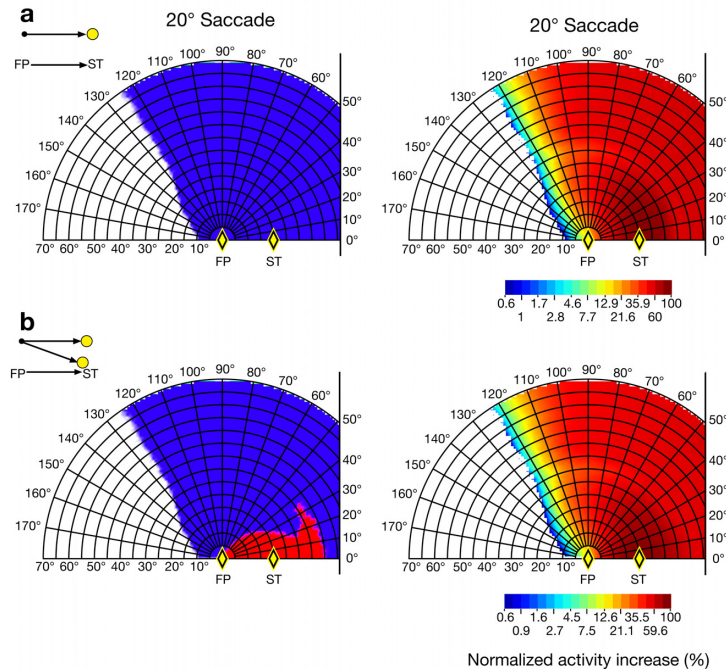


**Figure 17.** Results of the one-probe test and the two-probe test of the pooling stage of layer 2. (a) The blue area consists of the positions of current receptive field centers in visual space where cells are classified as predictive remapping cells. (b) Peri-saccadic activity increase shown as a function of the current receptive field center in visual space. Yellow diamonds indicate the fixation point (FP) and the saccade target (ST).

pattern closely resembles the shape of the feedback signal in visual space. Figure 16 shows the results for the input stage of layer 2. As for the results of the change in the size of receptive fields (Section 2.3.3), the results of the one-probe test for the input stage of layer 2 are essentially the same as for the pooling stage of layer 1. The main difference is that the region in visual space where cells are affected by the feedback signal is larger for the former due to the larger receptive fields in this stage. Figure 17a shows the results for the one-probe test for the pooling stage of layer 2 for the 20° saccade. Due to the additional broader feedback signal in layer 2, the area in visual space where cells are classified as remapping cells is much larger as compared to the pooling stage of layer 1 and the input stage of layer 2.

### 2.3.6 Two-probe remapping test

The second test was introduced by Sommer & Wurtz (2006) and was designed to differentiate between remapping and the V4 receptive field dynamics. Two probes are used. As in the one-probe test, the first probe is presented in the center of the future receptive field. The second probe is placed close to the saccade target (Figure 14b), in order to test for receptive field shifts towards the saccade target. If

the receptive field translates parallel to the saccade, the first probe should evoke a stronger activation of a neuron than the second probe. If the receptive field shifts towards the saccade target, the second probe should evoke a stronger activation of a neuron than the first probe. This test will be referred to as the *two-probe test*. In the model the activity increase of a cell to a probe in the future receptive field was compared to the activity increase to a probe presented closer to the saccade target, that is, to a probe which was placed at the endpoint of a vector pointing directly towards the saccade target. The origin of this vector is equal to the center of the current receptive field and its length is equal to the saccade amplitude. If the distance between the current receptive field center and the saccade target was shorter than the saccade amplitude, the probe was presented directly at the saccade target location. As in the one-probe test, to be considered as a significant change, a probe had to cause at least an activity increase of five percent relative to the maximum activity in the fixation condition. If the activity increase to a probe in the future receptive field was higher than the activity increase to a probe presented closer to the saccade target, it was classified as a remapping cell.

The results of the two-probe test for the pooling stage of layer 1 are shown in Figure 18. Again, the results for the 12° and the 16° saccade and the results for the 20° and the 24° saccade are very similar. The blue area denotes the region in which cells show a higher response to a probe presented in the future receptive field than to a probe presented closer to the saccade target. It becomes obvious that the region where cells are classified as remapping cells is roughly the same for all saccadic amplitudes, that is cells with their current receptive field centers located above the fixation point. Thus, the majority of receptive field positions which are classified as remapping cells according to the one-probe test do not pass the more sophisticated two-probe test. However, the remaining regions of remapping cells seem to be consistent with the location of the current receptive field of remapping cells as reported in the literature. Figure 18b shows the normalized increase of the activity of a given cell. The results are qualitatively the same as for the one-probe test (see above). Note that the activity increase is shown for the probe eliciting the higher response. That is, for remapping cells (blue region in Figure 18a) the activity increase depends on the probe which was presented in the future receptive field. For the rest of the cells (red region in Figure 18a) the activity increase depends on the probe which was presented closer to the saccade target. Figure 19 shows the results for the input stage of layer 2. Again, the results for this stage and the pooling stage of layer 1 are essentially the same. Figure 17b shows the results of the two-probe test for the pooling stage of layer 2. Here, the area of visual space where cells pass

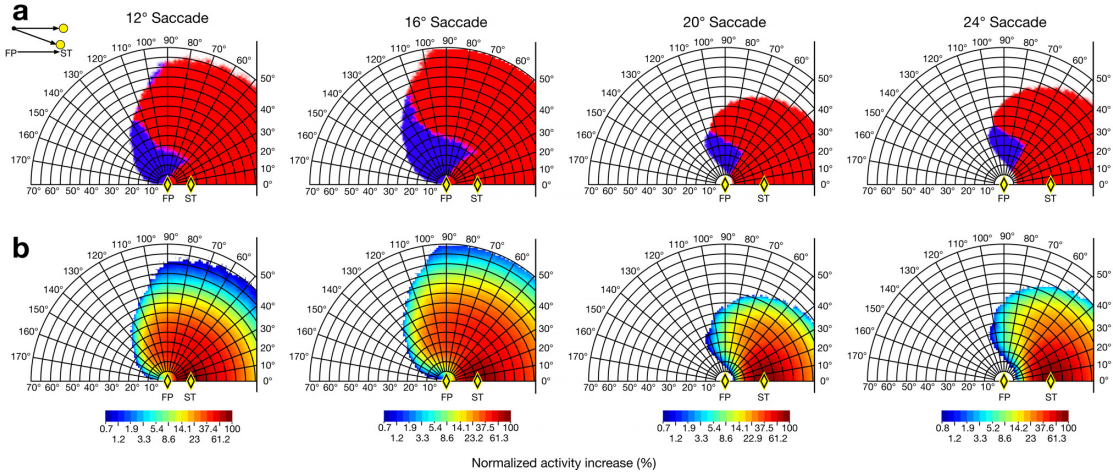


**Figure 18.** Results of the two-probe test for the pooling stage of layer 1. (a) The blue area consists of positions of current receptive field centers in visual space where cells are classified as predictive remapping cells. The red area consists of the positions of current receptive field centers in visual space where cells respond stronger to the probe which is presented closer to the saccade target. (b) Peri-saccadic activity increase shown as a function of the current receptive field center in visual space. Yellow diamonds indicate the fixation point (FP) and the saccade target (ST).

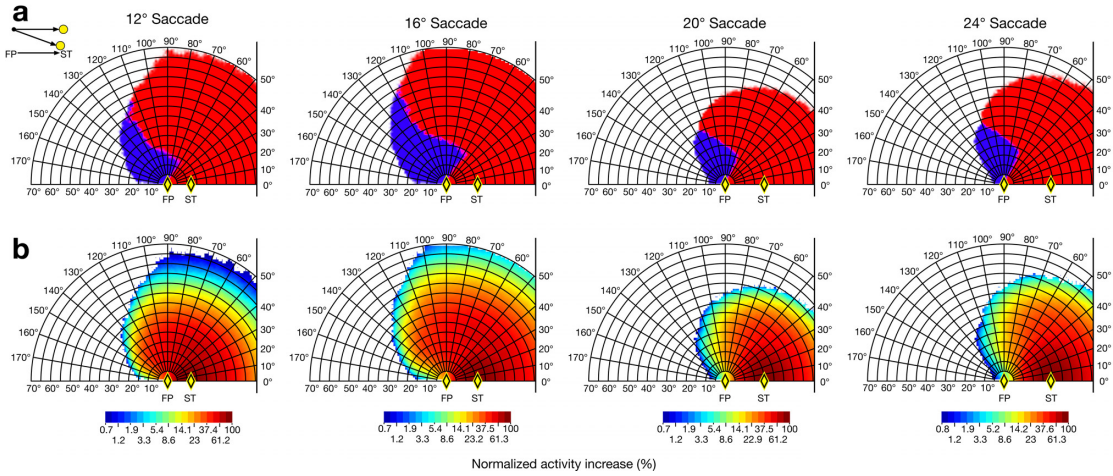


**Figure 19.** Results of the two-probe test for the input stage of layer 2. Same notation as in Figure 18.

the two-probe remapping test, that is, the area (blue) where cells are still classified as remapping cells after the test, is much larger as compared to the pooling stage of layer 1 and the input stage of layer 2. The area in visual space where cells respond stronger to the probe which is presented closer to the saccade target is restricted to a relative small region between the fixation point and the wider saccade target area.

### 2.3.7 Continuous remapping test

The above described procedures for receptive field mapping in the model match the typical procedures used in electrophysiological experiments as closely as possible. However, with the model it is also possible to use procedures that cannot reasonably be performed in electrophysiological experiments due to time or method restrictions. Although such procedures do not allow a direct comparison to physiological data, they can be very useful to illustrate the mechanism at work. Therefore, an additional remapping test was included. For each cell the position  $p_{max}$  in visual space was determined where the increase of the peri-saccadic receptive field as compared to the fixation receptive field is maximal

$$p_{max} = \arg \max_{p_i} (r^{\text{peri}}(p_i) - r^{\text{fix}}(p_i)),$$

where  $r^{\text{peri}}$  and  $r^{\text{fix}}$  denote the activity for a given cell to a probe presented at position  $p_i$  for the peri-saccadic and the fixation condition, respectively. To be considered as a significant shift, the maximum activity increase  $p_{max}$  had to be at least five percent of the maximum activity in the fixation condition, equal to the one- and two-probe tests described above. Then a displacement vector  $\mathbf{v}$  was computed with the current receptive field center as origin and  $p_{max}$  as endpoint. When the magnitude of this vector was greater than  $1^\circ$ , the direction  $\phi_v$  of  $\mathbf{v}$  was compared to the direction predicted by remapping  $\phi_R$  and to the direction pointing directly towards the saccade target  $\phi_{ST}$ . That is, the minimal angle  $\phi_{min}$  between  $\phi_v$  and  $\phi_R$ , and between  $\phi_v$  and  $\phi_{ST}$  was determined with

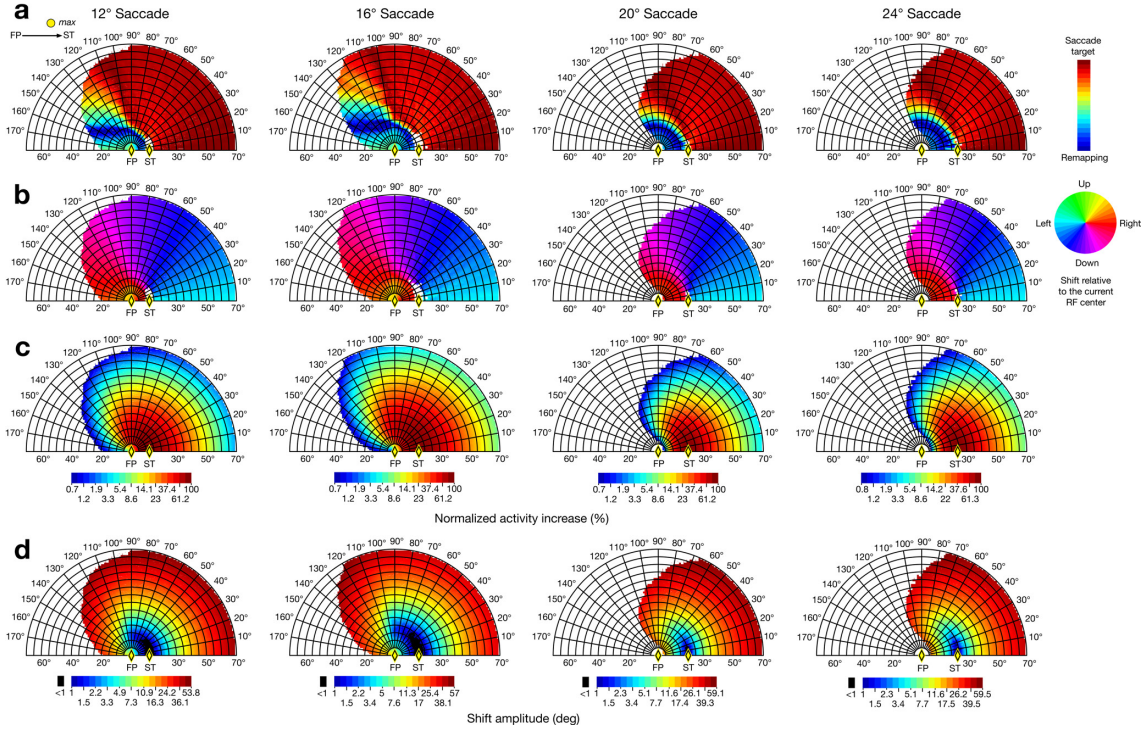
$$\phi_{min} = f(\phi_1, \phi_2) = \begin{cases} 2\pi - |\phi_1 - \phi_2| & \text{if } |\phi_1 - \phi_2| > \pi \\ |\phi_1 - \phi_2| & \text{else} \end{cases}.$$

These angles were then used to compute a shift index

$$S = \frac{f(\phi_v, \phi_R)}{f(\phi_v, \phi_R) + f(\phi_v, \phi_{ST})},$$

where  $S \in [0, 1]$  indicates the relative similarity between  $\phi_v$  and  $\phi_{ST}$ , respectively the similarity between  $\phi_v$  and  $\phi_R$ , with  $S = 1$  if  $\phi_v = \phi_{ST}$  and  $S = 0$  if  $\phi_v = \phi_R$  (Figure 14c).

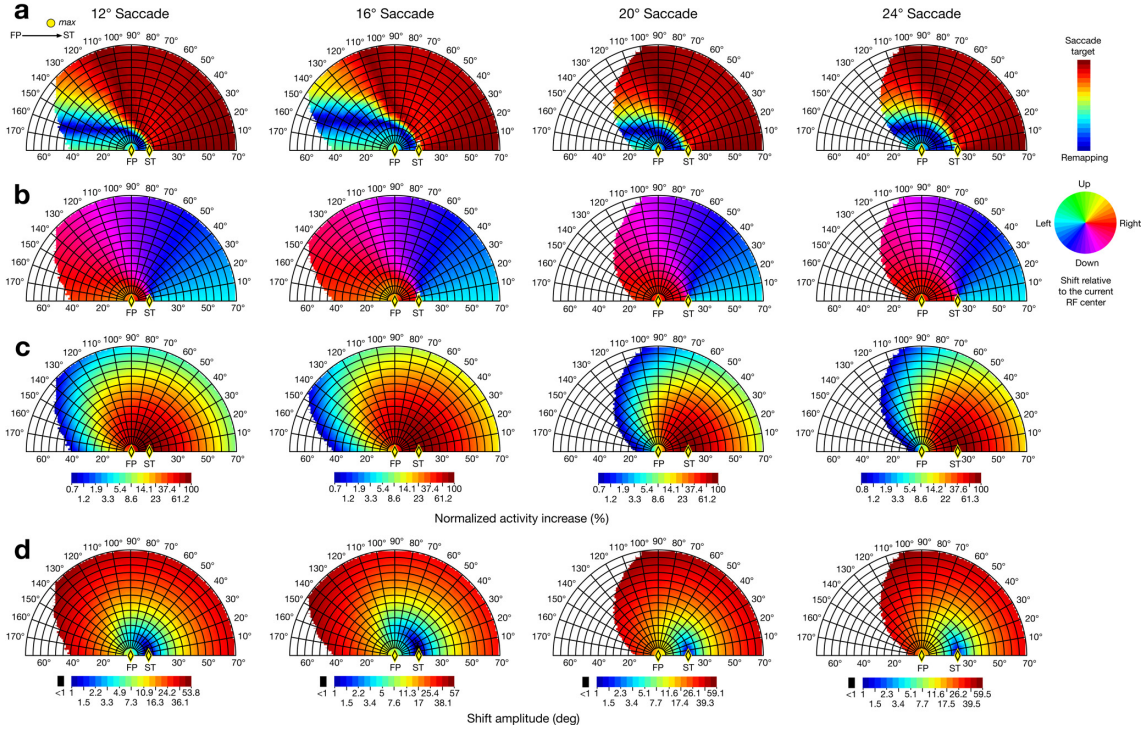
Figure 20 shows the results of the continuous remapping test for the pooling stage of layer 1. As for the two-probe test, cells with a displacement direction close to the predicted remapping direction (dark blue regions in Figure 20a) are located above the fixation point. In general, due to the different test condition (see Section 2.3.6)



**Figure 20.** Results of the continuous remapping test for the pooling stage of layer 1. (a) Visualization of the shift index  $S$ . (b) Shift direction of the maximum activity increase of the peri-saccadic receptive field relative to its current receptive field center. (c) Maximum peri-saccadic activity increase. (d) Shift magnitude of the maximum peri-saccadic activity increase. All measures are shown as a function of the current receptive field center in visual space. Yellow diamonds indicate the fixation point (FP) and the saccade target (ST).

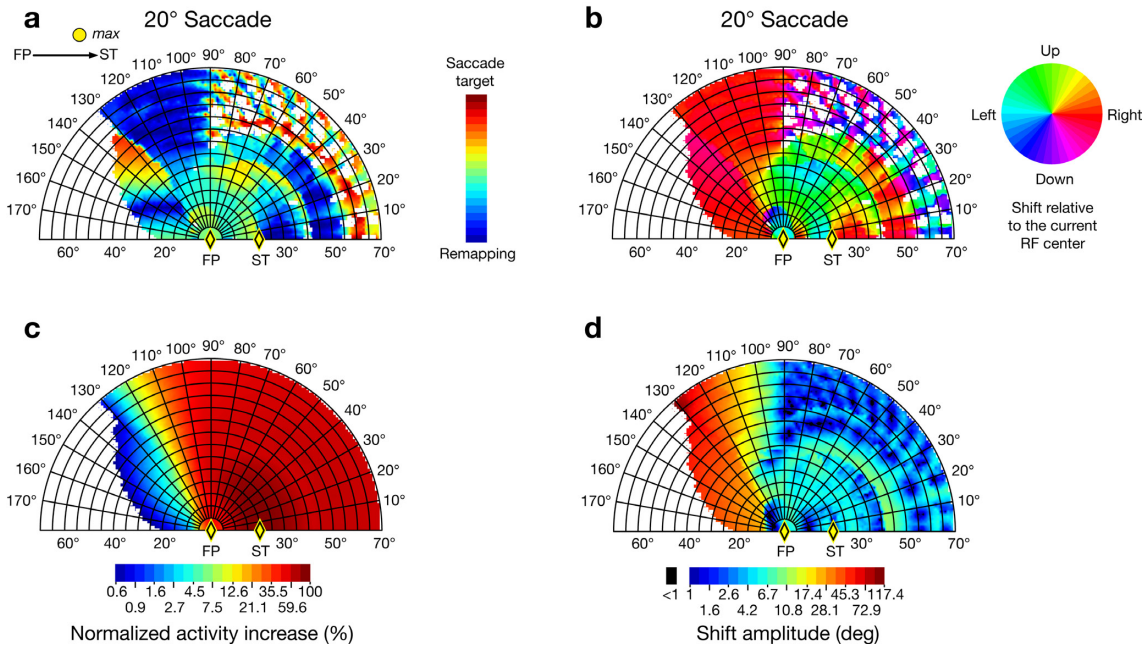
the area of remapping cells is larger for the continuous test as compared to the two-probe test, which is especially true for the 20° and the 24° saccade. Yellow and light blue regions denote current receptive field centers for which the displacement direction lies in between the predicted remapping direction and the direction of a displacement towards the saccade target, whereas red regions denote a displacement direction pointing close towards the saccade target.

Figure 20b shows the displacement directions relative to the current receptive field center (see also Figure 14d). As can be seen for the 12° and the 16° saccade for some cell positions close to the fixation point the displacement is actually directed more upwards (denoted in yellow) than expected by a predictive remapping displacement. Figure 20c shows the maximum normalized increase of the activity of a given cell. The results are qualitatively the same as for the one-probe and the two-probe test. The increase is highest for cells with current receptive field centers located close to the saccade target. Figure 20d shows the magnitude of the displacement. Although there are regions where cells show a displacement direction consistent with predictive remapping (Figure 20a), the amplitudes of the shifts in these regions



**Figure 21.** Results of the continuous remapping test for the input stage of layer 2. (a) Visualization of the shift index  $S$ . (b) Shift direction of the maximum activity increase of the peri-saccadic receptive field relative to its current receptive field center. (c) Maximum peri-saccadic activity increase. (d) Shift magnitude of the maximum peri-saccadic activity increase. All measures are shown as a function of the current receptive field center in visual space. Yellow diamonds indicate the fixation point (FP) and the saccade target (ST).

show larger variations as compared to a stringent remapping conception. Often the amplitudes are either smaller or larger than the saccade vector. Furthermore, cells with their current receptive field centers located close to the saccade target do not show a significant shift ( $> 1^\circ$ ) at all. Figure 21 shows the results of the continuous remapping test for the input stage of layer 2. With the exception of the larger region in visual space where cells are affected by the feedback signal, the results are essentially the same as for the pooling stage of layer 1. Figure 22 shows the results of the continuous remapping test for the pooling stage of layer 2. Here, in contrast to the results of the pooling stage of layer 1 and the input stage of layer 2 topography, that is, a transition of remapping towards saccade target shifts depending on the position of cells in visual space, is much coarser. As Figure 22a shows, a large part of the upper left hemisphere, with an eccentricity larger than  $40^\circ$ , consists of cells which are close to remapping, while less eccentric parts lie somewhere in between remapping and saccade target shifts, while a relative small part left to the fixation point again shows remapping. In the right hemisphere remapping regions can be observed right to the saccade target. At an eccentricity of  $60^\circ$  small patches



**Figure 22.** Results of the continuous remapping test for the pooling stage of layer 2. (a) Visualization of the shift index  $S$ . (b) Shift direction of the maximum activity increase of the peri-saccadic receptive field relative to its current receptive field center. (c) Maximum peri-saccadic activity increase. (d) Shift magnitude of the maximum peri-saccadic activity increase. All measures are shown as a function of the current receptive field center in visual space. Yellow diamonds indicate the fixation point (FP) and the saccade target (ST).

are localized which consist of saccade target shifts. For larger eccentricities the index lies again somewhere in between remapping and saccade target shifts. Figure 22b reflects this complexity in terms of the displacement direction relative to the current receptive field center. Most remarkably, cells with their current receptive field center located in the region above the fixation point and the saccade target show an upwards shift of the maximal increase of the peri-saccadic receptive field. Figure 22c shows the normalized activity increase which is largest in the right hemisphere with the maximum at the saccade target region. Figure 22d shows the magnitude of the displacement. Again for the greater amount of regions where cells show a displacement direction consistent with predictive remapping, the magnitude of the shift is either too large (left hemisphere) or too small (right hemisphere) as compared to a stringent remapping conception.

### 2.3.8 Discussion

In the previous sections the receptive field dynamics predicted by the model were illustrated in detail in order to compare them to the known peri-saccadic receptive field dynamics, that is, predictive remapping and saccade target shifts. As the results

show, the model is able to explain a wide spectrum of receptive field dynamics. They consist of combinations of shrinkages, expansions and shifts, which can in principle reproduce both the observed V4 dynamics and the receptive field effects of predictive remapping, providing a proof of concept. However, the exact pattern of the simulated model dynamics depends on a number of factors such as the center of the current receptive field, the size of the current receptive field, the size of the feedback signal, and the saccade amplitude, confining the occurrence of particular types of receptive field dynamics to restricted regions of the visual field. Therefore, it is suggested that the understanding of the receptive field dynamics of cells in the mentioned areas (V4, V3, V3a, LIP, FEF, SC) of the visual system might benefit from an analysis that takes the position and size of the current receptive field center in visual space systematically into account. Such an analysis may reveal whether the experimentally observed receptive field dynamics might indeed be caused by the same mechanism as it is implemented in the model.

Further, the simulations suggest that the one-probe test which is used in most of the remapping studies (Duhamel et al., 1992; Walker et al., 1995; Umeno & Goldberg, 1997; Nakamura & Colby, 2002) cannot fully discriminate between predictive remapping and saccade target shifts. Many model cells that were classified as remapping cells according to the one-probe test did not pass the more sophisticated two-probe test. The two-probe test restricted the areas consistent with predictive remapping to a relatively small part of the visual space around the fixation point, which seems to correspond to areas where the current receptive field of cells in the above mentioned studies were located. Thus, the one-probe test in general might indicate whether a tested cell gets more responsive to a probe presented in its future receptive field, but it does not provide strong evidence for predictive remapping.

By assuming that the model is true, several implications may be discussed. As the results of the pooling stage of layer 1 and the input stage of layer 2 suggest, the most obvious implication is that instead of representing a global phenomenon, predictive remapping might be limited to a certain region of visual space. Depending on the type of measurement, it roughly encompasses the region around the fixation point (two-probe and continuous remapping test) or the region between the fixation point and the saccade target (continuous remapping test). Although this conception seems to be reasonable with respect to the results of the two-probe test and the direction of the shift in the continuous remapping test a more in depth analysis of the receptive field dynamics leads to an even more complex picture. That is, although there are cells which shift their receptive fields parallel to the saccade, the amplitude of these shifts indicates that the peri-saccadic receptive fields are located closer to

the saccade target, as it is reported for cells in V4. Furthermore, part of these cells also show an expansion of their receptive fields. This expansion seems to be consistent with changes in the average receptive field reported in the FEF (Sommer & Wurtz, 2006). There, receptive fields might not undergo a complete translation as it is commonly associated with the predictive remapping conception, but they rather stretch or develop a bimodal profile in order to cover a greater amount of the saccade target region as it is also observed for cells in the pooling stage of layer 2. Thus, it might be argued that these cells rather participate in an enhanced processing of the saccade target region, but do not update an internal reference frame which is often suggested to play an important role in visual stability. For example, Wurtz (2008) suggested that since each neuron gains information from the same region of visual space before and after the eye movement, this information could possibly be used to mediate the subjective experience of a stable world. While in general the conception of predictive remapping suggests a global account for spatial stability, others have stressed the importance of local visual information provided after a saccade. Both the saccade target theory (Irwin, McConkie, Carlson-Radvansky, & Currie, 1994; McConkie & Currie, 1996; Currie et al., 2000) and the object reference theory (Deubel, Schneider, & Bridgeman, 1996; Deubel, Bridgeman, & Schneider, 1998) propose an important role of the saccade target. It is suggested that the visual system possesses a built-in stability assumption which is only rejected if there is sufficient evidence for an alternative interpretation. Prior to an eye movement visual information at the future eye position is stored and is compared to the visual input after the eyes have landed. If there is a reasonable match, perceived stability will be maintained. In this conception there is no need for a global trans-saccadic memory, only the saccade target region is used to assess stability. Indeed, it has been demonstrated that the saccade target region is more likely to be stored into trans-saccadic memory than other locations (Irwin 1992; Irwin & Andrews, 1996; Irwin & Gordon, 1998; Henderson & Hollingworth, 1999; Henderson & Hollingworth, 2003). Thus, the observed model receptive field dynamics which lead to an increase of responsive cells, that is, an enhanced processing capacity at the saccade target region, seem to support rather such a local conception of visual stability. Note, recent psychophysical evidence for predictive remapping in humans seem to contradict this view. Melcher (2007) used the tilt aftereffect to assess predictive remapping. It was demonstrated that for an adaptor presented close to the fixation point just before a saccade, the tilt aftereffect is stronger at the future post-saccadic position of the adapted region than at the current adaptor position in visual space. This result was interpreted as evidence for remapping of receptive fields to their future position

immediately before a saccade. It was further demonstrated that the tilt aftereffect is reduced for adaptors presented directly at the saccade target. However, in contrast to the former experiment the future position was not tested. Thus, evidence for predictive remapping in this case is somewhat limited. That is, consistent with the model, the reduced tilt aftereffect at the saccade target could also be explained by a processing of an increasing amount of unadapted cells whose receptive fields are shifted towards the saccade target prior to the eye movement.

Finally, it is possible that both receptive field dynamics, the reported V4 shifts and predictive remapping, may exist in parallel but take place at different levels of the processing hierarchy. Areas like V3a, TEO, MT and MST might show similar effects as V4 in order to extract relevant features of the future fixation while areas like LIP of the parietal cortex, which is traditionally assumed to play an important role in space perception, might take part in an updating process.

To conclude, more detailed measurements of peri-saccadic receptive field dynamics in both the ventral and dorsal pathway are needed in order to differentiate between the above mentioned possibilities and functional implications, and to improve our understanding of peri-saccadic perception and ultimately the subjective experience of visual stability.

## 2.4 Discussion

It was demonstrated that the present model of peri-saccadic processing is able to account for the essentials of peri-saccadic compression and for the reported peri-saccadic receptive field dynamics in terms of an attentional explanation. It was argued that a spatially selective feedback signal originating in oculomotor related areas is fed back to visual areas where it causes gain modulations of individual neurons. Those gain modulations are strongest for cells processing the saccade target region. As a consequence the neural population response gets distorted leading to the mislocalization of briefly presented visual stimuli and in turn to receptive field dynamics. As a whole, the receptive field dynamics lead to an enhanced processing capacity of the saccade target region consisting of an increase in the number of cells which are effectively processing this region. It is suggested that this enhanced processing capacity in interaction with the gain increase leads to the observed performance boost at the future fixation (Shepherd et al., 1986; Hoffman & Subramaniam, 1995; Kowler et al., 1995; Deubel & Schneider, 1996; Godijn & Pratt, 2002; Peterson et al., 2004). Furthermore, consistent with the observed V4 dynamics (Tolias et al., 2001) the model predicts that for relative early areas of the visual hierarchy the peri-saccadic receptive fields often possess an increased spatial

selectivity. That means that they are finer tuned and can in principle enable the visual system to extract details of a given scene that will otherwise only be available after the eye movement. For higher visual areas an increased spatial selectivity of receptive fields might be of less functional relevance since cells in these areas generalize over visual details, including spatial position, with the result of more global and abstract representations (Maunsell & Newsome, 1987; Vogels & Orban, 1996). Although one can show that by certain assumptions the increase of the number of cells within a population improves the accuracy of coding in general (Abbott & Dayan, 1999; Shamir & Sompolinsky, 2006) an improvement in object recognition must be investigated with more elaborated future models which explicitly account for feature selectivity in addition to spatial position. However, if we assume that each cell in the model is sensitive to a specific (non-spatial) feature at a certain position in the visual field, the model predicts a shift in the spatial arrangement of feature detectors. This suggests that the structure of objects, as determined by those detectors, remains uncompressed but the position of an object is subject to change. This is consistent with the observation that despite the peri-saccadic mislocalization of objects their features including size are maintained (Matsumiya & Uchikawa, 2001; Lappe, Kuhlmann, Oerke, & Kaiser, 2006; Noritake et al., 2009; for a discussion of conflicting results obtained by Sogo & Osaka [2005] see Noritake et al. [2009]).

What is the function of the enhanced processing of the future fixation? Every saccade is accompanied by a rapid shift of the projected images on our retinas. However, we do not perceive motion or a “gray out” in this period. It has been hypothesized that the visual system might accomplish this by forward and backward masking of the weakened saccadic representation (e.g., Matin, Clymer, Matin, 1972; Campbell & Wurtz, 1978; Brooks, Impelman, Lum, 1981; see also Ross et al., 2001). While it is convenient that the post-saccadic image provides a strong visual signal, the neural representation for stable stimuli strongly decays after stimulus onset. Moore et al. (1998) have argued that the observed pre-saccadic reactivation of such a decaying representation might serve in the proposed forward masking of the retinal motion during saccades. A related issue is the previously mentioned role of the enhanced processing of the future fixation in mediating visual stability as suggested by the saccade target theory (Irwin et al., 1994; McConkie & Currie, 1996; Currie et al., 2000) and the object reference theory (Deubel et al., 1996; Deubel et al., 1998). That is, pre-saccadic information of the future fixation is stored and compared to the post-saccadic visual input. Thus, the enhanced processing of the future fixation caused by the oculomotor feedback signal might play an important

role in the mediation of a clear and stable percept across saccades (see also Hamker, 2005b). Furthermore, while the saccade target and the object reference theory both emphasize the detection of changes between pre- and post-saccadic representations, others have stressed the notion of trans-saccadic integration of visual information. While it appears now unlikely that trans-saccadic integration operates as a fine scale visual buffer (for a review see Irwin, 1996), it has nevertheless been observed that the post-saccadic processing of a stimulus, serving as the saccade target, can be facilitated by a pre-saccadic preview at the same spatiotopic position (Pollatsek, Rayner, & Collins, 1984). Moreover, Pollatsek et al. have demonstrated that the preview effect is only partly mediated by visual features and thus their study provides evidence that the pre-saccadic enhanced processing of the saccade target is already sufficient to generate a high-level semantic representation of this region even before we look at it (see also Gordon & Irwin, 2000). Finally, in addition to its perceptual function, the enhanced processing of the future fixation might also play a role in oculomotor programming, that is, the extracted features are used to guide the upcoming eye movement (Moore, 1999; Hamker, 2003, 2005a).

How does the present work of peri-saccadic processing relate to covert shifts of space-based attention? The model predicts that the effective feedback signal is driven by saccade related activity and thus, with this respect, is consistent with a premotor view of space-based attention. According to the premotor theory (Rizzolatti, Riggio, Dascola, & Umiltà, 1987) covert shifts of attention are mediated by the motor system, that is, the system that generates overt shifts of attention as well. Thus, covert shifts of attention are conceptualized as planned but not executed saccades. However, the issue whether the mechanisms of covert attention shifts are the same as for eye movements is still under debate (for reviews see Awh, Armstrong, Moore, 2006 and Moore 2006). For example, studies investigating the physiological basis for both saccades and covert attention shifts have provided evidence that although there seems to exist a large overlap for both (e.g., Corbetta et al., 1998; Perry & Zeki, 2000; Beauchamp, Petit, Ellmore, Ingeholm, & Haxby, 2001) there also exist distinct areas for covert and overt shifts of attention (Corbetta & Shulman, 1998). Furthermore, in other studies it was argued that shifts of attention can be dissociated from saccades (Murthy, Thompson, & Schall, 2001; Juan, Shorter-Jacobi, & Schall, 2004). Regardless of the exact source, however, the orienting of covert space-based attention reveals similar effects as observed around the time of a saccade. That is, as for saccades (Fischer and Boch, 1981a, 1981b; Moore et al., 1998; Mazer and Gallant, 2003) covert shifts of space-based attention are accompanied by an enhancement of cells processing the attended region (Treue

& Maunsell, 1996; McAdams & Maunsell, 1999; Reynolds et al., 2000). Furthermore receptive fields in V4 and MT tend to shift towards the center of attention (Connor, Gallant, Preddie, & Van Essen, 1996; Connor, Preddie, Gallant, & Van Essen, 1997; Womelsdorf, Anton-Erxleben, Pieper, & Treue, 2006; Womelsdorf, Anton-Erxleben, & Treue, 2008). If these effects are caused by a related mechanism, as it was outlined in the above sections, we will also expect distortions of the population response and thus the mislocalization of visual stimuli. Indeed, although far less in magnitude than the peri-saccadic mislocalization, some perceptual effects have also been observed during covert shifts of attention. Here, however, a repulsion away from the attended region (Suzuki & Cavanagh, 1997; Pratt & Turk-Browne, 2003) as well as an attraction towards the attended region (Yamada, Kawabe, & Miura, 2008) has been reported. Although at present it cannot be excluded that these different results are due to methodical issues (see Yamada et al., 2008), it might be that these observations can also be caused by a center-surround profile of the gain modulation (see Section 3), that is, a gain modulation which consists of a central excitatory region and surrounding inhibition (Hopf et al., 2006), which might be less pronounced in the peri-saccadic cases considered here. Thus, independent of the source it seems that related mechanisms, namely distortion inducing gain modulations, are involved at the level of neural populations within the target areas in both the covert and overt domain of space-based attention.

To conclude, each saccade is accompanied by an oculomotor feedback signal which is conveyed to multiple visual areas and enhances the gain of cells located around the saccade target. These gain increases lead to an advantage for the processing of stimuli located at or near the saccade target so that they are represented more actively. Moreover, the population response for stimuli presented around the saccade target is distorted. From the viewpoint of a single cell, oculomotor feedback increases its gain and alters its receptive field. On a macroscopic level the changes in receptive field size and location dynamically increase the processing capacity around the saccade target. The spatial mislocalization occurs as a cost of the enhanced processing whenever the brain must rely on the distorted population response in this period in order to generate the percept of an object, other than the saccade target, in space.

---

## 3 Directing global feature-based attention

### 3.1 Introduction

In the preceding part of this thesis it was argued that three of the major peri-saccadic phenomena, that is, the enhanced visual performance at the future fixation, the dynamic changes of receptive fields, and the brief perceptual distortions are caused by a single mechanism: a spatially selective feedback signal. It was demonstrated that due to local gain modulations this signal enhances the response of neurons located near the center of the signal leading to distortions of the population response. These distortions in turn cause receptive field dynamics and the mislocalization of stimuli in visual space. If a similar mechanism also works in the domain of feature-based attention, we should be able to observe related effects. Most obviously, due to distorted population responses, we will expect a misperception of stimuli in feature space.

As outlined in the General Introduction, attending to a particular location in visual space enhances neural responses to stimuli presented at this location, known as space-based attention (for a review see Reynolds & Chelazzi, 2004). Similar effects have been reported if attention is directed towards specific non-spatial attributes (Chelazzi et al., 1993; Motter, 1994a, 1994b; Chelazzi et al., 1998; Treue & Martinez-Trujillo, 1999; Martinez-Trujillo & Treue, 2004; Bichot et al., 2005). Remember, this feature-based attention is supposed to operate globally throughout visual space. That means that the activity of neurons is modulated according to a function of their tuning characteristics with respect to the attended feature even if their receptive field location is distinct from the present focus of space-based attention. For example, it was reported by Treue and Martinez-Trujillo (1999) that the response of direction-selective neurons in MT to their preferred direction were enhanced if the monkey attended to a second stimulus, presented outside of the recorded cells' receptive field, that matched the cells' characteristic. Furthermore, the response to the preferred direction was suppressed if the monkey attended to the anti-preferred direction of the recorded neuron. Related effects have also been observed in humans in terms of the strength of the haemodynamic response (Sàenz et al., 2002), the strength of the motion aftereffect (Boynton et al., 2006), and detection performance (Sàenz et al., 2003).

While the above mentioned observations are in accordance to a global up- and down-regulation of the neural representation of features according to the feature similarity gain model of attention (Treue & Martinez-Trujillo, 1999) it remains unknown in how far feature-based attention has a direct impact on feature space.

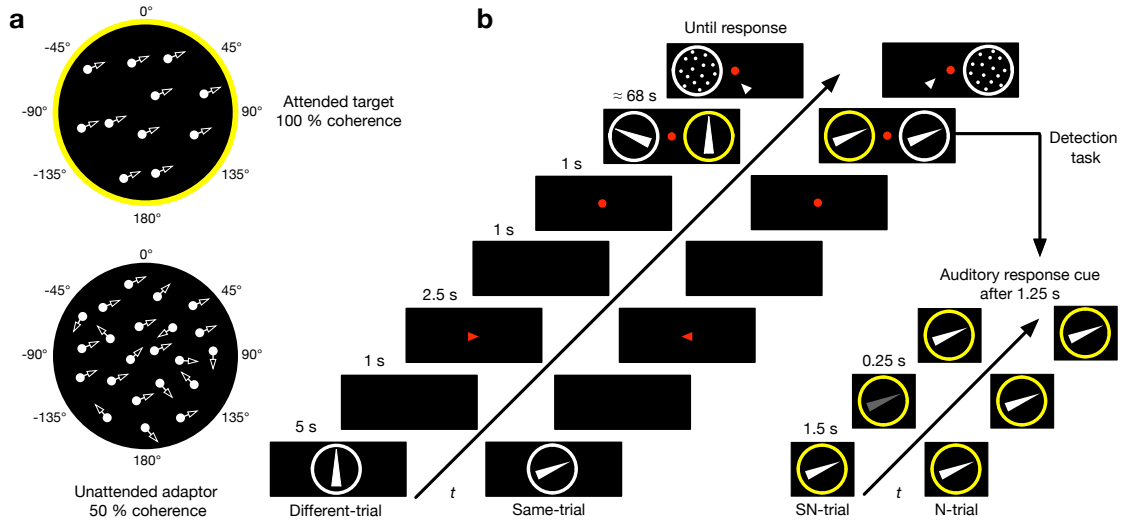


**Figure 23.** Stimuli and experimental procedure. (a) Illustration of RDKs used in the experiment. The yellow circle indicates the attended target RDK. The circle was not present in the experiments. (b) In different-trials the target was always directed upwards ( $0^\circ$ ) while the dots in the adaptor were moving in a different direction. In same-trials both target and adaptor were moving in the same direction. Yellow circles indicate the attended site. During the adaptation period the subjects' task was the detection of a recurring luminance change as illustrated in the lower right. During so-called signal-plus-noise trials (SN-trials) the luminance of the target RDK changed. In so-called noise trials (N-trials) the luminance of the target remained constant. After multiple detection trials in the prolonged adaptation period the static test pattern was presented.

That is, does feature-based attention merely result in a gating of relevant features or does it in addition alter the metric of feature space? This hypothesis was tested in an experiment using the perceived direction of the static motion aftereffect (SMAE) to probe the representation of motion direction in feature space.

The SMAE is the consequence of viewing a moving pattern for a prolonged period and designates the experience of motion while observing a stationary pattern. Thereby, the perceived direction of the stationary pattern points in the opposite direction of the moving pattern. The common explanation of the SMAE is an unbalanced population response to the stationary pattern due to neural adaptation towards the previously viewed motion (for a review see Mather, Pavan, Campana, & Caso, 2008). If attending to a given direction of motion does influence the representation of another, different direction of motion during the encoding phase, it should be reflected after the adaptation period in the direction of the SMAE.

While maintaining central fixation subjects attended to a peripheral random-dot kinematogram (RDK), which will be referred to as the *target*. Simultaneously, a second RDK was presented in the opposite hemifield which will be called the *adaptor* (Figure 23a). While ignoring the adaptor the subjects' task was to detect a small recurring luminance change of the target. After a certain time, the target

disappeared and the adaptor stopped moving, providing the stationary test pattern. Subjects had to indicate the perceived direction of the test pattern. Two types of trials were applied. In so-called *same*-trials the target and the adaptor always moved in the same direction. In *different*-trials the target always moved upwards while the adaptor moved in a different direction (Figure 23b). If feature-based attention only modulates the neural representation of a given feature in terms of strength, no systematic differences of the perceived direction between the same-condition and the different-condition should be found. If in contrast feature based attention alters the metric of feature space, systematic differences of the perceived directions between both conditions should be observed.

## 3.2 Experimental procedure

Four subjects ( $S_1, \dots, S_4$ ), two female, with normal or corrected to normal vision volunteered in the experiments. With the exception of  $S_2$  who was the author of this thesis all subjects were naive with respect to the purpose of the study. Subjects were instructed to keep central fixation throughout a trial. Further, they were instructed to detect not only the luminance change of the target, but to also attend to its exact direction. Before the experiment, subjects were made familiar with the SMAE in both central and peripheral viewing conditions using the same stimuli as described below with 100 % coherence.

In the main experiment the target RDK consisted of 100 and the adaptor RDK consisted of 200 white dots with 100 % and 50 % coherence, respectively. Note the coherence of the adaptor was reduced in order to decrease the population response (Britten & Newsome, 1998) and thus to maximize the expected effect (see Section 3.4). Dots were  $0.28^\circ$  in size, had a luminance of  $85.6 \text{ cd/m}^2$  (MINOLTA LS -110), and moved in a circular aperture of  $8^\circ$  in diameter with a velocity of  $7.6^\circ/\text{s}$ . The random part of the adaptor changed direction every two frames. All dots had unlimited lifetime as long as they stayed inside the aperture. When a dot left the aperture it was randomly placed at a new position of the borders and ensured that the dot would move inside the aperture again. The apertures were centered  $9^\circ$  left and right to a small ( $0.37^\circ$ ) red fixation point with a luminance of  $20.2 \text{ cd/m}^2$  placed in the center of the screen on a black background with a luminance of  $2.2 \text{ cd/m}^2$ . Stimuli were presented on a CRT-monitor (EIZO FlexScan F930) of 40 cm in width and 30 cm in height with a resolution of  $1856 \times 1392$  pixel and 85 Hz driven by a NVIDIA GeForce 7300 GT graphic-card placed in a Mac Pro 1.1. Stimuli were generated with customized software programmed in C using OpenGL. Subjects were placed 53 cm in front of the monitor. A chin-rest was used to stabilize the head.

The room was dimly illuminated with 5 lx.

A single trial was structured as follows. To cue the target direction, the to be attended RDK was first presented centrally for 5 s. After the presentation of a blank (1 s) a small red arrow cued the attended site for 2.5 s. After another blank (1 s) the fixation point appeared and 1 s later, both target and adaptor were shown. After 1.75 s the luminance of the target was decreased in half of the detection trials for 0.25 s. 1.25 s later, a short auditory response cue was provided. After the response of the subject, by pressing one of the two mouse buttons, feedback was given by the same auditory cue for a correct answer and the next detection trial was started. After 20 detection trials (end of adaptation period with an average duration of 68 s) the target disappeared and the adaptor stopped moving thereby providing the stationary test pattern. If the subjects perceived an aftereffect, they indicated its direction by a mouse-click relative to the fixation point. After a blank of 2.5 s the next trial began. During three consecutive trials the direction of the target and the adaptor never changed. The same is true for the attended site. Note, if detection performance of the luminance change as determined across these three trials fell outside a predefined range ( $min = d' = 1.35, max = d' = 2.56$ ) responses were discarded. The initial value of the luminance change was obtained with the method of constant stimuli for each subject, where the value corresponding to  $d' = 1.69$  was chosen. If performance fell outside the predefined range these values were adjusted in small steps. Information regarding the size of the luminance changes is shown in Table 4 in Section 6. After a 3 min break the attended site was changed and, depending on the condition, also the direction of the target and the adaptor. Note that this rather long period was chosen to avoid transfer-effects of adaptation across conditions and to give subjects time to recover, since the task was experienced by all subjects as quite exhaustive. An experimental session consisted of 18 trials lasting approximately 50 min.

Same-trials and different-trials were randomized within and across sessions. In same-trials both target and adaptor had the same direction. In different-trials the target direction was always upwards ( $0^\circ$ ) and as in same-trials the direction of the adaptor was randomly selected out of 10 possible directions ( $-135^\circ, -112.5^\circ, -90^\circ, -67.5^\circ, -45^\circ, 45^\circ, 67.5^\circ, 90^\circ, 112.5^\circ, 135^\circ$ ). Note for  $S_1$  the adaptor was always directed outwards with respect to the fovea and for all other subjects it was directed inwards. Further note that only for  $S_1$  and  $S_2$  all directions were used.  $S_3$  and  $S_4$  performed a subset consisting of  $-67.5^\circ$  and  $67.5^\circ$ .

In separate sessions the baseline for the same-trials was measured. Instead of detecting a luminance change subjects had to simply indicate the direction of the

target. The general procedure was the same as described above with the exception that the central presentation of the target direction and the 3 min break were omitted.

The whole experiment lasted over several weeks until for each subject 15 measures were available for each direction in all types of trials. Altogether over 50 h of measurement were required. About 22 % of the total number of trials in the same and different condition were excluded because the detection performance of the subjects fell outside the predefined range. The performance of the subjects is shown in Table 5 in Section 6. From the remaining trials further 10 % had to be excluded because subjects indicated that they did not perceive an aftereffect. Finally, less than 0.01 % of all these trials were identified and excluded as outliers, that is, they fell outside the region of  $\pm 2.5$  *SDs* around the respective mean. The results are summarized in Figure 24 and Table 6 in Section 6.

### 3.3 The altered metric of feature space

It is observed that direction estimates of the SMAE drastically change when, in the encoding phase, attention is directed to a stimulus whose motion direction differs from the one of the adaptor. For a given adaptor, the perceived direction of the SMAE can deviate more than  $30^\circ$  from the expected direction. Figure 24 summarizes the main results. The resulting SMAEs of the same-condition are close to the perceived directions of the target, which were measured separately and are referred to as *baseline*. However, for all subjects all SMAEs of the different-condition are significantly different (see Section 6.3 for statistical details) from their respective SMAEs of the same-condition. Two patterns are observed. For adaptor directions differing up to  $90^\circ$  from the target direction the resulting SMAEs seem to arise from adaptor directions being closer to the target as they actually are, that is, they are attracted. This can be seen for the  $-90^\circ$ ,  $-45^\circ$ ,  $45^\circ$ , and  $90^\circ$  adaptor direction in Figure 24a and for the  $-67.5^\circ$  and  $67.5^\circ$  adaptor direction in Figure 24b. For adaptor directions farther away from the target the opposite is found, that is, the adaptor directions are repelled with respect to the target, as it can be seen for the  $-135^\circ$  and the  $135^\circ$  adaptor direction in Figure 24a. Thus, the distance in feature space between attracted and repelled directions is increased.

It seems unlikely that a response bias can account for the observed pattern. If there was a simple tendency of subjects to indicate the direction of the SMAEs as being closer to the attended target, no repulsion should have been found. Moreover, consistent with previously reported findings in the attention domain (Reynolds et al., 2000; Martinez-Trujillo & Treue, 2002), the magnitude of the effect inversely scales

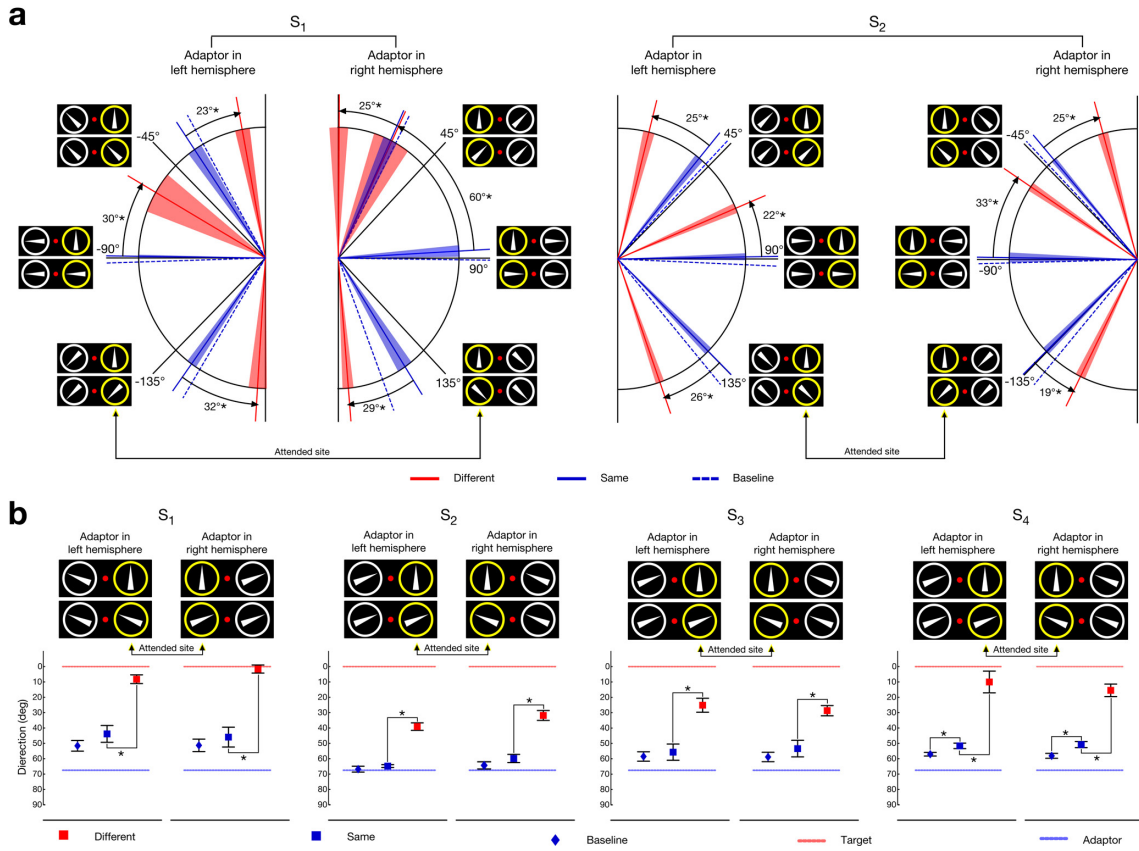


**Figure 24.** Dependency of the SMAE on the similarity of the attended stimulus and the adaptor. (a) Perceived direction of SMAE for two subjects ( $S_1$  and  $S_2$ ) for six adaptor directions ( $-135^\circ$ ,  $-90^\circ$ ,  $-45^\circ$ ,  $45^\circ$ ,  $90^\circ$ ,  $135^\circ$ ). For  $S_1$  the adaptor was always directed outwards with respect to the fovea and for  $S_2$  it was always directed inwards. The panel at each of the six adaptor directions indicates the presented motion directions in the different and same condition. Mean baselines (dashed blue lines) indicate the perceived directions of the target. Mean SMAEs from same-trials (solid blue lines) are close to the perceived baselines. Mean SMAEs of different-trials (red lines) strongly deviate from those in same-trials. Please note that for better readability the indicated SMAEs are transformed to the direction of motion which would have caused the SMAEs assuming a simple reversal. The colored region around the respective means represent 95 % confidence intervals. Arrows denote the differences between the same-condition and the different-condition. Asterisks denote statistical significance. For both subjects all differences between the same-condition and different-condition are statistically significant. None of the differences between same-conditions and baselines are statistically significant. (b) Results for subjects  $S_1$ ,  $S_2$ ,  $S_3$ , and  $S_4$  ( $-67.5^\circ$ ,  $67.5^\circ$ ). For  $S_1$  the adaptor was always directed outwards with respect to the fovea. For all other subjects it was directed inwards. Mean SMAEs of different-conditions are indicated by red squares. Mean SMAEs of different conditions are indicated by blue squares and mean baselines are indicated by blue diamonds. SMAEs are shown as the unsigned direction which would have caused them. Dashed blue lines indicate the unsigned adaptor direction and dashed red lines indicate the attended direction. Error bars denote 95 % confidence intervals. Asterisks denote statistical significance. For all subjects all differences between same-conditions and different-conditions are statistically significant. None of the differences between same-conditions and baselines are statistically significant with the exception of  $S_4$ .

with the contrast of the adaptor as revealed by a control experiment in which high contrast and low contrast adaptors with 100 % coherence were used (see Section 6.1). For both the high and the low contrast condition significant deviations are found, but the magnitude in the high contrast condition is significantly smaller than the one in the low contrast condition (see Figure 25 and Table 9).

Another potential caveat for an explanation based on a global influence of feature-based attention will arise when both target and adaptor are simultaneously processed by a single population of cells with large receptive fields covering both stimuli. If this was true, attention would simply increase the contribution of the attended stimulus to the net SMAE (Alais & Blake, 1999) as known from the biased competition framework (Desimone & Duncan, 1995). While this again cannot explain the repulsion effect it could be a possible explanation for the observed attraction. Thus, a second control experiment was conducted in which subjects had to detect a recurring luminance change of the fixation point and to ignore both target and adaptor (see Section 6.2). Given the assumption that target and distractor are both processed simultaneously by the same cells, the biased competition framework predicts that SMAEs in the different-condition lie somewhere in between the SMAEs of the target and the adaptor. However, this is not what has been observed. Thus, it is concluded that both stimuli are not significantly processed by the same neural population. Consistent with an attentional explanation the data show that when the target is ignored, the effect disappears and no significant differences between the same and the different-condition are observed (see Figure 26 and Table 11). Finally, the results are also unlikely to result from eye movements (see Section 6.5). Instead, the observed results can be explained by a model in which properties of the attended stimulus are fed back to early sensory areas and induce modulations of the population response (Figure 27). While such attentional gain modulation relates to earlier models of feature-based attention (Hamker, 2005a; Ardid, Wang, & Compte, 2007; Reynolds & Heeger, 2009), feature-based distortions of the population responses have not been predicted, except for a study simulating a masking phenomenon known as feature-inheritance (Hamker, 2007). A quantitative model evaluation revealed that the net gain modulation ought to have a center-surround profile, that is, neurons which prefer directions close to the attended target are enhanced while neurons which prefer directions farther away are suppressed (Figure 27b). Note that the model does not attempt to explain the SMAE per se, but it explains the impact of gain modulation on the population response during adaptation. Consistent with electrophysiological recordings (Martinez-Trujillo & Treue, 2004) this results in a sharpening of the

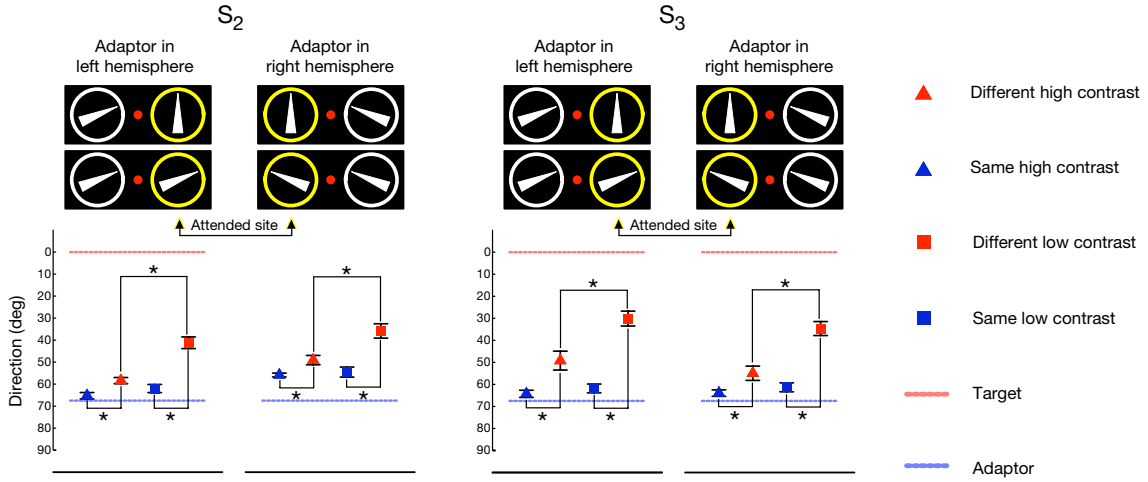


**Figure 25.** Contrast dependency of the SMAE (control experiment 1). For both subjects the adaptor ( $-67.5^\circ$ ,  $67.5^\circ$ ) was always directed inwards with respect to the fovea. For the high contrast condition mean SMAEs of different-conditions are indicated by red triangles and mean SMAEs of same-conditions are indicated by blue triangles. For the low contrast condition mean SMAEs of different-conditions are indicated by red squares and mean SMAEs of same-conditions are indicated by blue squares. Note SMAEs are shown as the unsigned direction which would have caused them assuming a simple reversal. Dashed blue lines indicate the unsigned adaptor direction and dashed red lines indicate the attended direction. Error bars denote 95 % confidence intervals. Asterisks denote statistical significance. For both subjects all differences between the same-condition and the different-condition for both the high and low contrast condition are statistically significant. Further, for both subjects the differences between the different-conditions of the high contrast condition and different-condition of the low contrast condition are statistically significant.

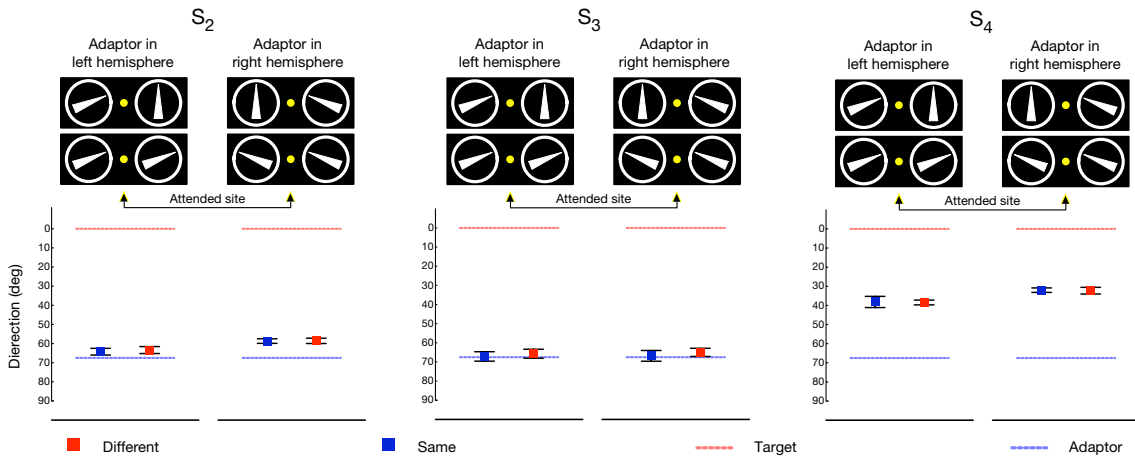


**Figure 26.** Results of the unattended motion condition (control experiment 2). Subjects attended to the fixation point as indicated by the yellow color. For all subjects the adaptor ( $-67.5^\circ$ ,  $67.5^\circ$ ) was always directed inwards with respect to the fovea. Mean SMAEs of different-conditions are indicated by red squares. Mean SMAEs of same-conditions are indicated by blue squares. Note SMAEs are shown as the unsigned direction which would have caused them assuming a simple reversal. Dashed blue lines indicate the unsigned adaptor direction and dashed red lines indicate the attended direction. Error bars denote 95 % confidence intervals. For all subjects none of the differences between the same-condition and the different-condition are statistically significant.

population response if target and adaptor have the same direction (Figure 27c) as determined by the half-maximum width of the response profile (see Section 6.4). For adaptors close to the target, however, the gain modulation leads to a distortion of the population in a way that the center of mass is shifted towards the target direction (Figure 27d). Similarly, the center of mass of the population response to adaptors which lie in the suppressive surround is shifted away from the target direction. Altogether, the distortions lead to local magnifications in feature space (Figure 27e). While these effects already occur due to simple gain changes of single neurons without shifts in the tuning curve, neurons that compute a weighted sum of the distorted population response ought to alter also their tuning properties, as predicted by the model (Figure 27f). These tuning curve shifts lead to an increased number of cells (see Section 6.4 for technical details) which are processing the attended and the opposite direction. However, since cells preferring directions farther away from the attended direction are suppressed, an effective increase in processing should occur for the attended direction (see also Abbott & Dayan, 1999; Shamir & Sompolinsky, 2006).

### 3.4 Discussion

Attention is well known to integrate features allowing for a coherent percept (e.g., Treisman, 2006). However, the present results suggest, that the features themselves can be changed during the process. That is, the study reveals that feature-based attention alters the metric of feature space since the direction of the SMAE depends on the attended feature in the adaptation phase. These observations conceptually extend the feature-similarity gain model of attention (Treue & Martinez-Trujillo, 1999), according to which attention increases or decreases the response of neurons to a stimulus dependent on a gain factor which relies on the similarity between the attended feature and the preferred feature of the particular neuron. While previous experiments have only reported an up- or downregulation of the neural response in early visual areas (Treue & Martinez-Trujillo, 1999; Sàenz et al., 2002; Liu, Larsson, & Carrasco, 2007), the present observations suggest distortions of the population response governed by the feature-similarity principle, which enable the visual system to increase the distance between relevant and irrelevant features in feature space.

The model suggests that the physiological correlate of the perceptual changes is mediated by feedback connections which distort the population response. Distorted population responses would lead to tuning curve changes in neurons that are driven by these responses, for example, neurons that compute a weighted sum of the population response (Rust, Mante, Simoncelli, & Movshon, 2006). This could

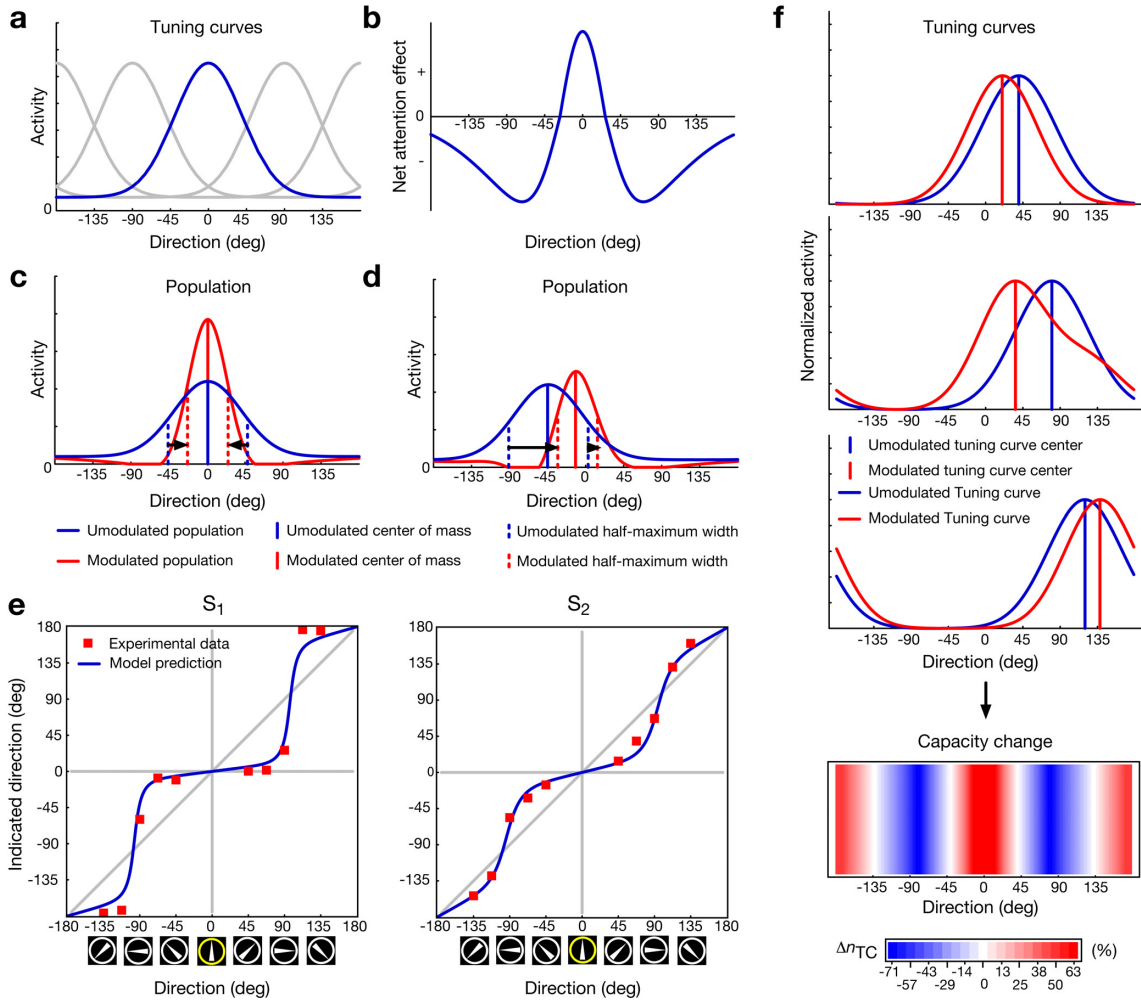


**Figure 27.** Model of feature-based attention. (a) Tuning curves of sensory neurons located on a circle. The bandwidth of the tuning curves is within the range of V1 and MT (Albright, 1984). (b) The net effect of attention. Directions close to the attended direction ( $0^\circ$ ) are enhanced while directions farther away are suppressed. (c) Consistent with experimental data (Martinez-Trujillo & Treue, 2004) the population response is sharpened as indicated by the half-maximum if the stimulus direction is equal to the attended direction. (d) For a stimulus with a direction of  $-45^\circ$  the population response is distorted, that is, the center of mass of the neural activity is attracted towards the attended direction. (e) Indicated SMAEs of subject  $S_1$  and  $S_2$  for all ten directions ( $-135^\circ$ ,  $-112.5^\circ$ ,  $-90^\circ$ ,  $-67.5^\circ$ ,  $-45^\circ$ ,  $45^\circ$ ,  $67.5^\circ$ ,  $90^\circ$ ,  $112.5^\circ$ ,  $135^\circ$ ) denoted by the red squares shown together with the model fits denoted by the blue lines as a function of the veridical direction. Note again SMAEs are shown as the direction which would have caused them assuming a direct reversal. While directions near the attended direction ( $0^\circ$ ) are attracted directions farther away are repelled. (f) Exemplary tuning curve shifts of three model neurons. The center of the unmodulated tuning curve is  $40^\circ$ ,  $80^\circ$ , and  $120^\circ$  from top to bottom. While the center of the tuning curve shifts towards the attended feature for tuning curves with unmodulated centers close to the attended direction, it is shifted away for tuning curves with unmodulated centers farther away. This results in an increase of tuning curves which are processing the attended and the opposite direction. However, since the tuning curves with preferred direction farther away from the attended direction are suppressed, an effective increase in processing occurs at the attended direction, that is, tuning curves of neurons shift their preferred direction such that the whole population preferably processes the attended properties.

explain the change in the spectral tuning of V4 neurons during a naturalistic visual search task, where cells became more sensitive to features of the attended search target (David, Hayden, Mazer, & Gallant, 2008). Thus, the model links physiological observations with subjective perceptual experience. As far as the origin of the distorted percept is concerned, it seems that a widely distributed network is involved in generating motion aftereffects (Taylor et al., 2000). However, since there is a general agreement that for the SMAE early areas as V1 and MT participate significantly (Mather et al., 2008), it appears reasonable that distortions of the population response should be observable in these areas.

Because the content of attention during adaptation affects the SMAE, feature-based attention appears to influence the representation of stimuli already before the final decision level. Although the distinction between encoding and decoding might be smoother than traditionally thought, earlier studies that focused on the discrimination of features rather attributed the misperception of stimuli to the level of decoding (Jazayeri & Movshon, 2007), for example, by optimally chosen top-down signals (Navalpakkam & Itti, 2007).

To conclude, feature-based attention has typically been attributed to a mere control of information flow, that is, a gating of relevant features for further processing, whereas the observations of perceptual distortions suggests that feature-based attention operates by local magnifications of feature space between relevant and irrelevant features. Thus, the information itself is altered by feature-based attention. As a result, a stimulus matching the content of feature-based attention is encoded more similar to the attended one whereas other stimuli are repelled in feature space.

---

## 4 General discussion

It was argued that both overt space-based attention and feature-based attention can fundamentally alter the neural representation of their specific spaces at the level of population responses as well as at the level of single cells. In both domains attention, that is, modulatory feedback, leads to distorted population responses causing mislocalizations of stimuli respectively features and altered receptive fields and tuning curves. So far space-based and feature-based attention have been treated rather independently. While space-based attention is often supposed to “highlight” a specific region in space irrespective of specific non-spatial features, the opposite is true for feature-based attention. That is, the latter is suggested to highlight specific non-spatial features irrespective of space. However, from a functional point of view both are highly interdependent and can act synergistically (Hayden & Gallant, 2009; Patzwahl & Treue, 2009) in order to process behaviorally relevant information.

Let us assume, as it is often the case in our daily behavior, that we are searching for a certain object. We do not know its exact location in space but we know how it looks like, that is, we have knowledge about the featural composition of the object such as its color and shape. According to the work of Hamker (e.g., 2003, 2004a, 2005a), space-based and feature-based attention might act in concert to find the desired object as follows. A given visual scene provides the visual system the bottom-up input. The resulting activity is then modulated with respect to task dependent constraints, the goal of our search. That is, top-down feature-based feedback can be provided by a memorized “target template” of the searched object. The activity of cells in visual areas whose tuning characteristics match the characteristics of the template is enhanced. Furthermore, these cells project to oculomotor related areas in topographic correspondence. Some of these oculomotor cells again project back to visual areas where they modulate cells as a function of position, that is, they are able to provide a top-down space-based feedback signal. During this process, cells or populations which do not match either the featural composition of the template or the targeted positions of the space-based feedback signal are progressively suppressed via competition inducing inhibitory mechanisms. Finally, if successful, the whole dynamic leads to the selection of the desired object in space.

The present work, which can be considered in many aspects as a direct derivative of the original work by Hamker, thereby extends the understanding of the above described process. Firstly, during the process of selection, competition does not only take place for the mere representation of stimuli respectively features, but it is suggested to take place for processing recourses as well. In both the space and

feature domain, the modulatory impact of the feedback leads to structural changes of receptive fields and tuning curves, respectively. As a result the processing of the respective neural populations as a whole is biased towards the “dominant” feature, including spatial position. Secondly, this biased processing, mediated by distorted population responses, leads to quantitative changes of the encoded feature. Thus, the competition causes changes of the very meaning of the neural representation. While it is argued that the distortions of the population response in the space domain and thus the mislocalization of stimuli in visual space, which appear in a critical period of the spatial competition, are the inevitable costs the visual system has to pay for an enhanced processing of a favored location, the distortions in the feature-based domain seem to be of inherent use for the visual system. That is, these distortions enable the system to separate relevant and irrelevant features by increasing their relative distance in feature space.

To conclude, it is supposed that attention does not merely strengthen the neural representation of relevant features and weakens the representation of irrelevant ones, but that attention does directly alter both the contents that are processed respectively represented by single neurons and the populations they constitute. Thereby, in accordance with the gain modulation, the changes of receptive fields and tuning curves are suggested to result in an enhanced processing capacity of the current contents of attention.

---

## References

- Abbott, L. F. (1994). Decoding neuronal firing and modeling neural networks. *Quarterly Review of Biophysics*, *27*, 291-331.
- Abbott, L. F., & Dayan, P. (1999). The effect of correlated variability on the accuracy of a population code. *Neural computation*, *11*, 91-101.
- Adams, D. L., & Horton, J. C. (2003). A precise retinotopic map of primate striate cortex generated from the representation of angioscotomas. *The Journal of Neuroscience*, *23*, 3771-3789.
- Alais, D., & Blake, R. (1999). Neural strength of visual attention gauged by motion adaptation. *Nature neuroscience*, *2*, 1015-1018.
- Albright, T. D. (1984). Direction and orientation selectivity of neurons in visual area MT of the macaque. *Journal of Neurophysiology*, *52*, 1106-1130.
- Albright, T. D., & Desimone, R. (1987). Local precision of visuotopic organization in the middle temporal area (MT) of the macaque. *Experimental Brain Research*, *65*, 582-592.
- Anderson, R. W., Das, S., & Keller, E. L. (1998). Estimation of spatiotemporal neural activity using radial basis function networks. *Journal of Computational Neuroscience*, *5*, 421-441.
- Ardid, S., Wang, X. J., & Compte, A. (2007). An integrated microcircuit model of attentional processing in the neocortex. *The Journal of Neuroscience*, *27*, 8486-8495.
- Armstrong, K.M., Fitzgerald, J.K., & Moore, T. (2006). Changes in visual receptive fields with microstimulation of frontal cortex. *Neuron*, *50*, 791-798.
- Armstrong, K. M., & Moore, T. (2007). Rapid enhancement of visual cortical response discriminability by microstimulation of the frontal eye field. *Proceedings of the National Academy of Sciences of the United States of America*, *104*, 9499-9504.
- Awater, H., Burr, D., Lappe, M., Morrone, M. C., & Goldberg, M. E. (2005). Effect of saccadic adaptation on localization of visual targets. *Journal of Neurophysiology*, *93*, 3605-3614.

- Awater, H., & Lappe, M. (2006). Mislocalization of perceived saccade target position induced by perisaccadic visual stimulation, *Journal of Neuroscience*, *26*, 12-20.
- Awh, E., Armstrong, K. M., & Moore, T. (2006). Visual and oculomotor selection: links causes and implications for spatial attention, *Trends in Cognitive Sciences*, *10*, 124-130.
- Beauchamp, M. S., Petit, L., Ellmore, T. M., Ingeholm, J., & Haxby, J. V. (2001). A parametric fMRI study of overt and covert shifts of visuospatial attention. *NeuroImage*, *14*, 310-321.
- Becker, W. (1991). Saccades. In R. H. S. Carpenter (Ed.), *Eye Movements, Vision and visual dysfunctions* (pp.95-117). London: Macmillian Press.
- Ben Hamed, S., Duhamel, J. R., & Bremmer, F. (2001). Representation of the visual field in the lateral intraparietal area of macaque monkeys: a quantitative receptive field analysis. *Experimental Brain Research*, *140*, 127-144.
- Bichot, N. P., Rossi, A. F., & Desimone, R. (2005). Parallel and serial neural mechanisms for visual search in macaque area V4. *Science*, *308*, 529-534.
- Binda, P., Bruno, A., Burr, D. C., & Morrone, M. C. (2007). Fusion of visual and auditory stimuli during saccades: a Bayesian explanation for perisaccadic distortions. *The Journal of Neuroscience*, *27*, 8525-8532.
- Bischof, N., & Kramer, E. (1968). Investigations and considerations of directional perception during voluntary saccadic eye movements. *Psychologische Forschung*, *32*, 185-218.
- Blatt, G. J., Andersen, R. A., & Stoner, G. R. (1990). Visual receptive field organization and cortico-cortical connections of the lateral intraparietal area (Area LIP) in the macaque. *The Journal of Comparative Neurology*, *299*, 421-445.
- Boussaoud, D., Desimone, R., & Ungerleider, L. G. (1991). Visual topography of area TEO in the macaque. *The Journal of Comparative Neurology*, *306*, 554-575.
- Boynton, G. M., Ciaramitaro, V. M., & Arman, A. C. (2006). Effects of feature-based attention on the motion aftereffect at remote locations. *Vision Research*, *46*, 2968-2976.

- Brefczynski-Lewis, J. A., Datta, R., Lewis, J. W., & DeYoe, E. A. (2009). The topography of visuospatial attention as revealed by a novel visual field mapping technique. *Journal of Cognitive Neuroscience*, *21*, 1447-1460.
- Britten, K. H., & Newsome, W. T. (1998). Tuning bandwidths for near-threshold stimuli in area MT. *Journal of Neurophysiology*, *80*, 762-770.
- Brooks, B. A., Impelman, D. M., & Lum, J. T. (1981). Backward and forward masking associated with saccadic eye movement. *Perception & Psychophysics*, *30*, 62-70.
- Bruce, C. J., & Goldberg, M. E. (1985). Primate frontal eye fields. I. Single neurons discharging before saccades. *Journal of Neurophysiology*, *53*, 603-635.
- Bullier, J., Schall, J. D., & Morel, A. (1996). Functional streams in occipito-frontal connections in the monkey. *Behavioural Brain Research*, *76*, 89-97.
- Burr, D. C., Morrone, M. C., & Ross, J. (2001). Separate visual representations for perception and action revealed by saccadic eye movements. *Current Biology*, *11*, 798-802.
- Cai, R. H., Pouget, A., Schlag-Rey, M., & Schlag, J. (1997). Perceived geometrical relationships affected by eye-movement signals. *Nature*, *386*, 601-604.
- Campbell, F. W., & Wurtz, R. H. (1978). Saccadic omission: why we do not see a grey-out during a saccadic eye movement. *Vision Research*, *18*, 1297-1303.
- Carrasco, M., Ling, S., & Read, S. (2004). Attention alters appearance. *Nature Neuroscience*, *7*, 308-313.
- Carrasco, M., Penpeci-Talgar, C., & Eckstein, M. (2000). Spatial covert attention increases contrast sensitivity across the CSF: support for signal enhancement. *Vision Research*, *40*, 1203-1215.
- Cavanaugh, J., & Wurtz, R. H. (2004). Subcortical modulation of attention counters change blindness. *The Journal of Neuroscience*, *24*, 11236-11243.
- Chelazzi, L., Duncan, J., Miller, E. K., & Desimone, R. (1998). Responses of neurons in inferior temporal cortex during memory-guided visual search. *Journal of Neurophysiology* *80*, 2918-2940.
- Chelazzi, L., Miller, E. K., Duncan, J., & Desimone, R. (1993). A neural basis for visual search in inferior temporal cortex. *Nature*, *363*, 345-347.

- Collins, T., Doré-Mazars, K., & Lappe, M. (2007). Motor space structures perceptual space: evidence from human saccadic adaptation. *Brain Research, 1172*, 32-39.
- Connor, C. E., Gallant, J. L., Preddie, D. C., & Van Essen, D. C. (1996). Responses in area V4 depend on the spatial relationship between stimulus and attention. *Journal of Neurophysiology, 75*, 1306-1308.
- Connor, C. E., Preddie, D. C., Gallant, J. L., & Van Essen, D. C. (1997). Spatial attention effects in macaque area V4. *The Journal of Neuroscience, 17*, 3201-3214.
- Corbetta, M., Akbudak, E., Conturo, T. E., Snyder, A. Z., Ollinger, J. M., Drury, H. A., Linenweber, M. R., Petersen, S. E., Raichle, M. E., Van Essen, D. C., & Shulman, G. L. (1998). A common network of functional areas for attention and eye movements. *Neuron, 21*, 761-773.
- Corbetta, M., & Shulman, G. L. (1998). Human cortical mechanism of visual attention during orienting and search. *Philosophical Transactions of the Royal Society of London. Series B, Biological Sciences, 353*, 1353-1362.
- Currie, C. B., McConkie, G. W., Carlson-Radvansky, L. A., & Irwin, D. E. (2000). The role of the saccade target object in the perception of a visually stable world. *Perception & Psychophysics, 62*, 673-683.
- Daniel, P. M., & Whitteridge, D. (1961). The representation of the visual field on the cerebral cortex in monkeys. *Journal of Physiology, 159*, 203-221.
- Dassonville, P., Schlag, J., & Schlag-Rey, M. (1992). Oculomotor localization relies on a damped representation of saccadic eye displacement in human and nonhuman primates. *Visual Neuroscience, 9*, 261-269.
- Dassonville, P., Schlag, J., & Schlag-Rey, M. (1995). The use of egocentric and exocentric location cues in saccadic programming. *Vision Research, 35*, 2191-2199.
- Datta, R., & DeYoe, E. A. (2009). I know where you are secretly attending! The topography of human visual attention revealed with fMRI. *Vision Research, 49*, 1037-1044.
- David, S. V., Hayden, B. Y., Mazer, J. A., & Gallant, J. L. (2008). Attention to stimulus features shifts spectral tuning of V4 neurons during natural vision. *Neuron, 59*, 509-521.

- Deneve, S., Latham, P. E., & Pouget, A. (1999). Reading population codes: a neural implementation of ideal observers. *Nature Neuroscience*, *2*, 740-745.
- Desimone, R., & Duncan, J. (1995). Neural mechanisms of selective visual attention. *Annual Review of Neuroscience*, *18*, 193-222.
- Desimone, R., & Schein, J. S. (1987). Visual properties of neurons in area V4 of the macaque: sensitivity to stimulus form. *Journal of Neurophysiology*, *57*, 835-868.
- Deubel, H., Bridgeman, B., & Schneider, W. X. (1998). Immediate post-saccadic information mediates space constancy. *Vision Research*, *38*, 3147-3159.
- Deubel, H., & Schneider, W. X. (1996). Saccade target selection and object recognition: Evidence for a common attentional mechanism. *Vision Research*, *36*, 1827-1837.
- Deubel, H., Schneider, W. X., & Bridgeman, B. (1996). Postsaccadic target blanking prevents saccadic suppression of image displacement. *Vision Research*, *36*, 985-996.
- Deubel, H., Schneider, W. X., & Bridgeman, B. (2002). Transsaccadic memory of position and form. *Progress in Brain Research*, *140*, 165-180.
- Doré-Mazars, K., & Collins, T. (2005). Saccadic adaptation shifts the pre-saccadic attention focus. *Experimental Brain Research*, *162*, 537-542.
- Dow, B. M., Snyder, A. Z., Vautin, R. G., & Bauer, R. (1981). Magnification factor and receptive field size in foveal striate cortex of the monkey. *Experimental Brain Research*, *44*, 213-228.
- Draper, N. R., & Smith, H. (1998). *Applied regression analysis* pp. 567-584. New York: John Wiley & Sons.
- Duhamel, J. R., Colby, C. L., & Goldberg, M. E. (1992). The updating of the representation of visual space in parietal cortex by intended eye movements. *Science*, *25*, 90-92.
- Duncan, R. O., & Boynton, G. M. (2003). Cortical magnification within human primary visual cortex correlates with acuity thresholds. *Neuron*, *38*, 659-671.
- Edelman, J. A., & Goldberg, M. E. (2001). Dependence of saccade-related activity in the primate superior colliculus on visual target presence. *Journal of Neurophysiology*, *86*, 676-691.

- 
- Edelman, J. A., & Goldberg, M. E. (2003). Saccade-related activity in the primate superior colliculus depends on the presence of local landmarks at the saccade endpoint. *Journal of Neurophysiology*, *90*, 1728-1736.
- Felleman, J. D., & Kaas, J. H. (1984). Receptive-field properties of neurons in middle temporal visual area (MT) of owl monkeys. *Journal of Neurophysiology*, *52*, 488-513.
- Fischer, B., & Boch, R. (1981a). Selection of visual targets activates prelunate cortical cells in trained rhesus monkey. *Experimental Brain Research*, *41*, 431-433.
- Fischer, B., & Boch, R. (1981b). Enhanced activation of neurons in prelunate cortex before visually guided saccades of trained rhesus monkeys. *Experimental Brain Research*, *44*, 129-137.
- Frens, M. A., & Van Opstal, A. J. (1997). Monkey superior colliculus activity during short-term saccadic adaptation. *Brain Research Bulletin*, *43*, 473-483.
- Fukushima, K. (1980). Neocognitron: A self-organizing neural network model for a mechanism of pattern recognition unaffected by shift in position. *Biological Cybernetics*, *36*, 193-202.
- Galletti, C., & Battaglini, P.P. (1989). Gaze-dependent visual neurons in area V3A of monkey prestriate cortex. *The Journal of Neuroscience*, *9*, 1112-1125.
- Gattass R., Gross, C. G., & Sandell, J. H. (1981). Visual topography of V2 in the macaque. *The Journal of Comparative Neurology*, *201*, 519-539.
- Gattass, R., Sousa, A. P. B., & Gross, C. G. (1988). Visuotopic organization and extent of V3 and V4 of the macaque. *Journal of Neuroscience*, *201*, 519-539.
- Gattass, R., Sousa, A. P. B., & Rosa, M. G. (1987). Visual topography of V1 in the cebus monkey. *The Journal of Comparative Neurology*, *259*, 529-548.
- Georg, K., Hamker, F. H., & Lappe, M. (2008). Influence of adaptation state and stimulus luminance on peri-saccadic localization. *Journal of Vision*, *8*, 1.1-13.
- Georg, K., & Lappe, M. (2009). Effects of saccadic adaptation on visual localization before and during saccades. *Experimental Brain Research*, *192*, 9-23.
- Godijn, R., & Pratt, J. (2002). Endogenous saccades are preceded by shifts of visual attention: evidence from cross-saccadic priming effects. *Acta Psychologica*, *110*, 83-102.

- 
- Gordon, R. D., & Irwin, D. E. (2000). The role of physical and conceptual properties in preserving object continuity. *Journal of Experimental Psychology. Learning, Memory, and Cognition*, *26*, 136-150.
- Hamker, F. H. (2003). The reentry hypothesis: linking eye movements to visual perception. *Journal of Vision*, *3*, 808-816.
- Hamker, F. H. (2004a). A dynamic model of how feature cues guide spatial attention. *Vision Research*, *44*, 501-521.
- Hamker, F. H. (2004b). Predictions of a model of spatial attention using sum- and max-pooling functions. *Neurocomputing*, *56C*, 329-343.
- Hamker, F. H. (2005a). The reentry hypothesis: the putative interaction of the frontal eye field, ventrolateral prefrontal cortex, and areas V4, IT for attention and eye movement. *Cerebral Cortex*, *15*, 431-447.
- Hamker, F. H. (2005b). A computational model of visual stability and change detection during eye movements in real-world scenes. *Visual Cognition*, *12*, 1161-1176.
- Hamker, F. H. (2005c). Modeling Attention: From computational neuroscience to computer vision. In L. Paletta et al. (Ed.), *International workshop on attention and performance in computer vision (WAPCV 2004)* (pp. 118-132). Berlin, Heidelberg: Springer-Verlag.
- Hamker, F. H. (2007). The mechanisms of feature inheritance as predicted by a systems-level model of visual attention and decision making. *Advances in Cognitive Psychology*, *3*, 111-123.
- Hamker, F. H., Zirnsak, M., Calow, D. & Lappe, M. (2004). Planned action determines perception: A computational model of saccadic mislocalization. In U. J., Ilg, H. H. Bülthoff, & H. A. Mallot (Eds.), *Dynamic perception* (pp. 71-76). St. Augustin, Germany: Infix.
- Hayden, B. Y., & Gallant, J. L. (2009). Combined effects of spatial and feature-based attention on responses of V4 neurons. *Vision Research*, *49*, 1082-1087.
- Henderson, J. M., & Hollingworth, A. (1999). The role of fixation position in detecting scene changes across saccades. *Psychological Science*, *10*, 438-443.

- Henderson, J. M., & Hollingworth, A. (2003). Eye movements and visual memory: detecting changes to saccade targets in scenes. *Perception & Psychophysics*, *65*, 58-71.
- Helmholtz, H. von (1867/1925). *Treatise on physiological optics* (translated from the 3rd German edition). New York: Dover.
- Hoffman, J. E., & Subramaniam, B. (1995). The role of visual attention in saccadic eye movements. *Perception & Psychophysics*, *57*, 787-795.
- Honda, H. (1989). Perceptual localization of visual stimuli flashed during saccades. *Perception & Psychophysics*, *45*, 162-174.
- Honda, H. (1991). The time course of visual mislocalization and of extraretinal eye position signals at the time of vertical saccades. *Vision Research*, *31*, 1915-1921.
- Honda, H. (1993). Saccade-contingent displacement of the apparent position of visual stimuli flashed on a dimly illuminated structured background. *Vision Research*, *33*, 709-716.
- Hopf, J. M., Boehler, C. N., Luck, S. J., Tsotsos, J. K., Heinze, H. J., & Schoenfeld, M. A. (2006). Direct neurophysiological evidence for spatial suppression surrounding the focus of attention in vision. *Proceedings of the National Academy of Sciences of the United States of America*, *103*, 1053-1058.
- Hopp, J. J., & Fuchs, A.F. (2004). The characteristics and neuronal substrate of saccadic eye movement plasticity. *Progress in Neurobiology*, *72*, 27-53.
- Hupé, J. M., James, A. C., Girard, P., Lomber, S. G., Payne, B. R., & Bullier, J. (2001). Feedback connections act on the early part of the responses in monkey visual cortex. *Journal of Neurophysiology*, *85*, 134-145.
- Irwin, D. E. (1992). Memory for position and identity across eye movements. *Journal of Experimental Psychology. Learning, Memory, and Cognition*, *18*, 307-317.
- Irwin, D. E. (1996). Integrating information across saccadic eye movements. *Current Directions in Psychological Science*, *5*, 94-100.
- Irwin, D. E., & Andrews, R. (1996). Integration and accumulation of information across saccadic eye movements. In T. Inui, & J. L. McClelland (Eds.),

- 
- Attention and performance XVI: Information integration in perception and communication* (pp. 125-155). Cambridge, MA: MIT Press.
- Irwin, D. E., & Gordon, R. D. (1998). Eye movements, attention and trans-saccadic memory. *Visual Cognition*, *5*, 127-155.
- Irwin, D. E., McConkie, G. W., Carlson-Radvansky, L., & Currie, C. (1994). A localist evaluation solution for visual stability across saccades. *Behavioral and Brain Sciences*, *17*, 265-266.
- Jazayeri, M., & Movshon, J. A. (2007). A new perceptual illusion reveals mechanisms of sensory decoding. *Nature*, *446*, 912-915.
- Juan, C. H., Shorter-Jacobi, S. M., & Schall, J. D. (2004). Dissociation of spatial attention and saccade preparation. *Proceedings of the National Academy of Sciences of the United States of America*, *101*, 15541-15544.
- Kaiser, M., & Lappe, M. (2004). Perisaccadic mislocalization orthogonal to saccade direction. *Neuron*, *41*, 293-300.
- Kastner, S., De Weerd, P., Pinsk, M. A., Elizondo, M. I., Desimone, R., & Ungerleider, L. G. (2001). Modulation of sensory suppression: implications for receptive field sizes in the human visual cortex. *Journal of Neurophysiology*, *86*, 1398-1411.
- Komatsu, H., & Wurtz, R. H. (1988). Relation of cortical areas MT and MST to pursuit eye movements. I. Localization and visual properties of neurons. *Journal of Neurophysiology*, *60*, 580-603.
- Kowler, E., Anderson, E., Doshier, B., & Blaser, E. (1995). The role of attention in the programming of saccades. *Vision Research*, *35*, 1897-1916.
- Krekelberg, B., Kubischik, M., Hoffmann, K. P., & Bremmer, F. (2003). Neural correlates of visual localization and perisaccadic mislocalization. *Neuron*, *37*, 537-545.
- Lappe, M., Awater, H., & Krekelberg, B. (2000). Postsaccadic visual references generate presaccadic compression of space. *Nature*, *403*, 892-895.
- Lappe, M., Kuhlmann, S., Oerke, B., & Kaiser, M. (2006). The fate of object features during perisaccadic mislocalization. *Journal of Vision*, *6*, 1282-1293.

- 
- Liu, T., Larsson, J., & Carrasco, M. (2007). Feature-based attention modulates orientation-selective responses in human visual cortex. *Neuron*, *55*, 313-323.
- Lu, Z. L., & Doshier, B. A. (1998). External noise distinguishes attention mechanism. *Vision Research*, *38*, 1183-1198.
- Luck, S. J., Chelazzi, L., Hillyard, S. A., & Desimone, R. (1997). Neural mechanisms of spatial selective attention in areas V1, V2, and V4 of macaque visual cortex. *Journal of Neurophysiology*, *77*, 24-42.
- Martinez-Trujillo, J. C., & Treue, S. (2002). Attentional modulation strength in cortical area MT depends on stimulus contrast. *Neuron*, *35*, 365-370.
- Martinez-Trujillo, J. C., & Treue, S. (2004). Feature-based attention increases the selectivity of population responses in primate visual cortex. *Current Biology*, *14*, 744-751.
- Mather, G., Pavan, A., Campana, G., & Caso, C. (2008). The motion aftereffect reloaded. *Trends in cognitive sciences*, *12*, 481-487.
- Matin, E., Clymer, A. B., & Matin, L. (1972). Metacontrast and saccadic suppression. *Science*, *178*, 179-182.
- Matin, L., & Pearce, D. G. (1965). Visual perception of direction for stimuli flashed during voluntary saccadic eye movements. *Science*, *148*, 1485-1488.
- Matin, L., Pearce, E., & Pearce, D. G. (1969). Visual perception of direction when voluntary saccades occur: I. relation of visual directions of a fixation target extinguished before a saccade to a subsequent test flash presented during the saccade. *Perception & Psychophysics*, *5*, 65-80.
- Matsumiya, K., & Uchikawa, K. (2001). Apparent size of an object remains uncompressed during presaccadic compression of visual space. *Vision Research*, *41*, 3039-3050.
- Maunsell, J. H., & Newsome, W. T. (1987). Visual processing in monkey extrastriate cortex. *Annual Review of Neuroscience*, *10*, 363-401.
- Mazer, J. A., & Gallant, J. L. (2003). Goal-related activity in V4 during free viewing visual search: Evidence for a ventral stream visual salience map. *Neuron*, *40*, 1241-1250.

- McAdams, C. J., & Maunsell, J. H. (1999). Effects of attention on orientation-tuning functions of single neurons in macaque cortical area V4. *The Journal of Neuroscience*, *19*, 431-441.
- McConkie, G. W., & Currie, C. B. (1996). Visual stability across saccades while viewing complex pictures. *Journal of Experimental Psychology. Human Perception and Performance*, *22*, 563-581.
- Melcher, D. (2007). Predictive remapping of visual features precedes saccadic eye movements. *Nature Neuroscience*, *10*, 903-907.
- Melcher, D., & Colby, C. L. (2008). Trans-saccadic perception. *Trends in Cognitive Sciences*, *12*, 466-473.
- Michels, L., & Lappe, M. (2004). Contrast dependency of saccadic compression and suppression. *Vision Research*, *44*, 2327-2336.
- Moore, T. (1999). Shape representation and visual guidance of saccadic eye movements. *Science*, *285*, 1914-1917.
- Moore, T. (2006). The neurobiology of visual attention: finding sources. *Current Opinion in Neurobiology*, *285*, 1914-1917.
- Moore, T., & Armstrong, K. M. (2003). Selective gating of visual signals by microstimulation of frontal cortex. *Nature*, *421*, 370-373.
- Moore, T., & Chang, M. H. (2009). Presaccadic discrimination of receptive field stimuli by area V4 neurons. *Vision Research*, *49*, 1227-1232.
- Moore, T., & Fallah, M. (2004). Microstimulation of the frontal eye field and its effects of covert spatial attention. *Journal of Neurophysiology*, *91*, 152-162.
- Moore, T., Tolias, A. S., & Schiller, P. H. (1998). Visual representation during saccadic eye movements. *Proceedings of the National Academy of Sciences of the United States of America*, *95*, 8981-8984.
- Moran, J., & Desimone, R. (1985). Selective attention gates visual processing in the extrastriate cortex. *Science*, *229*, 782-784.
- Morrone, M. C., Ma-Wyatt, A., & Ross, J. (2005). Seeing and ballistic pointing at perisaccadic targets. *Journal of Vision*, *5*, 741-754.

- Morrone, M. C., Ross, J., & Burr, D. C. (1997). Apparent position of visual targets during real and simulated saccadic eye movements. *The Journal of Neuroscience*, *17*, 7941-7953.
- Motter, B. C. (1994a). Neural correlates of attentive selection for color or luminance in extrastriate area V4. *The Journal of Neuroscience*, *14*, 2178-2189.
- Motter, B. C. (1994b). Neural correlates of feature selective memory and pop-out in extrastriate area V4. *The Journal of Neuroscience* *14*, 2190-2199.
- Moulden, B., Kingdom, F., & Gatley, L. F. (1990). The standard deviation of luminance as a metric for contrast in random-dot images. *Perception*, *19*, 79-101.
- Müller, J. R., Philiastides, M. G., & Newsome, W. T. (2005). Microstimulation of the superior colliculus focuses attention without moving the eyes. *Proceedings of the National Academy of Sciences of the United States of America*, *102*, 524-529.
- Munoz, D. P., & Wurtz, R. H. (1995). Saccade-related activity in monkey superior colliculus. I. Characteristics of burst and buildup cells. *Journal of Neurophysiology*, *73*, 2313-2333.
- Murthy, A., Thompson, K. G. & Schall, J. D. (2001). Dynamic dissociation of visual selection from saccade programming in frontal eye field. *Journal of Neurophysiology*, *86*, 2634-2637.
- Nakamura, K., & Colby, L.C. (2000). Visual, saccade-related, and cognitive activation of single neurons in monkey extrastriate area V3a. *Journal of Neurophysiology*, *84*, 677-692.
- Nakamura, K., & Colby, C. L. (2002). Updating of the visual representation in monkey striate and extrastriate cortex during saccades. *Proceedings of the National Academy of Sciences of the United States of America*, *99*, 4026-4031.
- Navalpakkam, V., & Itti, L. (2007). Search goal tunes features optimally. *Neuron*, *53*, 605-617.
- Noritake, A., Utti, B., Terao, M., Nagai, M., Watanabe, J., & Yagi, A. (2009). Saccadic compression of rectangle and kanizsa figures: Now you see it, now you don't. *PLoS One*, *4*, e6383.

- Nowak, L. G., & Bullier, J. (1997). The timing of information transfer in the visual system. In J. H. Kaas, K. Rockland, & A. Peters (Eds.), *Cerebral cortex, volume 12: extrastriate cortex*. New York: Plenum.
- O'Regan, J. K. (1984). Retinal versus extraretinal influences in flash localization during saccadic eye movements in the presence of a visible background. *Perception & Psychophysics*, *36*, 1-14.
- Ostendorf, F., Fischer, C., Finke, C., & Ploner, C.J (2007) Perisaccadic compression correlates with saccadic peak velocity: differential association of eye movement dynamics with perceptual mislocalization patterns. *The Journal of Neuroscience*, *27*, 7559-7563.
- Patzwahl, D. R., & Treue, S. (2009). Combining spatial and feature-based attention within the receptive field of MT neurons. *Vision Research*, *49*, 1088-1093.
- Perry, R. J., & Zeki, S. (2000). The neurology of saccades and covert shifts in spatial attention: an event-related fMRI study. *Brain*, *123*, 2273-2288.
- Peterson, M. S., Kramer, A. F., & Irwin, D. E. (2004). Covert shifts of attention precede involuntary eye movements. *Perception & Psychophysics*, *66*, 398-405.
- Pola, J. (2004). Models of the mechanism underlying perceived location of a perisaccadic flash. *Vision Research*, *44*, 2799-2813.
- Pollatsek, A., Rayner, K., & Collins, W. E. (1984). Integrating pictorial information across eye movements. *Journal of Experimental Psychology. General*, *113*, 426-442.
- Posner, M. I., Nissen, M. J., & Ogden, W. C. (1978). Attended and unattended processing modes: The role of set for spatial location. In H. L. Pick & I. J. Saltzman (Eds.), *Modes of perceiving and processing information*. Hillsdale, NJ: Erlbaum.
- Posner, M. I., Snyder, C. R. R., & Davidson, B. J. (1980). Attention and the detection of signals. *Journal of Experimental Psychology. General*, *109*, 160-174.
- Pratt, J., & Turk-Browne, N. B. (2003). The attentional repulsion effect in perception and action. *Experimental Brain Research*, *152*, 376-382.
- Reynolds, J. H., & Chelazzi, L. (2004). Attentional modulation of visual processing. *Annual Review of Neuroscience*, *27*, 611-647.

- Reynolds, J. H., Chelazzi, L., & Desimone, R. (1999). Competitive mechanisms subserve attention in macaque areas V2 and V4. *The Journal of Neuroscience*, *19*, 1736-1753.
- Reynolds, J. H., & Heeger, D. J. (2009). The normalization model of attention. *Neuron*, *61*, 168-185.
- Reynolds, J. H., Pasternak, T., & Desimone, R. (2000). Attention increases sensitivity of V4 neurons. *Neuron*, *26*, 703-714.
- Riesenhuber, M., & Poggio, T. (1999). Hierarchical models of object recognition in cortex. *Nature Neuroscience*, *2*, 1019-1025.
- Rizzolatti, G., & Matelli, M. (2003). Two different streams form the dorsal visual system: anatomy and functions. *Experimental Brain Research*, *153*, 146-157.
- Rizzolatti, G., Riggio, L., Dascola, I., & Umiltá, C. (1987). Reorientation attention across the horizontal and vertical meridians: evidence in favor of a premotor theory of attention. *Neuropsychologia*, *25*, 31-40.
- Ross, J., Morrone, M. C., & Burr, D. C. (1997). Compression of visual space before saccades. *Nature*, *386*, 598-601.
- Ross, J., Morrone, M.C., Goldberg, M.E., & Burr, D.C. (2001). Changes in visual perception at the time of saccades. *Trends in Neurosciences*, *24*, 113-121.
- Rovamo, J., & Virsu, V. (1983). Isotropy of cortical magnification and topography of striate cortex. *Vision Research*, *24*, 283-286.
- Rust, N. C., Mante, V., Simoncelli, E. P., & Movshon, J. A. (2006). How MT cells analyze the motion of visual patterns. *Nature Neuroscience*, *9*, 1421-1431.
- Sàenz, M., Buraças, G. T., & Boynton, G. M. (2002). Global effects of feature-based attention in human visual cortex. *Nature Neuroscience*, *5*, 631-632.
- Sàenz, M., Buraças, G. T., & Boynton, G. M. (2003). Global feature-based attention for motion and color. *Vision Research*, *43*, 629-637.
- Salinas, E., & Abbott, L. F. (1994). Vector reconstructing from firing rates. *Journal of Computational Neuroscience*, *1*, 89-107.
- Schall, J. D., Morel, A., King, D.J., & Bullier, J. (1995). Topography of visual cortex connections with frontal eye field in macaque: Convergence

- and segregation of processing streams. *The Journal of Neuroscience*, *15*, 4464-4487.
- Schira, M. M., Wade, A. R., & Tyler, C. W. (2007). Two-dimensional mapping of the central and parafoveal visual field to human visual cortex. *Journal of Neurophysiology*, *97*, 4284-4295.
- Schlag, J., & Schlag-Rey, M. (1995). Illusory localization of stimuli flashed in the dark before saccades. *Vision Research*, *35*, 2347-2357.
- Schlag, J., & Schlag-Rey, M. (2002). Through the eye, slowly: delays and localization errors in the visual system. *Nature Reviews. Neuroscience*, *3*, 191-215.
- Seitz, A. R., Nanez, J., E., Holloway, S. R., & Watanabe, T. (1993). Perceptual learning of motion leads to faster flicker perception. *PLoS One*, *1*, e28.
- Seung, H. S., & Sompolinsky, H. (1993). Simple models for reading neuronal population codes. *Proceedings of the National Academy of Sciences of the United States of America*, *90*, 10749-10753.
- Schmolesky, M. T., Wang, Y., Hanes, D. P., Thompson, K. G., Leutgeb, S, Schall, J. D., & Leventhal, A. G. (1998). Signal timing across the macaque visual system. *Journal of Neurophysiology*, *79*, 3272-3278.
- Shamir, M., & Sompolinsky, H. (2006). Implications of neuronal diversity on population coding. *Neural computation*, *18*, 1951-1986.
- Shepherd, M., Findlay, J. M., & Hockey R. J. (1986). The relationship between eye movements and spatial attention. *The Quarterly Journal of Experimental Psychology Section A*, *38*, 475-491.
- Sogo, H., & Osaka, N. (2005). Kanizsa figure does not defend against saccadic compression of visual space. *Vision Research*, *45*, 301-309.
- Sommer, M. A., & Wurtz, R. H. (2004). What the brain stem tells the frontal cortex. I. Oculomotor signals sent from superior colliculus to frontal eye field via mediodorsal thalamus. *Journal of Neurophysiology*, *91*, 1381-1402.
- Sommer, M. A., & Wurtz, R. H. (2006). Influence of the thalamus on spatial visual processing in frontal cortex. *Nature*, *444*, 374-377.

- Stanton, G. B., Bruce, C. J., & Goldberg, M. E. (1995). Topography of projections to posterior cortical areas from the macaque frontal eye fields. *The Journal of Comparative Neurology*, *353*, 291-305.
- Stojanoski, B., & Niemeier, M. (2007). Feature-based attention modulates the perception of object contours. *Journal of Vision*, *7*, 18.1-11.
- Suzuki, S., & Cavanagh, P. (1997). Focussed attention distorts visual space: an attentional repulsion effect. *Journal of Experimental Psychology. Human Perception and Performance*, *23*, 443-463.
- Takagi, M., Abe, H., Hasegawa, S., Yoshizawa, T., & Usui, T. (1993). Velocity profile of human horizontal saccades. *Ophthalmologica*, *206*, 169-176.
- Takeichi, N., Kaneko, C. R., & Fuchs, A. F. (2007). Activity changes in monkey superior colliculus during saccade adaptation. *Journal of Neurophysiology*, *97*, 4096-4107.
- Tanaka, K., Sugita, Y., Moriya, M., & Saito, H. (1993). Analysis of object motion in the ventral part of the medial superior temporal area of the macaque visual cortex. *Journal of Neurophysiology*, *69*, 128-142.
- Taylor, J. G., Schmitz, N., Ziemons, K., Grosse-Ruyken, M. L., Gruber, O., Mueller-Gaertner, H. W., & Shah, N. J. (2000). The network of brain areas involved in the motion aftereffect. *NeuroImage*, *11*, 257-270.
- Thompson, K. G., Biscoe, K. L., & Sato, T. R. (2005). Neuronal basis of covert attention in the frontal eye field. *The Journal of Neuroscience*, *25*, 9479-9487.
- Tolias, A. S., Moore, T., Smirnakis, S. M., Tehovnik, E. J., Siapas, A.G., & Schiller, P. H. (2001). Eye movements modulate visual receptive fields of V4 neurons. *Neuron*, *29*, 757-767.
- Treisman, A. (2006). How the deployment of attention determines what we see. *Visual Cognition*, *14*, 41-443.
- Treue, S., & Martinez-Trujillo, J. C. (1999). Feature-based attention influences motion processing gain in macaque visual cortex. *Nature*, *399*, 575-579.
- Treue, S., & Maunsell, J. H. (1996). Attentional modulation of visual motion processing in cortical areas MT and MST. *Nature*, *382*, 539-541.

- Umeno, M. M., & Goldberg, M. E. (1997). Spatial processing in the monkey frontal eye field. I. Predictive responses. *Journal of Neurophysiology*, *78*, 1373-1383.
- Van Essen, D. C., Newsome, W. T., & Maunsell, J. H. (1984). The visual field representation in striate cortex of the macaque monkey: asymmetries, anisotropies, and individual variability. *Vision Research*, *24*, 429-448.
- VanRullen, R. (2004). A simple translation in cortical log-coordinates may account for the pattern of saccadic localization errors. *Biological Cybernetics*, *91*, 131-137.
- Vogels, R., & Orban, G. A. (1996). Coding of stimulus invariances by inferior temporal neurons. *Progress in Brain Research*, *112*, 195-211.
- Waizman, D. M., Ma, T. P., Optican, L. M., & Wurtz, R. H. (1991). Superior colliculus neurons mediate the dynamic characteristics of saccades. *Journal of Neurophysiology*, *66*, 1716-1737.
- Walker, M. F., Fitzgibbon, E. J., & Goldberg, M. E. (1995). Neurons in the monkey superior colliculus predict the visual result of impending saccadic eye movements. *Journal of Neurophysiology*, *73*, 1988-2003.
- Webster, M. J., Bachevalier, J., & Ungerleider, L. G. (1994). Connections of inferior temporal areas TEO and TE with parietal and frontal cortex in macaque monkeys. *Cerebral cortex*, *149*, 470-483.
- Williford, T., & Maunsell, J. H. (2006). Effects of spatial attention on contrast response functions in macaque area V4. *Journal of Neurophysiology*, *96*, 40-54.
- Womelsdorf, T., Anton-Erxleben, K., Pieper, F., & Treue, S. (2006). Dynamic shifts of visual receptive fields in cortical area MT by spatial attention. *Nature Neuroscience*, *9*, 1156-1160.
- Womelsdorf, T., Anton-Erxleben, & Treue, S. (2008). Receptive field shift and shrinkage in macaque temporal area through attentional gain modulation. *The Journal of Neuroscience*, *28*, 8934-8944.
- Wurtz, R. H. (2008). Neuronal mechanism of visual stability. *Vision Research*, *48*, 2070-2089.
- Wurtz, R. H., Sommer, M.A, & Cavanaugh, J. (2005). Drivers from the deep: the contribution of collicular input to thalamocortical processing. *Progress in Brain Research*, *149*, 207-225.

- Yamada, Y., Kawabe, T., & Miura, K. (2008). Mislocalization of a target toward subjective contours: attentional modulation of location signals. *Psychological Research*, *72*, 273-280.
- Zirnsak, M. (2004). *A computational account for perisaccadic compression of visual space based on spatial reentry*. Unpublished diploma thesis, Westfälische Wilhelms-Universität Münster.

---

## 5 Appendix A: Space-based attention

### 5.1 Mathematical description of the model

The present model of peri-saccadic processing aims at linking psychophysical data to their underlying brain processes. Although the general idea of the model is very simple, the emphasis on certain neuroanatomical and physiological details, such as the visuo-cortical mapping, requires some advanced techniques. These are described in detail in the following sections.

#### 5.1.1 Hierarchical visual processing

The model consists of two visual, hierarchically organized layers  $L_1$  and  $L_2$ . The computation in each layer is divided into three functional stages. The first stage either represents the input from earlier areas or is driven directly by a stimulus. The second stage implements a gain modulation of the input, and the third stage pools the gain modulated activity (cf., Fukushima, 1980; Riesenhuber & Poggio, 1999). Cortical magnification changes along with spatial pooling to account for the fact that higher areas typically show a less pronounced magnification at the fovea. The cortical space is mathematically described as a curved surface (Rovamo & Virsu, 1983). The shape of this surface depends on the changes in cortical magnification along the horizontal meridian of the visual field  $M_p(\epsilon)$  and along isoeccentric rings  $M_e(\epsilon)$ , where  $\epsilon$  denotes eccentricity (see Section 5.1.3 for details). Let  $V$  be the visual space,  $C^{L_1, \text{in}}$  the cortical space of the input into  $L_1$ ,  $C^{L_1, \text{gain}} = C^{L_1, \text{in}}$  the cortical space of the gain modulated stage and  $C^{L_1, \text{pool}}$  the cortical space of  $L_1, \text{pool}$ . Gaussian functions were used to model the receptive fields. Let  $c_i^{L_1} \in V$  be the position of the receptive field center, that is, the point in visual space which maximally activates the cell  $i$  in  $L_1$ . The width of the receptive field is determined by  $\sigma_i^{L_1}$ , which is a function of eccentricity ( $\sigma_i^{L_1} = \sigma_i^{L_1}(\epsilon)$ ). Let  $p_s \in V$  be the position of a stimulus in the visual field. For simplicity, the stimulus width is ignored. The activity of a given  $L_1, \text{in}$  cell is then defined by

$$r_i^{L_1, \text{in}} = k \exp \left( -\frac{\|p_s - c_i^{L_1, \text{in}}\|^2}{2(\sigma_i^{L_1, \text{in}})^2} \right).$$

Note that  $\|p_s - c_i^{L_1, \text{in}}\|$  is the distance (see Section 5.1.4) between the receptive field center and the stimulus position and  $k$  is a constant which relates to the contrast, respectively to the luminance of the stimulus. Since in the relevant experiments (Morrone et al., 1997; Kaiser & Lappe, 2004) the contrast of the stimulus was low,

$k$  was set to  $k = .1$ . Note that the dynamic range of any given cell is  $[0, 1]$ . Thus, the initial stimulus driven activity was 10 % of the maximum activity. After saccade onset the retinal position of the stimulus is computed according to the position of the eye in space. The computation of the eye movements is described in Section 5.1.6.

Formally, the gain modulated response  $r_i^{\text{gain}}$  can be described by a sensitivity increase of a cell  $i$  to its input  $r_i^{\text{in}}$  dependent on the oculomotor feedback signal  $\hat{r}_i$ . As derived in Section 5.1.2, the activity of a given  $L_{1,\text{gain}}$  cell  $i$  is defined as a function of the input  $r_i^{\text{L}_{1,\text{in}}}$ , the gain and a term which normalizes the activity:

$$r_i^{\text{L}_{1,\text{gain}}} = \frac{r_i^{\text{L}_{1,\text{in}}}(1 + w \hat{r}_i^{\text{L}_{1,1}})}{1 + w \max_j \left( r_j^{\text{L}_{1,\text{in}}} \right) \hat{r}_i^{\text{L}_{1,1}}}. \quad (1)$$

The weight factor  $w$  is equal for all layers. The feedback signal is denoted by  $\hat{r}_i^{\text{L}_{1,1}}$ . The feedback signal might have its origin in an oculomotor map in which an activity hill is built up around the target location of a planned eye movement. The oculomotor map is fully connected with  $L_1$  and  $L_2$ . The feedback signal from the oculomotor map to  $L_1$  and  $L_2$  is determined as a Gaussian in cortical space which changes in amplitude, that is, strength as a function of time:

$$\hat{r}_i^{\text{L}_{1,1}} = \exp \left( - \frac{\|p_i^{\text{L}_{1,\text{in}}} - c^{\text{ST}}\|^2}{2(\sigma_{\text{SA}}^{\text{L}_{1,1}})^2} \right) f(t), \quad (2)$$

where  $p_i^{\text{L}_{1,\text{in}}} \in C^{\text{L}_{1,\text{in}}}$  denotes the cortical position of the cell  $i$  in  $L_{1,\text{in}}$ ,  $c^{\text{ST}} \in C^{\text{L}_{1,\text{in}}}$  denotes the center of the feedback signal in cortical coordinates. For all performed simulations it is assumed that the center of the feedback signal is equal to the saccade target used in the relevant experiments (Morrone et al., 1997; Kaiser & Lappe, 2004). The distance between the position of a given  $L_{1,\text{in}}$  cell and the saccade target in cortical space is denoted by  $\|p_i^{\text{L}_{1,\text{in}}} - c^{\text{ST}}\|$ . The description of cortical space is given in Section 5.1.3 and the computation of distances in cortical space is explained in Section 5.1.5.  $\sigma_{\text{SA}}^{\text{L}_{1,1}}$  is the saccade amplitude dependent width of the feedback signal with  $\text{SA} \in \{12^\circ, 16^\circ, 20^\circ, 24^\circ\}$ . The assumption of a gradual spatial decrease of the feedback signal relative to the saccade target is supported by a recent observation in V4 using below threshold microstimulation in the frontal eye field (Armstrong, Fitzgerald, & Moore, 2006). That is, the microstimulation does not cause a saccade. In this study, the increase of the separation between the saccade endpoint (as determined by above threshold stimulation) and the stimulus in the receptive field of a cell resulted in a decrease of the enhancement effect. Thus,

the closer the stimulus is to the saccade target, the stronger is the gain increase by microstimulation. Note that the predictions of the model do not depend on a retinotopic projection as long as the connections between oculomotor areas and the visual areas correspond with each other in visual space.

As far as the temporal characteristics  $f(t)$  are concerned, the oculomotor feedback should increase for  $t \leq 0$ , and decrease for  $t > 0$ , where  $t = 0$  denotes the onset of the saccade. Thus, the strength of the feedback signal is maximal for a stimulus presented at saccade onset. The center of the feedback signal moves with the eye, that is, it remains at its original position in a retinocentric coordinate system. In order to test how far the feedback signal relates to the typical time course of movement-related cells in the FEF or the SC, the time course of the feedback signal was systematically varied. For  $f(t)$  exponential functions

$$f(t) = f_e(t) = \begin{cases} \exp(\alpha t) & \text{if } t \leq 0 \\ \exp(-\beta t) & \text{else} \end{cases} \quad (3)$$

and Gaussian functions

$$f(t) = f_g(t) = \begin{cases} \exp\left(-\frac{t^2}{2\alpha^2}\right) & \text{if } t \leq 0 \\ \exp\left(-\frac{t^2}{2\beta^2}\right) & \text{else} \end{cases} \quad (4)$$

were used, where  $\alpha$  determines the increase and  $\beta$  the decrease of the activity over time in both cases.

The activity  $r_j^{\text{L}_{1,\text{pool}}}$  of a given  $\text{L}_{1,\text{pool}}$  cell  $j$  is determined by pooling the gain modulated input activities of the respective  $\text{L}_1$  cells. The classical receptive fields of  $\text{L}_{1,\text{pool}}$  cells are incorporated into the model using Gaussian functions. The activities of  $\text{L}_{1,\text{pool}}$  cells are weighted with respect to the distance  $\|c_i^{\text{L}_{1,\text{in}}} - c_j^{\text{L}_{1,\text{pool}}}\|$  in visual space between the receptive field center of the cell  $i$  in  $\text{L}_{1,\text{in}}$ , that is,  $c_i^{\text{L}_{1,\text{in}}} \in V$  and the receptive field center of the  $\text{L}_{1,\text{pool}}$  cell  $c_j^{\text{L}_{1,\text{pool}}} \in V$ . These weighted  $\text{L}_1$  cell activities are then spatially pooled using a max operation (Hamker, 2004b)

$$r_j^{\text{L}_{1,\text{pool}}} = \max_i \left( r_i^{\text{L}_{1,\text{gain}}} \exp\left(-\frac{\|c_i^{\text{L}_{1,\text{in}}} - c_j^{\text{L}_{1,\text{pool}}}\|^2}{2(\sigma_j^{\text{L}_{1,\text{pool}}})^2}\right) \right), \quad (5)$$

where  $\sigma_j^{\text{L}_{1,\text{pool}}} = \sigma_j^{\text{L}_{1,\text{pool}}}(\epsilon)$  relates to the width of the receptive field of the respective cell. These receptive field kernels only indirectly define the final receptive field size of each layer. Thus, the given estimates of the receptive field size were obtained from

mappings of the receptive fields (Section 5.3). The activities in  $L_2$  are computed equivalently using Equations 1 - 5. Note that the described model is completely static, that is, the model does not possess any neural dynamics such as latencies or persistence. A stimulus presented at a given time immediately causes a neural population response which is assumed to encode the stimulus position. In order to relate this encoded position to the experimental data the population response has to be decoded (Section 5.4). In order to focus on the localization error predicted exclusively by the oculomotor feedback, any possible additional errors due to the mapping of a retinal coordinate system into a world centered coordinate system are not considered. Thus, the position of the eye  $\theta$  (Section 5.1.6) is added to the estimated stimulus position in retinal coordinates  $\hat{p}_s$  to obtain the estimated stimulus position  $\hat{\theta}_s$  in eye-position invariant coordinates  $\hat{\theta}_s = \hat{p}_s + \theta$ . This is assumed to correspond to the final response of subjects in the experiments of Morrone et al. (1997) and Kaiser and Lappe (2004).

More than 48,000 cells per layer, which were equally distributed in cortical space up to  $70^\circ$  eccentricity were simulated. The parameters and the final number of layers in the model were iteratively determined (see Section 5.2) from the fit of the model to three mentioned experimental data sets, namely the time course of compression, the spatial range of compression, and the two-dimensional spatial pattern of compression.

### 5.1.2 Gain modulation

In the model static neurons are used. Here, the equation of gain modulation for static neurons from an equation used for dynamic neurons is derived. Let us assume, we have a set of gain modulated neurons. The firing rate of each neuron can be described by a differential equation (Hamker, 2004b, 2005a)

$$\tau \frac{d}{dt} r_i^{L_1, \text{gain}} = -r_i^{L_1, \text{gain}} + r_i^{L_1, \text{in}} + \left( A - \max_j \left( r_j^{L_1, \text{gain}} \right) \right)^+ w r_i^{L_1, \text{in}} \hat{r}_i^{L_1} - w_{inh} r_i^{L_1, \text{gain}} \sum_j r_j^{L_1, \text{gain}}.$$

Such a gain function is motivated by several electrophysiological studies which have shown that feedback signals have a modulatory influence (e.g., Hupé, James, Girard, Lomber, Payne, & Bullier, 2001; Moore & Armstrong, 2003) and it has successfully been applied to model the effect of feedback connections on feedforward processing (Hamker, 2005a). The term

$$\left( A - \max_j \left( r_j^{L_1, \text{gain}} \right) \right)^+$$

ensures that the efficiency of the feedback signal depends on the activity of the postsynaptic cell population, where  $(\cdot)^+$  denotes half-rectification, that means if the argument is negative, it is set equal to zero. If the maximal firing rate exceeds the value  $A$ , the feedback signal  $\hat{r}_i^{L1}$  no longer affects the gain. This term has been shown to be consistent with a multiplicative contrast gain modulation as observed in several single cell recordings (Hamker, 2005c).

When we numerically compute the firing rate and set the weight of the dynamic inhibition among the cells to  $w_{inh} = 0$ , the change of activity  $\Delta r_i^{L1, gain}$  in each time step is

$$\Delta r_i^{L1, gain} \approx -r_i^{L1, gain} + r_i^{L1, in} + \left( A - \max_j \left( r_j^{L1, gain} \right) \right)^+ w r_i^{L1, in} \hat{r}_i^{L1}$$

When we ensure that  $\max_j \left( r_j^{L1, gain} \right) \leq A$  and further approximate

$$\frac{r_i^{L1, in}}{\max_j \left( r_j^{L1, in} \right)} \approx \frac{r_i^{L1, gain}}{\max_j \left( r_j^{L1, gain} \right)}$$

we obtain for the equilibrium a non-recursive equation for the firing rate of the gain modulated neurons (Figure 28a):

$$r_i^{L1, gain} = r_i^{L1, in} \frac{1 + A w \hat{r}_i^{L1}}{1 + w \max_j \left( r_j^{L1, in} \right) \hat{r}_i^{L1}}.$$

This equation for the firing rate of a static gain modulated neuron is of course not equal to the dynamic recursive solution, but it captures the essentials as verified by simulations (not reported). In addition to the equation above, the following damped gain function (Figure 28b) was used in order to explore the source of the feedback signal (see Section 5.3):

$$r_i^{L1, gain} = r_i^{L1, in} \frac{1 + A w \left( \hat{r}_i^{L1} \right)^4}{1 + w \max_j \left( r_j^{L1, in} \right) \left( \hat{r}_i^{L1} \right)^4}.$$

This damped gain function only leads to small changes in gain for low feedback activity.

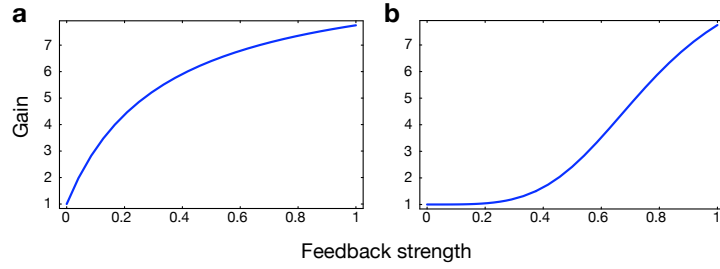


**Figure 28.** Gain of a neuron  $i$  with respect to the feedback strength  $\hat{r}_i^{L_1}$  for an input  $r_i^{L_1, \text{in}} = 0.1$ . The gain is equal to one, if no feedback signal is present. An increase of the feedback signal enhances the gain of a neuron. (a) Instantaneous gain function. (b) Damped gain function.

### 5.1.3 Visuo-cortical mapping

Neurophysiological findings in monkeys and humans indicate that central parts of the visual field are processed by a greater amount of cortical tissue as compared to peripheral parts (e.g., Dow et al., 1981; Duncan & Boynton, 2003). The amount of cortical tissue, which processes one degree of the visual field, is termed the cortical magnification factor and is usually denoted in millimeter per degree (Daniel & Whitteridge, 1961).

For the mapping of the visual field  $V$  into cortical space  $C$ , a procedure by Rovamo and Virsu (1983) was used according to which the cortical space is a topologically isomorphic distortion of the visual space, that is, a transformation of a sphere (Figure 29). A point in visual space is given by the coordinates  $(\epsilon, \phi)$  and the cortical space is described in cylindrical coordinates  $(r, \theta, z)$ . Note that the angle  $\epsilon$  is the eccentricity generating the meridians and the angle  $\phi$  generates the circles of constant eccentricity. To obtain the cortical representation  $C$  of the visual field  $V$ , the sphere is transformed according to the two cortical magnification functions  $M_p(\epsilon)$  and  $M_e(\epsilon)$ .  $M_p(\epsilon)$  describes the changes in cortical magnification along the meridians of the visual field and  $M_e(\epsilon)$  describes the changes along the circles with constant eccentricity. If both functions are equal, the cortical magnification is isotropic. That is, at each location in the visual field magnification along a circle of constant eccentricity is equal to magnification along a meridian. The magnification function  $M_p(\epsilon, \phi)$  along the meridian is defined by

$$M_p(\epsilon, \phi) = \left( \left( \frac{dz}{d\epsilon} \right)^2 + \left( \frac{dr}{d\epsilon} \right)^2 \right)^{0.5}, \quad (6)$$

and the magnification function  $M_e(\epsilon, \phi)$  along the circles of constant eccentricity is

defined by

$$M_e(\epsilon, \phi) = \left( \frac{r}{\sin(\epsilon)} \right) \left( \frac{d\theta}{d\phi} \right). \quad (7)$$

It is assumed that the cortical space is rotationally symmetric ( $\theta = \phi$ ), that is, the magnification functions do not depend on  $\phi$ . Solving Equation 6 and 7 yields the complete transformation rule

$$r(\epsilon, \phi) = M_e(\epsilon) \sin(\epsilon)$$

and

$$z(\epsilon) = \int_0^\epsilon \left( (M_p(\tilde{\epsilon}))^2 - \left( \frac{dr}{d\tilde{\epsilon}} \right)^2 \right)^{0.5} d\tilde{\epsilon}.$$

Figure 30 shows the cortical space of  $L_1$  and  $L_2$  and Figure 31 shows the corresponding magnification functions. The main factor leading to the stronger asymmetry of the compression pattern is the longer distances along the rays compared to the ones along the circles. The degree of overrepresentation around the fovea is not crucial for the results obtained. Please note that the assumed anisotropy across the whole visual field is a simplification. It is not claimed that the whole human visual field is subject to anisotropy.

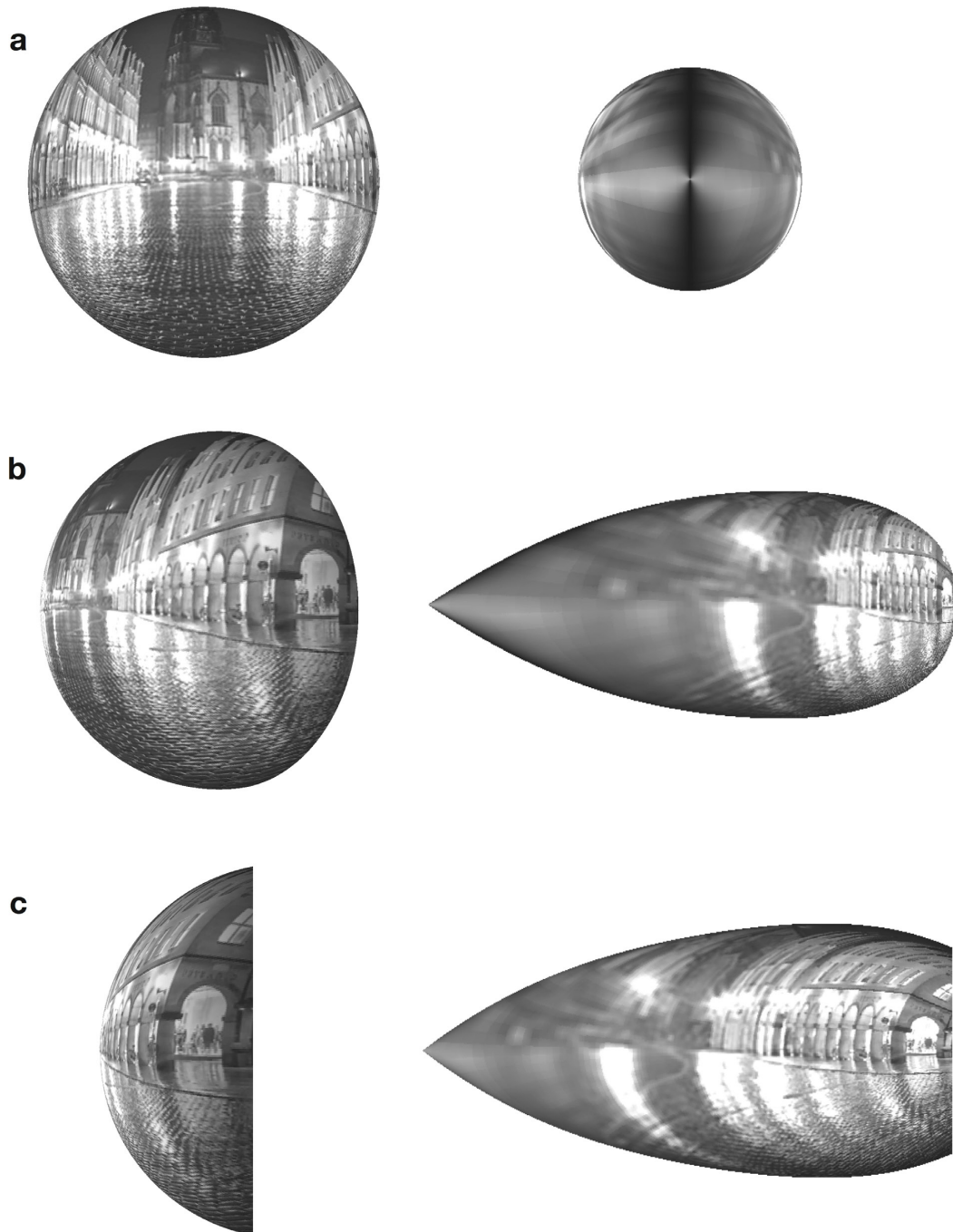


**Figure 29.** Illustration of the visuo-cortical mapping. Visual space is shown on the left and cortical space on the right. (a) Front view of the sphere and its projection. (b) 45° side view. (c) 90° side view.

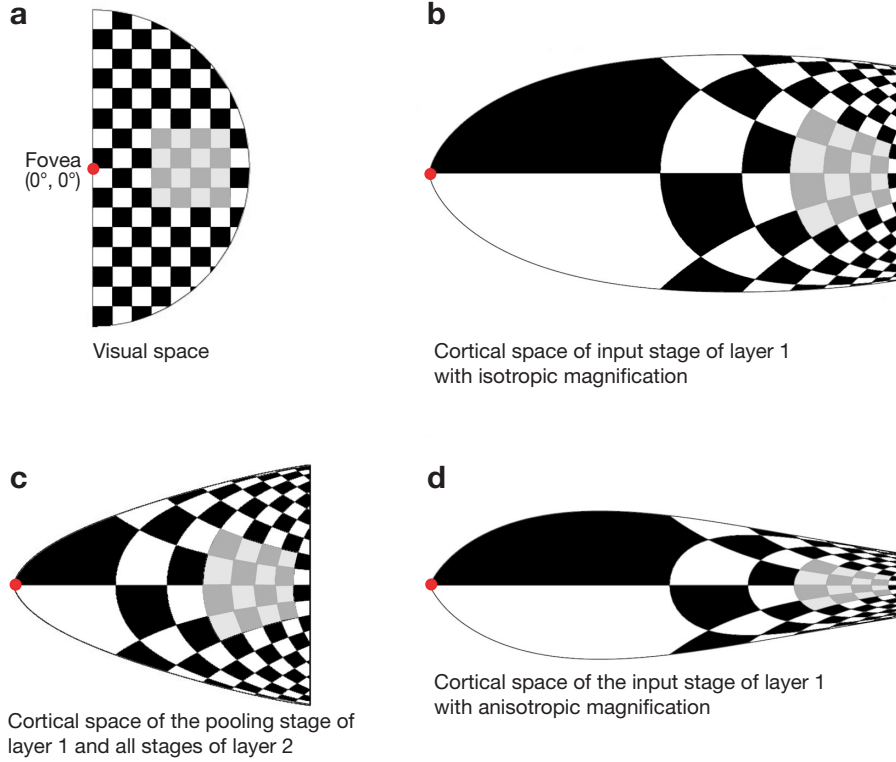


**Figure 30.** Visual hemifield and the respective side view of the different cortical surfaces from the fovea up to  $32^\circ$  eccentricity. The center of the visual field, that is, the fovea is indicated by the red dot. Each checkerboard element is  $4^\circ$  by  $4^\circ$  in visual space. The gray shaded part indicates the area where the dots in the experiment of Kaiser & Lappe (2004) were presented. (a) Visual space. (b) Input stage of layer 1 with isotropic magnification ( $M_p = M_e$ ). (c) Pooling stage of layer 1 and all stages of layer 2. (d) Input stage of layer 1 with anisotropic magnification ( $M_p > M_e$ ).

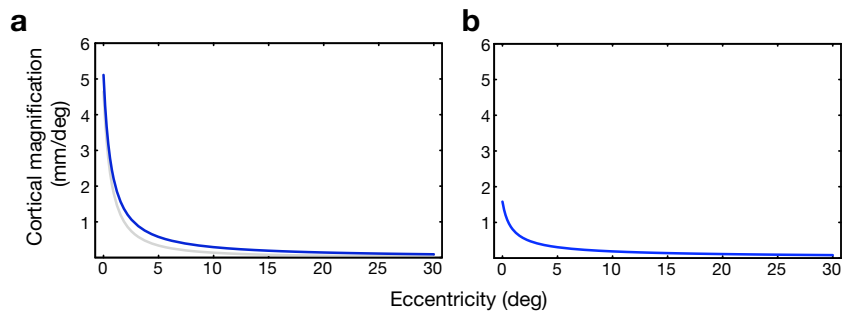


**Figure 31.** Illustration of cortical magnification functions used in the model. (a) Magnification functions for the input stage of layer 1. The blue curve denotes  $M_p$  and the gray curve denotes  $M_e$ . (b) Magnification function used for the pooling stage of layer 1 and for all stages in layer 2 ( $M_p = M_e$ ).

### 5.1.4 Computation of distances in visual space

The distance  $d$  between two points  $(\epsilon_1, \phi_1)$  and  $(\epsilon_2, \phi_2)$  located on a sphere with radius 1 is the angle between the three dimensional position vectors  $r_1$  and  $r_2$  determining the points. In the  $(x, y, z)$  coordinate system the components of the position vectors are ( $i = 1, 2$ )

$$\begin{aligned} x_i &= \cos(\phi_i) \sin(\epsilon_i) \\ y_i &= \sin(\phi_i) \sin(\epsilon_i) \\ z_i &= \cos(\epsilon_i). \end{aligned}$$

The angle  $\theta$  between  $r_1$  and  $r_2$  is determined by the inner product  $\theta = \arccos(r_1 \cdot r_2)$  and one obtains

$$d = \theta = \arccos(\cos(\epsilon_1) \cos(\epsilon_2) + \sin(\epsilon_1) \sin(\epsilon_2) \cos(\phi_1 - \phi_2)).$$

### 5.1.5 Computation of distances in cortical space

Since the oculomotor feedback signal is described as a Gaussian in cortical space, the distance between the center of the signal and the cortical position of each cell is required. In order to compute the distance one has to consider that the cortical space is a curved surface and the distance between two points is the length of the geodetic line connecting the two points. The geodetic line is the solution of the following variation problem. Let  $s$  be a real number from 0 to 1,  $g(x_1, x_2)$  be the metric tensor of the surface with respect to the local coordinates  $(x_1, x_2)$ , and let  $(x_1(s), x_2(s))$  be a path connecting the points  $(x_1(0), x_2(0))$  and  $(x_1(1), x_2(1))$ . Finding the geodetic line is done by minimizing

$$S = \int_0^1 (g_{ij}(x_1(s), x_2(s)) x'_i(s) x'_j(s))^{\frac{1}{2}} ds \quad (8)$$

by variation over the possible paths  $(x_1(s), x_2(s))$  connecting the points  $(x_1(0), x_2(0))$  and  $(x_1(1), x_2(1))$ .  $S$  is the length of the path  $x'_i = \frac{dx_i}{ds}$  and  $L(x_i, x'_i) = g_{ij} x'_i x'_j$  is called the Lagrange function of the variation problem. The solution of this variation problem is equivalent to the solution of the system of differential equations:

$$\frac{\partial L}{\partial x_i} - \frac{d}{ds} \frac{\partial L}{\partial x'_i} = 0$$

with respect to the boundary conditions  $(x_1(0), x_2(0))$  and  $(x_1(1), x_2(1))$ . The local coordinates describing the cortical space are the eccentricity  $x_1 = \epsilon$  generating the

meridians and the angle  $x_2 = \phi$  yielding the circles of constant eccentricity. The metric tensor  $g(\epsilon, \phi)$  can directly be calculated from Equation 6 and 7 as shown in the following. The infinitesimal path-length on the cortical space is in cylindrical coordinates:

$$(dS)^2 = (dz)^2 + (dr)^2 + r^2(d\theta)^2.$$

Using Equation 6 and 7 we obtain:

$$(dS)^2 = (M_p(\epsilon))^2(d\epsilon)^2 + (M_e(\epsilon))^2(\sin(\epsilon))^2(d\phi)^2. \quad (9)$$

Recall Equation 8, the components of the metric tensor  $g(\epsilon, \phi)$  can directly be taken from Equation 9:

$$\begin{aligned} g_{11} &= (M_p(\epsilon))^2 \\ g_{12} &= 0 \\ g_{21} &= 0 \\ g_{22} &= (M_e(\epsilon))^2(\sin(\epsilon))^2. \end{aligned}$$

In terms of the metric tensor  $g(\epsilon, \phi)$  one obtains the Lagrange function:

$$L = (M_p(\epsilon))^2 (\epsilon')^2 + (M_e(\epsilon))^2(\sin(\epsilon))^2 (\phi')^2.$$

This yields a system of differential equations of second order:

$$\begin{aligned} 0 &= \epsilon'' + \frac{M_p'(\epsilon)}{M_p(\epsilon)} (\epsilon')^2 - \left( \frac{M_e(\epsilon)M_e'(\epsilon)(\sin(\epsilon))^2}{(M_p(\epsilon))^2} + \frac{(M_e(\epsilon))^2 \sin(\epsilon) \cos(\epsilon)}{(M_p(\epsilon))^2} \right) (\phi')^2 \\ 0 &= \phi'' + 2 \left( \frac{M_e'(\epsilon)}{M_e(\epsilon)} + \frac{\cos(\epsilon)}{\sin(\epsilon)} \right) \epsilon' \phi', \end{aligned}$$

where  $M_p'(\epsilon) = \frac{dM_p(\epsilon)}{d\epsilon}$  and  $M_e'(\epsilon) = \frac{dM_e(\epsilon)}{d\epsilon}$ . Since this system of differential equations has no analytical solution, it was solved numerically with respect to the boundary condition, that is, the two points in visual coordinates ( $\epsilon(0) = \epsilon_0, \phi(0) = \phi_0$ ) and ( $\epsilon(1) = \epsilon_1, \phi(1) = \phi_1$ ). For each simulated cell its distance to the saccade target on the cortical surface was computed. When two points, that is, a given cell and the saccade target, are in different hemispheres the shortest distance through the fovea was used for all reported simulations. Control simulations using the shortest possible distance between a given cell located in the opposite hemisphere as the saccade target revealed virtually no differences for the mislocalization arising in

layer 1 ( $L_1$ ), due to the limited extension, that is, the width ( $\sigma_{SA}^{L_1}$ ) of the feedback signal (Figure 34 in Section 5.2). However, using the shortest possible distances as described above for layer 2 ( $L_2$ ) does not allow to fit the amount of mislocalization for stimuli presented in the opposite hemisphere as the saccade target (Figure 4a in Section 2.2.3). That is, the model predicts less compression as experimentally observed (not shown). Figure 32 shows the feedback signal of layer 2 using the different distances. Note that the prediction of a limited transfer of space-based attention to the opposite hemisphere as the center of attention receives support from a recent fMRI study (Brefczynski-Lewis, Datta, Lewis, & DeYoe, 2009).

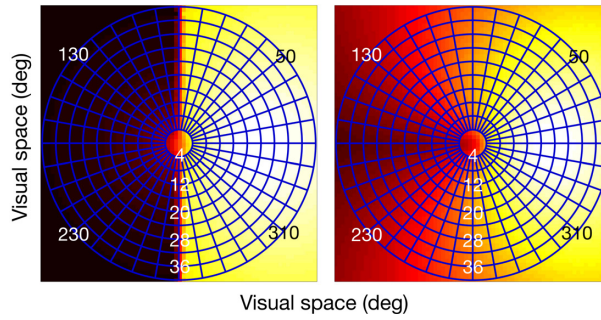


**Figure 32.** Resulting feedback shape in layer 2 for the  $20^\circ$  saccade. The left panel shows the feedback signal when the shortest distance crossing the fovea between cells of the left hemisphere and the saccade target (right hemisphere) was used. The right panel shows the feedback signal when the shortest possible distance between cells of the left hemisphere and the saccade target was used.

### 5.1.6 Simulation of eye movements

Since the subjects' eye position is not always available, a more general approach was used, that is the time course of each saccade was simulated by approximating its velocity profile using a sixth order polynomial

$$v(t) = b_0 + b_1t + b_2t^2 + b_3t^3 + b_4t^4 + b_5t^5 + b_6t^6. \quad (10)$$

Given the following constraints

$$\begin{aligned}
 v(0) &= 0 \\
 v(d) &= 0 \\
 v(t_{v_{max}}) &= v_{max} \\
 v'(t_{v_{max}}) &= 0 \\
 v'(0) &= 0 \\
 v'(d) &= 0 \\
 \int_0^d v(t)dt &= a
 \end{aligned}$$

it is possible to find a unique solution for the seven free parameters. If the amplitude  $a$  of a saccade is given, we have to determine the duration  $d$  of a saccade, the maximal velocity  $v_{max}$ , and the point in time  $t_{v_{max}}$  where the velocity reaches its maximum. The duration of each saccade was obtained by  $d = d_0 + d_1 a$  (Becker, 1991). Consistent with Becker (1991), who reported a range of 20-30 milliseconds for  $d_0$  and a range of 2-3 milliseconds per degree for  $d_1$ , we set  $d_0 = 25$  milliseconds and  $d_1 = 2.5$  milliseconds per degree. Knowing the duration of a saccade, the mean velocity  $\bar{v}$  is given by

$$\bar{v} = \frac{a}{d}$$

and the peak velocity of a saccade is

$$v_{max} = \bar{v}c,$$

where  $c$  denotes the ratio of the peak velocity to the mean velocity, i.e.  $c = \frac{v_{max}}{\bar{v}}$ . Becker (1991) approximated  $c$  with a constant value of  $c = 1.65$ .

Finally, we have to determine  $t_{v_{max}}$ . Takagi et al. (1993) defined the skewness  $S$  of the velocity profile by the ratio of the acceleration phase to the duration of the saccade. For rightward saccades they estimated the following linear regression equation

$$S = -md + 0.53$$

where  $m = 2.71 \frac{1}{s}$ . With  $S$  it is possible to determine

$$t_{v_{max}} = Sd.$$

After determining the parameters of Equation 10 with respect to the constraints for each saccade amplitude (Table 1), the velocity profile and the path of the eye movement (Figure 33) can be obtained. The angle  $\theta$  the eye moves within a time interval  $[t_1, t_2]$  is given by the integral

$$\theta(t_1, t_2) = \int_{t_1}^{t_2} v(t) dt.$$

$\theta$  is then used in the model to update the retinal position of a stimulus during a saccade. Assuming a stimulus is presented at time  $t_s$  at position  $\theta_s$  ( $t = 0$  denotes saccade onset), the retinal position  $p_s$  of the stimulus with respect to the actual eye position is then

$$p_s = \theta_s - \theta(0, t_s).$$

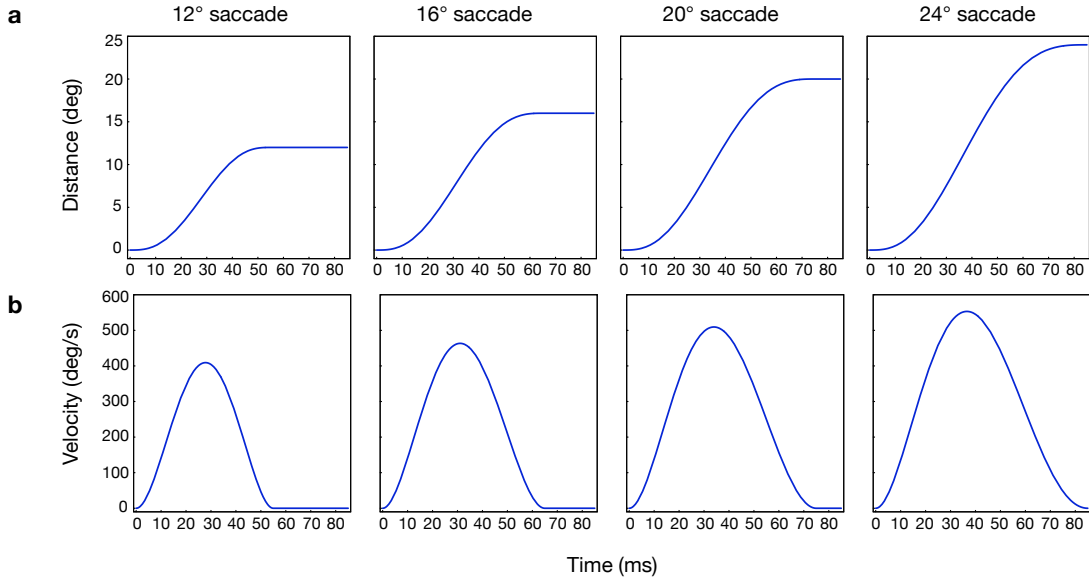


**Figure 33.** Simulated saccades. (a) Position of the eye relative to the fixation point at  $0^\circ$  for the four saccade amplitudes ( $12^\circ$ ,  $16^\circ$ ,  $20^\circ$ ,  $24^\circ$ ). (b) Velocity profiles.

**Table 1** Parameters for the simulation of the eye movement.

Amplitude	$b_0$ (deg/s)	$b_1$ (deg/s <sup>2</sup> )	$b_2$ (deg/s <sup>3</sup> )	$b_3$ (deg/s <sup>4</sup> )	$b_4$ (deg/s <sup>5</sup> )	$b_5$ (deg/s <sup>6</sup> )	$b_6$ (deg/s <sup>7</sup> )
$12^\circ$	0	0	$2.06 \cdot 10^6$	$-7.14 \cdot 10^7$	$5.49 \cdot 10^8$	$1.21 \cdot 10^9$	-2305.21
$16^\circ$	0	0	$2.06 \cdot 10^6$	$-7.3 \cdot 10^7$	$7.82 \cdot 10^8$	$2.27 \cdot 10^9$	-2309.89
$20^\circ$	0	0	$1.98 \cdot 10^6$	$-6.78 \cdot 10^7$	$7.5 \cdot 10^8$	$-2.66 \cdot 10^9$	-2402.27
$24^\circ$	0	0	$1.9 \cdot 10^6$	$-6.18 \cdot 10^7$	$6.66 \cdot 10^8$	$-2.37 \cdot 10^9$	-2579.91

## 5.2 Fitting procedure and parameters of the model

The model has been parameterized using mathematical functions to describe the anatomy and the neural dynamics, such as the shape and timing of the feedback signal and the receptive field size as a function of eccentricity. Nevertheless, there are unknown parameters which could not be determined by other independent investigations (Table 2). These unknown parameters were estimated by fitting the model to the experimental data.

The exact time course of the perceived stimulus position was simulated given the time and position of the flashed stimulus. In order to relate the model to data taken from a particular time window, the average value  $\bar{t}$  from all data points in the time window was determined. From the data showing the spatial pattern of compression (Kaiser and Lappe, 2004) the following values are obtained:  $\bar{t} = 15.01$  ms for the  $12^\circ$  saccade,  $\bar{t} = 13.79$  ms for the  $16^\circ$  saccade,  $\bar{t} = 9.61$  ms for the  $20^\circ$  saccade, and  $\bar{t} = 9.84$  ms for the  $24^\circ$  saccade. These values were then used for  $f(t)$  in Equation 3 or 4. Similar, the position of the eye was computed. All data points from 0-25 ms for the  $12^\circ$  and  $16^\circ$  saccade amplitude and from 0-20 ms for the  $20^\circ$  and  $24^\circ$  saccade amplitude were considered. The size of the window was chosen to obtain a sufficient number of trials in the time bin where the effect of compression is strongest. From the data showing the spatial range of compression in the critical phase from -25 to 0 ms (Morrone et al., 1997)  $\bar{t} = -11.38$  ms was obtained.

With respect to the receptive fields, only the receptive field sizes in the input of each layer ( $\sigma^{L_{1,\text{in}}}$ ,  $\sigma^{L_{2,\text{in}}}$ ) are constrained by the data, since the neural population in this layer provides the input for the gain modulation and thus the degree of distortion. For the simulations in Section 2.3 the following receptive field sizes (measured in degree as described in Section 5.3) were used:  $7+0.8\epsilon$  for  $L_{1,\text{in}}$ ,  $10+0.78\epsilon$  for  $L_{1,\text{pool}}$ ,  $19.9 + 0.37\epsilon$  for  $L_{2,\text{in}}$ , and  $22.21 + 0.36\epsilon$  for  $L_{2,\text{pool}}$ . Note that for  $L_{1,\text{in}}$  and  $L_{2,\text{in}}$  the values were obtained from the initial simulations described below. The data provides only little constraints about the overall magnitude of magnification, as verified by simulations with different magnification factors. However, since the ratio of cortical magnification along rays ( $M_p$ ) to magnification along circles ( $M_e$ ) has turned out to be relevant for fitting the spatial pattern of compression ( $M_p > M_e$ ), specific values have to be determined. To reflect the input of earlier stages the cortical magnification along the rays in  $L_{1,\text{in}}$  ( $M_p^{L_{1,\text{in}}}$ ) was chosen similar to the magnification of monkey V2 (Gattass et al., 1981) and the magnification in  $L_{1,\text{pool}}$  ( $M_p^{L_{1,\text{pool}}}$ ) similar to monkey MT (Albright & Desimone, 1987) and V4 (Gattass et al., 1988). Since I do not know direct measurements of cortical magnification in higher areas,  $M_p^{L_2}$  was set identical to  $M_p^{L_{1,\text{pool}}}$ . The magnification along the rings of

constant eccentricity  $M_e^{L1,in}$  could either be identical to  $M_p^{L1,in}$  (isotropic condition) or different (anisotropic condition). In all other model parts, magnification is isotropic. In the anisotropic condition,  $M_e^{L1,in}$  was roughly determined to obtain a sufficient fit of the data showing the spatial pattern of compression. After running these preliminary simulations to obtain plausible initial values, the fitting procedure was performed in two steps. Note that during these simulations exponential functions (Equation 3) were used for the time course of the feedback signal. In the first step, the fitting started with small receptive field sizes as well as with a small value for the strength of the feedback signal  $w$  which were both iteratively increased by allowing adjustments to the initial values of the other parameters ( $\alpha, \beta, \sigma_{20^\circ}^{L1}, \sigma_{20^\circ}^{L2}$ ) to fit the model to the data from Morrone et al. (1997). Besides determining the RF sizes, this fitting process resulted in the final values of  $\alpha, \beta$ , the strength  $w$  of the feedback signal and the width of the feedback signal in  $L_2$  ( $\sigma_{20^\circ}^{L2}$ ) for a  $20^\circ$  saccade amplitude (Figure 32). In the second step, the final values of the saccade amplitude dependent feedback width ( $\sigma_{SA}^{L1}$  with  $SA \in \{12^\circ, 16^\circ, 20^\circ, 24^\circ\}$ ) (Figure 34) were obtained by fitting the model to the data from Kaiser and Lappe (2004). This was done by minimizing the sum of the absolute errors between the model and the data, that is, the absolute differences in the x- and y-direction for each saccade amplitude, as a robust estimation procedure (Draper & Smith, 1998). The obtained value for the width of the feedback signal ( $\sigma_{20^\circ}^{L1}$ ) was then also used in the simulation of the data from Morrone et al. (1997). Thus, all data was fitted with a single parameter set (Table 2).

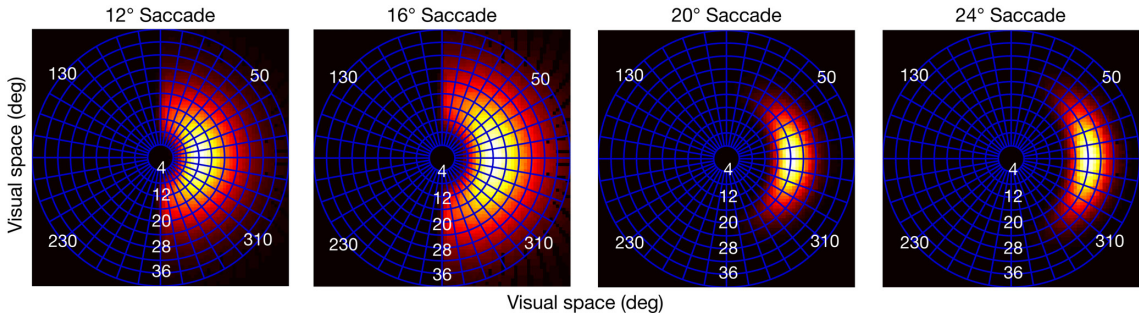


**Figure 34.** Resulting feedback shape in layer 1 for the four saccade amplitudes ( $12^\circ, 16^\circ, 20^\circ, 24^\circ$ ).

### 5.3 Predicting source and targets of the feedback signal

Since the predicted mislocalization of stimuli presented at different times relative to saccade onset critically depends on the time course  $f(t)$  of the cells in the oculomotor map, the time course and shape of the oculomotor feedback signal

**Table 2** List of model parameters.

Parameter	Explanation
$\sigma^{L1,in} = 3.5 + 0.4\epsilon$	Kernel for RF size in degree as a function of eccentricity in $L_{1,in}$
$\sigma^{L2,in} = 11.5 + 0.175\epsilon$	Kernel for RF size in degree as a function of eccentricity in $L_{2,in}$
$M_p^{L1,in} = 4(0.8 + \epsilon)^{-1.1}$	Magnification along the horizontal meridian in $L_{1,in}$
$M_e^{L1,in} = 5(1.05 + \epsilon)^{-1.5}$	Magnification along isoecentric rings in $L_{1,in}$
$M_p^{L1,pool} = M_e^{L1,pool} = 1.14(0.65 + \epsilon)^{-0.76}$	Magnification along the horizontal meridian in $L_{1,pool}$ and $L_{2,in}$
$\alpha = 0.095$ (Equation 3)	Increase of the feedback signal prior to saccade onset (Equation 3 or 4)
$\beta = 0.13$ (Equation 3)	Decay of the feedback signal after saccade onset (Equation 3 or 4)
$k = 0.1$	Fixed peak input activity, identical for all data sets
$\sigma_{12^\circ}^{L1} = 1.32, \sigma_{16^\circ}^{L1} = 1.19, \sigma_{20^\circ}^{L1} = 0.51, \sigma_{24^\circ}^{L1} = 0.43$	Saccade amplitude dependent width of the feedback signal in $L_1$
$\sigma_{20^\circ}^{L2} = 4.7$	Saccade amplitude dependent width of the feedback signal in $L_2$
$w = 30$	Weight of the feedback signal

were systematically varied to test whether the model is constrained by the typical behavior of cells in oculomotor areas such as the SC and FEF. These simulations were based on the parameters obtained by the fitting procedure described above (Section 5.2). The results of the simulations are summarized in Figure 3. In each case from left to right the time course of compression of four stimulus positions (Morrone et al., 1997), the time course of the feedback signal, and different snapshots in time of the shape of the feedback signal are shown. For each data fit the proportional reduction in error measure (*pre*, described in Section 5.6) was determined. Since the localization of the stimulus presented at  $20^\circ$  and  $-20^\circ$  shows a systematic mislocalization after saccade termination (shift in baseline) *pre\** measures were also computed for these locations to determine the goodness of fit ignoring the baseline shift. In addition, below each panel aggregated *pre*-measures are shown, where *pre*(sr) refers to the proportional reduction in error measure of the spatial range of compression, *pre*(tc) to the time course of compression, and *pre*(sc,tc) to the combined measure.

From Figure 35a to 35d the timing of the feedback signal was increased from a late, sharply bursting response to an earlier burst or even build-up activity. It is observed that the data can be fitted by either simulating the time course using an exponential function (Equation 3) with a half-maximum value, that is, the time where the feedback activity reaches half of its maximum activity, of 7.4 ms before and 5.3 ms after saccade (Figure 35a), or a Gaussian function (Equation 4) with a half-maximum value of 21.2 ms before and 14.1 ms after saccade (Figure 35b). A shift to earlier build-up activity (Figure 35c - half-maximum value of 23.5 ms

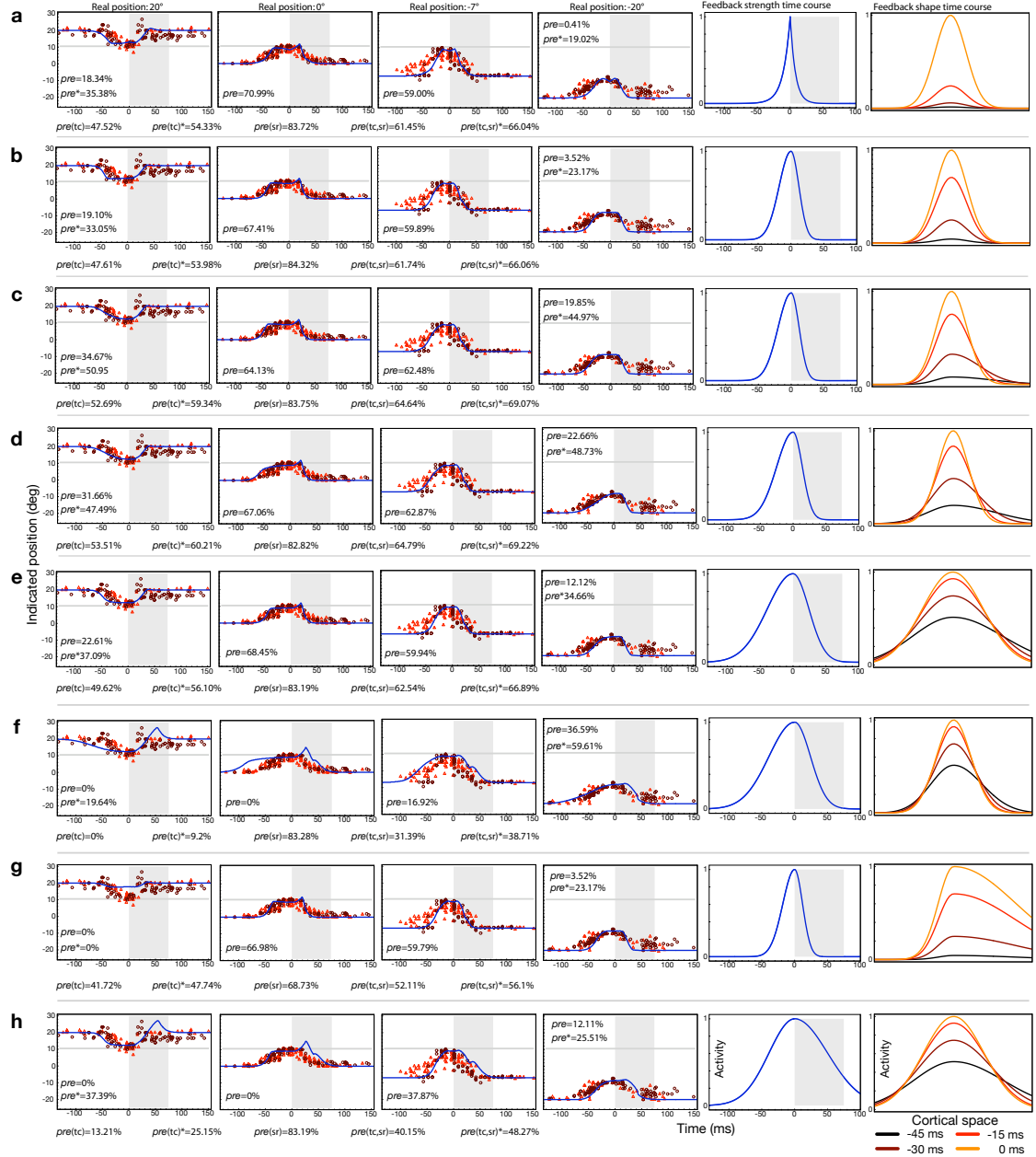


**Figure 35.** Variation of the oculomotor feedback signal in time and space. Details are given in in the Text. (a-e) Increase of the prelude activity in the feedback signal from late burst to build-up activity and the required changes in the shape of the feedback signal. (f) Effect of a strong early visual component in the feedback signal using an instantaneous gain function. (g) Effect of a strong contribution from cells with open movement fields. (h) Effect of a strong contribution from unclipped cells in the feedback signal.

before saccade) required to vary the width of the feedback signal with respect to the activity, with the result that the feedback is initially broadly tuned, and prior to saccade onset, it becomes more focused. Such a spatiotemporal pattern could well emerge by competitive interactions in oculomotor areas. Thus,  $\sigma_{SA}^{L_1}$  in Equation 2 is

now a function of time and for a 20° saccade (SA= 20) and  $\sigma_{SA}^{L1} = \sigma_{20}^{L1}(t)$ :

$$\sigma_{20}^{L1}(t) = \begin{cases} \frac{\sigma_{20}^{L1}(0)\gamma}{1 + (\gamma - 1)f(t)} & \text{if } t \leq 0 \\ \sigma_{20}^{L1}(0) & \text{else} \end{cases}$$

where  $\sigma_{20}^{L1}(0)$  is set to the value obtained by the fit of the spatial compression pattern (see Section 5.2) and  $\gamma = \gamma_1$  (if  $\epsilon(p_i^{L1}) \leq \epsilon(c^{ST})$ ) and  $\gamma = \gamma_2$  (if  $\epsilon(p_i^{L1}) > \epsilon(c^{ST})$ ) determines the width of the signal for  $t = -\infty$ . Note that  $\epsilon(p_i^{L1})$  indicates the eccentricity of a given cell in a certain layer and  $\epsilon(c^{ST})$  indicates the eccentricity of the saccade target.

In particular, an initially broader population into the direction of larger eccentricities with respect to the saccade target ( $\gamma_1 = 1$  and  $\gamma_2 > 1$ ) avoids a strong and early mislocalization of the bar presented at 20°. At most, it is possible to shift the half-maximum value to 29.4 ms prior to saccade by broadening the shape of the early oculomotor signal ( $\gamma_1 > 1$  and  $\gamma_2 > 1$ )(Figure 35d). An initially broader feedback signal leads to less compression in the near range of the saccade target early in time. However, by dropping the assumption that the gain increase is instantaneous, that is, leads to a sufficiently strong distortion of the population response for low feedback activities, it is possible to also account for earlier build-up activity (Figure 35e), where  $\hat{r}_i^{L1}(t)$  (Equation 1) is now  $(\hat{r}_i^{L1}(t))^n$  with  $n = 4$ . Dropping the assumption of an instantaneous gain increase suggests that the source of the feedback signal can either originate from burst-like cells or from build-up cells. However, it also predicts that the effective signal depends on the burst activity, since the early build-up activity has only little impact on the gain. By assuming an instantaneous gain function, early feedback from visual cells activated by the presentation of the saccade target would not be consistent with the model (Figure 35f).

Feedback from open movement cells (simulated by  $\sigma_{20}^{L1}(0) = k \sigma_{20}^{L1}(0)$  if  $\epsilon(p_i^{L1}) > \epsilon(c^{ST})$ ) impairs the data fit since the population response from stimuli presented at larger eccentricities do not get sufficiently distorted (Figure 35g). Note that for illustration proposes it was assumed for this simulation that open movement cells predominately encode larger saccades and their feedback connections topographically correspond to their respective movement fields. By assuming that open movement fields are uniformly distributed with respect to saccade amplitude, the shape of the feedback signal would be broadened to both sides of the saccade target with the result of even less compression, since the population response for

stimuli presented in between the fixation point and the saccade target would not be sufficiently distorted.

Furthermore, it has also been observed that some cells still show significant activity after the end of the saccade, known as partially-clipped or unclipped cells. A strong feedback signal during the saccade leads to stronger mislocalization effects into the direction of the saccade, since the center of the feedback signal moves with the eye relative to the stimulus location (Figure 35h).

A summary of the parameters used in the above simulations is given in Table 3. The goodness of fit in Figure 5a (Section 2.2) was obtained from the simulation results shown in Figure 35 (Unclipped from 35h, Clipped from 35e; Open movement from 35g, Closed movement from 35c, Build-up (Inst. gain) from 35f, Build-up (Damp. gain) from 35e, and Burst (Inst. gain) from 35b).

Note that the above described predictions must of course be seen in the context of the present model, that is, they are the results of a static model lacking neural dynamics. For example, the model does not explicitly account for visual latencies, that is, neither the time a stimulus needs to activate cells in a particular area of interest nor the delay of the oculomotor signal is simulated. So, it is assumed that the latencies of both visual and oculomotor signals are roughly the same. In a study investigating the influence of microstimulation in the FEF on the detection of a transient dimming of a target stimulus Moore and Fallah (2004) reported that the sensitivity was maximal when the temporal asynchrony between the target change and the microstimulation was near zero. Furthermore, Armstrong and Moore (2007) reported observable effects in V4 within 40 ms after the first pulse of microstimulation in the FEF. Similarly, the earliest activation of V4, V3, MT and MST neurons can be observed at about 50 ms after stimulus onset (Nowak & Bullier, 1997; Schmolesky et al., 1998). Thus, the model assumption of equal latencies for visual and oculomotor signals seems to be justified. However, we have to keep in mind that latencies are subject to substantial variability and that additional factors like neural persistence and the temporal integration of visual signals might provide different constraints for the properties of the feedback signal.

Furthermore, during the simulations described above it was possible to substantially lower the receptive sizes in layer 1 ( $L_{1,in}$ ) to provide an estimate of the minimal receptive sizes as required by the model (Section 2.2.6), which in turn were used to predict the brain areas which are involved in the mislocalization. Unfortunately, there exist no sufficient quantitative receptive field measurements in human visual cortex, but it is likely that the receptive field size is larger than in monkeys (Kastner et al., 2001). Thus, the required receptive field sizes of the model

were compared with the receptive field sizes from the areas of interest as measured in monkeys. Due to the max-pooling of the model cells the size of their receptive fields has to be compared to the maximum receptive field size as measured for a given area and eccentricity in electrophysiological studies and not to the average receptive field size. Therefore, for each area of question the maximal receptive field size for a given eccentricity ( $1^\circ$  bins) was extracted from the figures in the literature: V3a (Galletti & Battaglini, 1989; Nakamura & Colby, 2000), V4 (Desimone & Schein, 1987; Gattass et al., 1988; Boussaoud et al., 1991), TEO (Boussaoud et al., 1991), MT (Albright & Desimone, 1987; Komatsu & Wurtz, 1988; Felleman & Kaas, 1984; Tanaka et al., 1993) (whereas most of the large receptive fields in MT have been reported by Tanaka et al., 1993), V2 (Gattass et al., 1988; Nakamura & Colby, 2000), LIP (Blatt, Andersen, & Stoner, 1990), and (Ben Hamed, Duhamel, & Bremmer, 2001), and TE (Boussaoud et al., 1991). Remember that only the receptive field size of the input stage of layer 1 ( $L_{1,\text{pool}}$ ) is directly determined by the receptive field kernels ( $\sigma_i^{L_1} = \sigma_i^{L_1}(\epsilon)$ ). To obtain the size of the receptive fields in the remaining parts of the model the following procedure was used. In order to approximate the receptive field size, one dimensional activity profiles were obtained by presenting a point stimulus in steps of  $1^\circ$  along the horizontal meridian. Since the size of a given receptive field kernel only depends on the eccentricity of the receptive field center in visual space, only cells of one hemisphere with centers along the horizontal meridian were included into the mapping to speed up the procedure. As commonly done in electrophysiology, the obtained activity profiles were fitted using a Gaussian function, yielding a set of receptive field widths defined by the  $\sigma$  of the respective Gaussian. According to Albright and Desimone (1987) who approximated the size of receptive fields by Gaussian functions, the ratio of the width ( $\sigma$ ) to the manually mapped width of the receptive fields is about 0.5. Thus, in order to convert the set of the estimated  $L_{2,\text{in}}$  receptive field width into the usually used  $\sqrt{\text{area}}$ , each entry of the set was multiplied by a factor of 2. This converted set was then fitted with a linear function to obtain the final description of the receptive field size in  $L_{1,\text{pool}}$ ,  $L_{2,\text{in}}$ , and  $L_{2,\text{pool}}$ .

Figure 36 shows the resulting time course of mislocalization for four different stimulus positions using the minimal receptive field size required by the model (Figure 36a) and a too small receptive field size (Figure 36b). The parameters of the feedback signal used in both cases are given in Table 3.

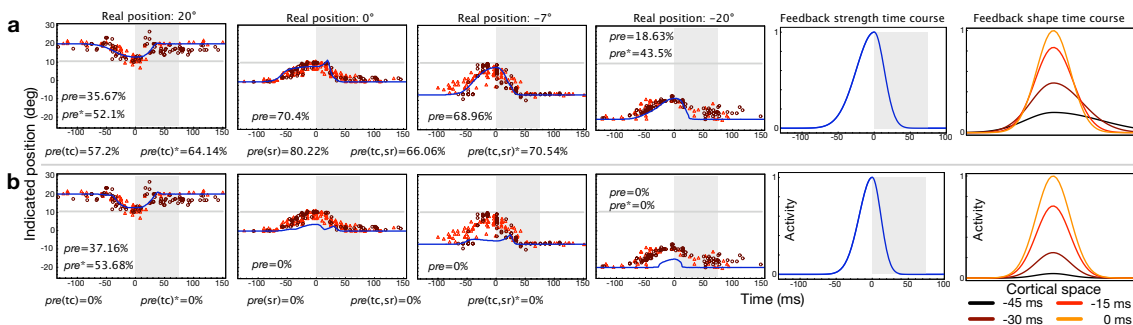


**Figure 36.** Variation of the receptive field sizes. For each data fit the proportional reduction in error measure ( $pre$ ) was determined. In addition, below each panel the aggregated  $pre$ -measures are given, where  $pre(sc)$  refers to the proportional reduction in error measure of the spatial range of compression,  $pre(tc)$  to the time course of compression, and  $pre(sc,tc)$  to the combined measure. In each case from left to right the time course of compression of four different stimulus positions, the time course of the feedback signal and different snapshots in time of the shape of the feedback signal are shown. (a) Resulting data fit of the minimal receptive field size (solid line in Figure 5d in Section 2.2). (b) Resulting data fit using a too small receptive field size (dashed line in Figure 5d).

**Table 3** Parameters of the simulations to predict source and targets of oculomotor feedback.

Figure	$f(t)$	$\alpha$	$\beta$	$w$	$\sigma_{20}^{L1}$	$\sigma_{20}^{L2}$	$\gamma_1$	$\gamma_2$	$n$	$k$
36a	$f_g(t)$	25	12	15	0.4	3.5	2	5	1	1
36b	$f_g(t)$	18	12	50	0.5	2.5	1	1	1	1
35a	$f_e(t)$	0.095	0.13	30	0.51	4.7	1	1	1	1
35b	$f_g(t)$	18	12	10.5	0.51	4.7	1	1	1	1
35c	$f_g(t)$	20	12	10.5	0.51	4.7	1	3	1	1
35d	$f_g(t)$	25	12	10.5	0.51	4.7	2	5	1	1
35e	$f_g(t)$	39	24	10.5	1	9.5	2	5	4	1
35f	$f_g(t)$	39	24	10.5	0.51	4.7	2	5	1	1
35g	$f_g(t)$	18	12	10.5	0.51	4.7	1	1	1	4
35h	$f_g(t)$	39	50	10.5	1	9.5	2	5	4	1

## 5.4 Decoding of the population response

The model provides a population response with respect to a specific stimulus. In order to compare the model’s output with the experimental data, we have to determine the “perceived” stimulus position by decoding the population response with regard to spatial position. Since the model is deterministic and noiseless, we have direct access to the exact or true population response for a given stimulus. It is assumed that a number of active cells  $N$  with firing rates  $r_i$  participate in encoding the stimulus location in retinocentric coordinates.  $\mathbf{r} = \{r_1, \dots, r_N\}$  can be considered as a vector in the  $N$ -dimensional space of neural responses. The unmodulated activity distribution, that is, the population long before a saccade which is not affected by the oculomotor feedback ( $\hat{r}_i = 0$ ), resulting from the presentation of a stimulus with the eye-centered position  $p_s$ , was used to generate

a set of templates  $\mathbf{f} = \mathbf{r}(p_s)$ . During the simulations, these templates were then compared to the current population response  $\mathbf{r}$  which could either be unmodulated ( $\hat{r}_i = 0$ ) or modulated ( $\hat{r}_i > 0$ ). The estimated eye-centered position  $\hat{p}_s$  is the one for which the angle between the two vectors  $\mathbf{r}$  and  $\mathbf{f}$  is minimized (Abbott, 1994), which is equivalent to the maximization of

$$\sum_i^N r_i \cdot f_i(\hat{p}_s) \left( \sum_i^N r_i^2 \right)^{-1/2} \left( \sum_i^N f_i^2(\hat{p}_s) \right)^{-1/2}$$

with respect to  $\hat{p}_s$ . Note that if an unmodulated population response is compared to the templates, the estimated position will be equal to the real stimulus position in retinal coordinates  $\hat{p}_s = p_s$ . The overall accuracy depends of course on the sampling of templates in visual space which was done in steps of  $0.2^\circ$ . Recall that in order to obtain the estimated stimulus position in eye-position invariant coordinates  $\hat{\theta}_s$ , the position of the eye  $\theta$  is added to the retinal stimulus position  $\hat{p}_s$ , that is,  $\hat{\theta}_s = \hat{p}_s + \theta$ . Note that the described decoding procedure tolerates the absolute increase in firing rate through the gain modulation. Further note that the reported results are not qualitatively dependent on this particular method of decoding. In Hamker, Zirnsak, Calow, and Lappe (2004) and in Zirnsak (2004) the population was read out by using the maximum of the activity distribution as an estimate of the stimulus position in retinal coordinates (see also Deneve, Latham, & Pouget, 1999). Further, using the center of mass of the neural population as an estimate of stimulus position, as it is done in Section 6.4, would also lead to compression as it is obvious from the distorted population responses towards the saccade target illustrated in Figure 3 (Section 2.2.2). For an overview of decoding methods see for example Seung and Sompolinsky (1993) and Salinas and Abbott (1994).

## 5.5 Computation of mean errors

Mean errors between data and model for the spatial range of compression (Figure 5c in Section 2.2.3) were computed as follows: for each of the eight conditions, that is each model specification (isotropy vs. anisotropy) and each saccade amplitude ( $12^\circ, 16^\circ, 20^\circ, 24^\circ$ ), the differences between the vector endpoints of the perceived and the predicted flash positions were obtained for the  $x$ - and  $y$ -direction, yielding a total of 48 differences (24 differences in the  $x$ - and 24 differences in the  $y$ -direction) for each condition. Then, the mean error for both the  $x$ - and  $y$ -direction was obtained by computing the respective arithmetic mean after the application of the algorithm which is defined below.

Let  $\mathbf{A} = (a_{ij})_{j=1,\dots,N}^{i=1,2}$ ,  $\mathbf{B} = (b_{ij})_{j=1,\dots,N}^{i=1,2}$ ,  $\mathbf{C} = (c_{ij})_{j=1,\dots,N}^{i=1,2}$ , and  $N = 24$ , where  $(a_{1j}, a_{2j})$ ,  $(b_{1j}, b_{2j})$ ,  $(c_{1j}, c_{2j})$  are the cartesian coordinates of the 24 flashed, perceived and predicted positions, respectively. Negative  $y$ -values indicate that the flash was presented below the horizontal meridian and positive  $y$ -values that the flash was presented above the horizontal meridian. Let us further define

$$\begin{aligned} \mathbf{D} &= (d_{ij})_{j=1,\dots,N}^{i=1,2} = \mathbf{B} - \mathbf{A} \\ \mathbf{E} &= (e_{ij})_{j=1,\dots,N}^{i=1,2} = \mathbf{B} - \mathbf{C} \\ \mathbf{F} &= (f_{ij})_{j=1,\dots,N}^{i=1,2} = \begin{cases} -|e_{ij}| & \text{if } [d_{ij}] = [e_{ij}] \\ |e_{ij}| & \text{else} \end{cases}, \end{aligned}$$

where  $|z|$  is the absolute value and  $[z]$  denotes the sign function of  $z$ .

Negative  $f_{ij}$  indicate an undershoot of the model, that is, the theoretically predicted component is smaller than the empirically obtained compression. Positive  $f_{ij}$  indicate an overshoot of the model, that is, the theoretically predicted is larger than the empirically obtained compression. The mean  $x$  error is then given by  $\bar{x} = 1/N \sum_j f_{1j}$  and the mean  $y$  error by  $\bar{y} = 1/N \sum_j f_{2j}$ .

It was tested separately for the x- and y-direction for each saccade amplitude if on average each model deviates statistically significant from the data (two-sided one-sample t-test,  $\alpha = .05$ ,  $df = 23$ ). Note, for a valid model it is desirable to maintain the nullhypothesis  $H_0$ . Thus, in order to increase statistical power no adjustments of the testwise  $\alpha'$ -level were conducted, that is  $\alpha' = \alpha$ . For the isotropic model all mean errors reach statistical significance ( $p < .05$ ) except for the error in the y-direction for the  $12^\circ$  and  $16^\circ$  saccade. For the anisotropic model none of the mean errors reaches statistical significance ( $p > .05$ ).

## 5.6 Proportional reduction in error measure

In order to quantify the model fit, the following proportional reduction in error measure

$$pre = 100 \frac{E_1 - E_2}{E_1}$$

was used. Thereby,  $E_1$  is the sum of squared error ( $SSE$ ) of the data with respect to a particular empirical mean value and  $E_2$  is the  $SSE$  with respect to the corresponding model predictions. If  $E_2 \geq E_1$ ,  $pre$  was set to zero. Since we have  $i = 1\dots 13$  pairs of  $(E_1, E_2)$  (8 of the spatial compression pattern, 4 of the time

course, 1 of the spatial range ), aggregated *pre*-measures were obtained by summing up the respective  $E_{1i}$  and  $E_{2i}$ , so that

$$pre = 100 \frac{\sum_i E_{1i} - \sum_i E_{2i}}{\sum_i E_{1i}}.$$

To exclude the apparent shift in baseline from the measurement, we additionally determined *pre*\*-measures of bars flashed at  $20^\circ$  and  $-20^\circ$  for which errors ( $E_1$  and  $E_2$ ) were computed using data points only in the period before  $t = 40\text{ms}$ .

---

## 6 Appendix B: Feature-based attention

### 6.1 Control experiment 1: Contrast dependency

In this control experiment the influence of contrast on the observed effect was tested using a high contrast and a low contrast condition. Subjects  $S_2$  and  $S_3$  participated in this experiment. The general procedure and the task were identical to the main experiment (see Section 3.2), but here, both stimuli had a coherence of 100 %. In the high contrast condition the dots of the target and the adaptor were white with a luminance of  $85.6 \text{ cd/m}^2$  on a black background ( $2.2 \text{ cd/m}^2$ ), resulting in a Weber contrast of 37.91 for a single dot and for the whole RDK in a root mean square (RMS) contrast (Moulden, Kingdom, & Gatley, 1990; Martinez-Tujillo & Treue, 2002; Seitz, Nanez, Holloway, & Watanabe, 2006) of 35.87. In the low contrast condition the dots of the target were also white with the same luminance as stated above, but the dots of the adaptor were gray with a luminance of  $5.2 \text{ cd/m}^2$ , resulting in a Weber contrast of 1.36 and a RMS contrast of 1.29. Two directions ( $-67.5^\circ, 67.5^\circ$ ) were used. Information about the size of the luminance change in the detection task is given in Table 7. About 20 % of the total number of trials were excluded because the luminance detection performance of the subjects fell outside the predefined range (see Section 3.2). The performance of the subjects is shown in Table 8. Less than 0.02 % of the remaining trials were identified and excluded as outliers because they fell outside the region of  $\pm 2.5 \text{ SDs}$  around the respective mean. The results are summarized in Figure 25 (Section 3) and Table 9.

### 6.2 Control experiment 2: Unattended motion

In this control experiment it was tested whether there is still a difference between the same-condition and the different-condition when attention is withdrawn from the target. Subjects  $S_2$ ,  $S_3$ , and  $S_4$  participated in this control. Both the general procedure and the task were identical to the main experiment (see Section 3.2) with the following exceptions. The presentation of the to be attended target direction was replaced by a blank of the same duration (5 s). Instead of detecting a luminance change of the target, subjects detected a luminance change of the central fixation point while ignoring both RDKs. The fixation point was white with a luminance of  $85.6 \text{ cd/m}^2$ . The magnitude of the luminance change required central fixation. That is, it was assured that the detection performance was at chance level if the subject fixated one of the two RDKs. The luminance change was  $8.4 \text{ cd/m}^2$  for  $S_2$  and  $S_3$ , and  $12.7 \text{ cd/m}^2$  for  $S_4$ . Subjects' performance is shown in Table 10. About 5 % of

the total numbers of trials were excluded because subjects indicated that they did not perceive an aftereffect. No outliers were detected. The results are summarized in Figure 26 (Section 3) and Table 11.

### 6.3 Statistical analysis

Since the variability of the data is reasonably low ( $\overline{SD} = 5.57, SD_{\overline{SD}} = 3.19, min = 1.27, max = 18.48$ ), ordinary statistics were used. It is assumed that all measurements are statistically independent. For all comparisons Welch's generalization of the independent two-sample  $t$ -test for unequal variances was used. All tests were conducted two sided. The test-wise  $\alpha'$ -level was adjusted due to Bonferroni correction so that  $\alpha' = \alpha/m$ , where  $m$  is the number of comparisons and  $\alpha = .05$ . The global null hypothesis is rejected if there exists at least one out of  $m$  multiple comparisons which is significant at the adjusted  $\alpha'$ -level.

In the main experiment it was tested separately for all subjects if there exists a statistically significant difference of the indicated SMAE directions between the same-condition and the different-condition and if there exists a difference between the same-condition and the baseline. This was done for all directions consisting in each case of 10 comparisons for  $S_1$  and  $S_2$  ( $\alpha' = .005$ ), and 2 comparisons for  $S_3$  and  $S_4$  ( $\alpha' = .025$ ). Statistics are summarized in Table 6.

In control experiment 1 it was tested if there exists a difference between the same-condition and the different-condition for the high and low contrast condition and if there exists a difference between the different-conditions of the high and the low contrast condition. In each case two comparisons were made per subject. Statistics are summarized in Table 9.

In control experiment 2 it was tested if there exists a difference of the indicated SMAE directions between the same-condition and the different-condition. For each subject two comparisons were made. Statistics are summarized in Table 11.

### 6.4 Model of feature-based attention

In order to explain the observed results a model was set up in which the impact of attention on the population response was simulated. The model can be considered as a static, simplified version of earlier formalizations (Hamker, 2005a, 2007). Thereby, the influences of attention were simulated in explicit terms as it is described below.

Let  $F = [0, 2\pi)$  be the feature space. Tuning curves are described as Gaussian functions located in  $F$ . For a given stimulus the unmodulated or input activity  $r^{\text{in}}$

of the  $i$ th cell is

$$r_i^{\text{in}} = b_0 + b_1 \exp\left(-\frac{\phi_i^2}{2(\sigma_{\text{TC}})^2}\right)$$

$$\phi_i = ((p_S - c_i^{\text{TC}} + \pi) \bmod 2\pi) - \pi,$$

with  $\phi \in [-\pi, \pi)$ . The preferred direction, that is, the center of the tuning curve in feature space is denoted by  $c_i^{\text{TC}} \in F$ . The direction of the stimulus is denoted by  $p_S \in F$ . The width of the tuning curve is determined by  $\sigma_{\text{TC}}$ , which was set to  $\sigma_{\text{TC}} = 0.7$ ,  $b_0$  is the baseline activity, which was set to  $b_0 = 1$  for all cells, and  $b_1$  determines the height of the Gaussian. For all cells  $b_1$  was set to  $b_1 = 10$ . Note cells have a bandwidth of  $94^\circ$  as determined by the half-maximum width after subtraction of the baseline activity  $b_0$ .

The influence of attention on the population response is formalized as a difference of Gaussians

$$a_i = \exp\left(-\frac{\phi_i^2}{2(\sigma_A)^2}\right) - c \exp\left(-\frac{\phi_i^2}{2(3\sigma_A)^2}\right)$$

$$\phi_i = ((p_i - c_A + \pi) \bmod 2\pi) - \pi,$$

where  $c_A \in F$  denotes the attended direction and  $p_i$  is the position of the  $i$ th cell in  $F$ . The extend of the central excitatory and the surrounding inhibitory region is determined by the constant  $c$  and by  $\sigma_A$ , which was set to  $\sigma_A = 0.52$ . Note that  $c = 0.9$  for subject  $S_1$  and  $c = 0.7$  for subject  $S_2$ . Further note that a simple Gaussian profile with central excitation and surrounding inhibition is inconsistent with the observed results since it cannot account for the repulsion effect, but predicts only attraction (not shown).

Finally, the modulated response  $r_i^{\text{gain}}$  of a given cell  $i$  is

$$r_i^{\text{gain}} = r_i^{\text{in}} (1 + w a_i),$$

where  $w$  is a weight which was set to  $w = 3$  for subject  $S_1$  and  $w = 2.5$  for subject  $S_2$ . Note if  $r_i^{\text{gain}} < 0$ , then  $r_i^{\text{gain}} = 0$ . For the simulations the whole population consisted of 360 cells which were equally spaced in  $F$ .

To decode the direction from the population response, the center of mass of the

neural activity in  $F$  was computed as follows

$$x = \frac{\sum_i r_i^{\text{gain}} \cos(c_i^{\text{TC}})}{\sum_i r_i^{\text{gain}}}$$

$$y = \frac{\sum_i r_i^{\text{gain}} \sin(c_i^{\text{TC}})}{\sum_i r_i^{\text{gain}}}.$$

The decoded direction is then given in Cartesian coordinates by the vector  $\mathbf{v} = (x, y)$ .

Note that the parameters were obtained by roughly fitting the model to the data of subjects  $S_1$  and  $S_2$  in order to provide a qualitative explanation of the observed effect. In order to keep the description as simple as possible, it was not accounted for the apparent asymmetries of the data in the two hemispheres (see Figure 24a in Section 3).

For the illustration of the tuning curve shifts a second population of cells was simulated. These cells pool the activity of the first population in feature space, that is, they are driven by a simple weighted sum of afferent responses (Rust et al., 2006). The bandwidth of the tuning curves of the second population is  $100^\circ$ . The modulated ( $w > 0$ ) and unmodulated ( $w = 0$ ) tuning curves were normalized after subtraction of the baseline, which was in this case defined as the minimal activity of a given tuning curve. Processing capacity is defined as the number of tuning curves  $n_{\text{TC}}$  for which the response to a given direction exceeds half of the maximum activity of the respective cell (please refer also Section 2.3) and  $\Delta n_{\text{TC}}$  is the change in capacity in the modulated case with respect to the unmodulated one. For the reported simulations (Figure 27f in Section 3) the parameters of  $S_2$  were used. Note same is true for the reported distortions of the population response (Figure 27c, 27d).

## 6.5 Eye movements

Although eye movements were not measured directly, it is unlikely that possible eye movements caused the observed results of the main experiment and of control experiment 1. The most reasonable case for subjects to break central fixation would be to direct their gaze at the target to optimize the detection of the luminance change. However, if the performance of subjects in the peripheral detection task of the main experiment and control experiment 1 is compared to the performance of a central detection task, where subjects were instructed to fixate the target, it

seems that subjects did not apply such a strategy as indicated by the performance in the respective conditions. If subjects had fixated the target during the peripheral detection task, a much higher detection rate should have been obtained as it is indicated by the performance of the central detection task.

The performance of the peripheral detection task is shown in Table 5 and Table 8. The mean performance across all subjects and the two experiments is 1.83 ( $min = 1.78, max = 1.87$ ) as measured in  $d'$  and corresponds to an unbiased proportion correct responses of  $p(c)_{max} = 81.67\%$ . For all subjects with the exception of  $S_4$  the unbiased proportions of correct responses  $p(c)_{max}$  are close to the empirical proportions of correct responses  $p(c)$ , indicating that the response bias in the detection task was low. In the central detection task for all subjects performance is close to perfect. For subject  $S_1$  the obtained performance is  $d' = 3.66$ ,  $p(c)_{max} = 96.66\%$ , and  $p(c) = 96.67\%$ . For  $S_2$  and  $S_3$  the obtained performance is  $d' = 4.24$ ,  $p(c)_{max} = 98.29\%$ , and  $p(c) = 100\%$ . Finally, for  $S_4$  the obtained performance is  $d' = 3.95$ ,  $p(c)_{max} = 97.6\%$ , and  $p(c) = 98.33\%$ . Note that for  $S_2$ ,  $S_3$ , and  $S_4$   $p(c)_{max}$  is less than  $p(c)$ . This is due to a common correction which was applied in order to estimate  $d'$  in the case of hit rates of  $h = 1$  and false alarm rates of  $f = 0$ . For  $h$  the correction is  $h = 1 - 1/N$  and for  $f$  the correction is  $f = f/N$ , where  $N = 60$  is the number of detection trials. For each subject the magnitude of the luminance change in this central task was set to the minimal luminance change which occurred for a specific subject in the peripheral task.

Furthermore, if subjects had fixated the target in the peripheral detection task, there would have been a foveal adaptation to the direction of the target. If we further assume that after the detection trials, where the target disappears and the adaptor stops moving, the subjects fixate the adaptor to indicate the SMAE, we will expect that in different-trials the indicated SMAE will always be directed opposite to  $0^\circ$ , that is, the SMAE should be  $180^\circ$  in the non-transformed description. As it is obvious from Figure 24 and Figure 25 (both in Section 3), the effect is more gradual and such a pattern of eye movements would not have resulted in the observed repulsion effect, which should not have been found either if subjects had altered between fixating the target and the adaptor.

**Table 4** Main experiment: Luminance change.

Subject	$n$	$M$	$SD$	$min$	$max$
S <sub>1</sub>	120	27.91	2.53	22.09	34.91
S <sub>2</sub>	111	28.2	1.78	23.36	31.66
S <sub>3</sub>	20	20.53	1.45	17.29	22.09
S <sub>4</sub>	33	32.63	5.57	21.27	41.08

*Note.* Unit of measurement is candela per square metre.

**Table 5** Main experiment: Performance.

Subject	$n$	$d'$			$p(c)_{max}$			$p(c)$		
		$M$	$SD$	$CI$	$M$	$SD$	$CI$	$M$	$SD$	$CI$
S <sub>1</sub>	120	1.81	0.31	[1.76, 1.87]	81.49	4.03	[80.76, 82.21]	80.08	4.41	[79.30, 80.87]
S <sub>2</sub>	111	1.82	0.3	[1.76, 1.87]	81.53	3.93	[88.8, 82.26]	80.74	3.86	[80.02, 81.45]
S <sub>3</sub>	20	1.85	0.31	[1.71, 1.99]	82.02	3.95	[80.29, 83.75]	80	4.65	[77.96, 82.04]
S <sub>4</sub>	33	1.87	0.34	[1.76, 1.99]	82.23	4.21	[80.8, 83.67]	73.64	5.9	[71.62, 75.65]

*Note.* 95 % confidence intervals are shown. Unbiased proportion correct is denoted by  $p(c)_{max}$ . Proportion correct is denoted by  $p(c)$ . Both measures are shown in percent.

Table 6 Main experiment: Statistics.

S <sub>1</sub>										
Adaptor	Baseline		Same		Different		Baseline vs. Same		Same vs. Different	
	<i>M</i>	<i>SD</i>	<i>M</i>	<i>SD</i>	<i>M</i>	<i>SD</i>	<i>t(df)</i>	<i>p</i>	<i>t(df)</i>	<i>p</i>
135	150.2	5.03	146.46	7.4	175.22	5.14	1.62(24)	.12	12.36(24)	$3.88 \cdot 10^{-12*}$
112.5	130.62	12.2	119.89	16.34	176.54	2.82	2.05(25)	.05	13.23(14)	$1.29 \cdot 10^{-9*}$
90	90.71	4.3	86.89	4.32	26.4	17.62	2.43(27)	.02	12.92(15)	$9.1 \cdot 10^{-10*}$
67.5	51.3	8.05	45.92	12.77	1.59	5.17	1.38(23)	.18	1.47(18)	$1.95 \cdot 10^{-10*}$
45	28.78	6.58	25.27	6.84	0.35	8.86	1.11(27)	.28	8.72(26)	$3.03 \cdot 10^{-9*}$
-45	-29.34	4.93	-33.93	6.77	-10.58	6.57	2.13(25)	.04	9.59(27)	$2.41 \cdot 10^{-10*}$
-67.5	-51.59	6.86	-43.84	10.8	-8.22	5.61	2.34(23)	.03	11.34(21)	$2.02 \cdot 10^{-10*}$
-90	-91.78	7.01	-89.26	1.27	-59.65	18.48	1.37(14)	.19	6.19(14)	$2.25 \cdot 10^{-5*}$
-112.5	-132.49	6.77	-129.66	8.21	-172.81	6.21	0.86(27)	.4	16.23(26)	$3.82 \cdot 10^{-15*}$
-135	-148.77	5.76	-144.34	4.69	-176.38	8.16	2.31(26)	.03	13.18(22)	$5.14 \cdot 10^{-12*}$

S <sub>2</sub>										
Adaptor	Baseline		Same		Different		Baseline vs. Same		Same vs. Different	
	<i>M</i>	<i>SD</i>	<i>M</i>	<i>SD</i>	<i>M</i>	<i>SD</i>	<i>t(df)</i>	<i>p</i>	<i>t(df)</i>	<i>p</i>
135	140.07	5.63	134.94	3.66	160.72	3.77	2.95(24)	$6.94 \cdot 10^{-3}$	19.02(27)	$1.54 \cdot 10^{-17*}$
112.5	117.77	4.65	116.19	3.58	131.18	3.98	1.05(26)	.3	10.85(27)	$1.75 \cdot 10^{-11*}$
90	92.53	3.65	89.09	3.04	67.17	4.36	2.8(27)	$9.21 \cdot 10^{-3}$	15.97(25)	$1.22 \cdot 10^{-14*}$
67.5	66.8	3.78	64.8	1.85	39.08	4.8	1.85(20)	.08	19.35(18)	$1.58 \cdot 10^{-13*}$
45	42.58	2.49	39.54	4.19	14.13	5.04	2.42(22)	.02	15.02(27)	$1.18 \cdot 10^{-14*}$
-45	-43.8	3.85	-40.5	2.47	-15.56	4.69	2.79(23)	.01	18.22(21)	$1.95 \cdot 10^{-14*}$
-67.5	-66.68	4.24	-59.84	5.26	-31.83	6.37	2.83(26)	$8.66 \cdot 10^{-3}$	13.14(27)	$3 \cdot 10^{-13*}$
-90	-91.51	2.27	-89.18	4.33	-56.23	3.9	1.84(21)	.08	21.88(27)	$5.14 \cdot 10^{-19*}$
-112.5	-117.49	3.12	-116.39	2.18	-128.7	4.8	1.11(25)	.28	7.76(19)	$3.84 \cdot 10^{-7*}$
-135	-139.91	6.28	-134.56	3.6	-153.6	4.48	2.85(22)	$9.15 \cdot 10^{-3}$	12.82(26)	$6.13 \cdot 10^{-13*}$

S <sub>3</sub>										
Adaptor	Baseline		Same		Different		Baseline vs. Same		Same vs. Different	
	<i>M</i>	<i>SD</i>	<i>M</i>	<i>SD</i>	<i>M</i>	<i>SD</i>	<i>t(df)</i>	<i>p</i>	<i>t(df)</i>	<i>p</i>
67.5	58.5	6.06	55.65	10.46	25.12	8.98	0.91(22)	.37	8.58(27)	$3.05 \cdot 10^{-9*}$
-67.5	58.82	6.09	-53.33	10.67	-28.68	6.58	1.73(22)	.1	7.61(23)	$9.28 \cdot 10^{-8*}$

S <sub>4</sub>										
Adaptor	Baseline		Same		Different		Baseline vs. Same		Same vs. Different	
	<i>M</i>	<i>SD</i>	<i>M</i>	<i>SD</i>	<i>M</i>	<i>SD</i>	<i>t(df)</i>	<i>p</i>	<i>t(df)</i>	<i>p</i>
67.5	57.05	2.33	51.63	3.53	10.17	13.98	4.96(24)	$4.4 \cdot 10^{-5*}$	11.14(15)	$7.02 \cdot 10^{-9*}$
-67.5	-58.12	3.16	-50.79	3.93	-15.46	8.06	5.63(26)	$5.74 \cdot 10^{-6*}$	15.27(20)	$1.37 \cdot 10^{-12*}$

Note. Unit of measurement is degree. Number of measurements in each condition is  $n = 15$ . Critical  $p$  values are

$p_{\text{crit}} = .005$  for S<sub>1</sub> and S<sub>2</sub>, and  $p_{\text{crit}} = .025$  for S<sub>3</sub> and S<sub>4</sub>

\* $p < p_{\text{crit}}$ , two-tailed.

**Table 7** Control experiment 1: Luminance change.

Subject	$n$	$M$	$SD$	$min$	$max$
S <sub>2</sub>	41	30.3	2.92	24.34	37.01
S <sub>3</sub>	41	17.96	2.55	10.67	22.09

*Note.* Unit of measurement is candela per square metre.

**Table 8** Control experiment 1: Performance.

Subject	$n$	$d'$			$p(c)_{max}$			$p(c)$		
		$M$	$SD$	$CI$	$M$	$SD$	$CI$	$M$	$SD$	$CI$
S <sub>2</sub>	41	1.84	0.31	[1.74, 1.93]	81.78	4.03	[80.54, 83.01]	80	4	[78.78, 81.22]
S <sub>3</sub>	41	1.78	0.32	[1.68, 1.87]	80.99	4.12	[79.73, 82.25]	80.33	4.27	[79.02, 81.63]

*Note.* 95 % confidence intervals are shown. Unbiased proportion correct is denoted by  $p(c)_{max}$ . Proportion correct is denoted by  $p(c)$ . Both measures are shown in percent.

Table 9 Control experiment 1: Statistics.

S <sub>2</sub>							
Contrast	Adaptor	Same		Different		Same vs. Different	
		<i>M</i>	<i>SD</i>	<i>M</i>	<i>SD</i>	<i>t(df)</i>	<i>p</i>
High	67.5	65.27	2.87	58.4	2.77	6.68(27)	$3.05 \cdot 10^{-7*}$
High	-67.5	-55.87	1.74	-49.09	4.19	5.79(18)	$1.5 \cdot 10^{-5*}$
Low	67.5	62	3.65	41.21	5.24	12.61(24)	$2.43 \cdot 10^{-12*}$
Low	-67.5	-54.53	4.5	-35.84	6.44	9.21(25)	$1.62 \cdot 10^{-9*}$
Different vs. Different							
		Adaptor	<i>t(df)</i>	<i>p</i>			
		67.5	11.23(21)	$2.07 \cdot 10^{-10*}$			
		-67.5	6.68(24)	$6.57 \cdot 10^{-7*}$			
S <sub>3</sub>							
Contrast	Adaptor	Same		Different		Same vs. Different	
		<i>M</i>	<i>SD</i>	<i>M</i>	<i>SD</i>	<i>t(df)</i>	<i>p</i>
High	67.5	64.29	3.21	49.2	8.46	6.46(17)	$4.55 \cdot 10^{-6*}$
High	-67.5	-67.95	2.89	-54.95	6.41	4.96(19)	$8.06 \cdot 10^{-5*}$
Low	67.5	61.84	3.91	30.13	6.67	15.87(22)	$9.53 \cdot 10^{-14*}$
Low	-67.5	-61.33	4.01	-34.65	6.27	13.88(23)	$6.54 \cdot 10^{-13*}$
Different vs. Different							
		Adaptor	<i>t(df)</i>	<i>p</i>			
		67.5	6.85(26)	$2.55 \cdot 10^{-7*}$			
		-67.5	8.77(27)	$1.61 \cdot 10^{-9*}$			

Note. Unit of measurement is degree. Number of measurements in each condition is  $n = 15$ . Critical  $p$  value is  $p_{\text{crit}} = .025$ .

\* $p < p_{\text{crit}}$ , two-tailed.

**Table 10** Control experiment 2: Performance.

Subject	$n$	$d'$			$p(c)_{max}$			$p(c)$		
		$M$	$SD$	$CI$	$M$	$SD$	$CI$	$M$	$SD$	$CI$
S <sub>2</sub>	21	3.09	0.5	[2.88, 3.3]	93.33	3.14	[91.99, 94.67]	92.86	3.54	[91.34, 94.37]
S <sub>3</sub>	22	3.54	0.53	[3.32, 3.77]	95.68	2.36	[94.7, 96.67]	95.61	3.66	[94.08, 97.13]
S <sub>4</sub>	24	3.09	0.62	[2.84, 3.34]	93.02	4.08	[91.39, 94.66]	92.57	4.58	[90.74, 94.4]

*Note.* 95 % confidence intervals are shown. Unbiased proportion correct is denoted by  $p(c)_{max}$ . Proportion correct is denoted by  $p(c)$ . Both measures are shown in percent.

**Table 11** Control experiment 2: Statistics.

S <sub>2</sub>							
Adaptor	Same		Different		Same vs. Different		$p$
	$M$	$SD$	$M$	$SD$	$t(df)$		
67.5	64.26	3.48	63.39	3.59	0.67(27)		.51
-67.5	-58.7	2.36	-58.59	2.74	0.12(27)		.91

S <sub>3</sub>							
Adaptor	Same		Different		Same vs. Different		$p$
	$M$	$SD$	$M$	$SD$	$t(df)$		
67.5	67.1	4.87	65.68	4.61	0.82(27)		.42
-67.5	-66.8	5.55	-64.99	4.23	1.01(26)		.32

S <sub>4</sub>							
Adaptor	Same		Different		Same vs. Different		$p$
	$M$	$SD$	$M$	$SD$	$t(df)$		
67.5	38.2	5.78	38.47	2.48	0.17(18)		.86
-67.5	-32.03	5.35	-32.29	3.45	0.24(23)		.81

*Note.* Unit of measurement is degree. Number of measurements in each condition is  $n = 15$ . Critical  $p$  value is  $p_{crit} = .025$ .

## Acknowledgements

This thesis could not have been completed without the help, support and encouragement of several people I would like to thank at this place.

First of all I would like to thank Prof. Dr. Fred Hamker for giving me the opportunity to write this thesis, for his professional leadership, and endless support. Further, I am grateful to Prof. Dr. Markus Lappe for his great support and discussions.

Moreover I would like to thank the following members of the lab for their patience, help or simply friendship:

Dr. Dirk Calow, Dr. Jeremy Fix, Dr. Harald Frenz, Ricarda Gerhards, Katharina Havermann, Ursula Husemann, Dr. Farid Kandil, Dr. Joachim Lange, Dr. Lars Michels, Stefanie Rau, Dr. Robert Volcic, Mark-Andre Voss, Andreas Wilmer, Jan Wiltschut, Karin Wittinghofer, and Eckart Zimmermann.

Finally, I would like to thank my whole family, especially Horst, Elke, and Hans Zirnsak.